ENGRAM PATHOLOGY IN DOWN SYNDROME: MOLECULAR AND CELLULAR MECHANISMS

Álvaro Fernández Blanco

TESI DOCTORAL UPF / ANY 2022

DIRECTORA DE LA TESI

Dra. Mara Dierssen

Biologia de sistemes - Centre de Regulació Genòmica

DEPARTAMENT CEXS-UPF-PHD PROGRAMME IN BIOMEDICINE

A mi familia, a Laura

“As long as our brain is a mystery, the universe,
the reflection of the structure of the brain,
will also be a mystery.”

Santiago Ramón y Cajal

Acknowledgements

Los agradecimientos es probablemente la parte más difícil de escribir, en parte debido a que la concepción y consecución de esta tesis no hubiera sido posible sin todas aquellas personas que me han acompañado en este camino. De todas ellas he aprendido y me han inspirado a ser mejor científico.

En primer lugar, me gustaría comenzar agradeciendo a Mara por la gran oportunidad que me brindó al poder realizar mi tesis doctoral en su laboratorio. Agradecer también su alta exigencia y altas expectativas porque gracias a ello pude aprender a hacerme las preguntas correctas. Agradecer su supervisión, guía, *feedback* y disponibilidad gracias a las cuales he podido madurar científicamente. Me gustaría agradecer también la oportunidad de asistir y de participar en diferentes conferencias internacionales de primer nivel, así como la posibilidad de haber realizado diferentes cursos de formación que me han ayudado a expandir mi mente a nivel científico. Tengo la total certeza de que, sin su supervisión y su guía, esta tesis no hubiera sido posible.

Me gustaría agradecer también el soporte y seguimiento por parte de los miembros de mi comité asesor de Tesis: Manuel Irimia, Gertrudis Perea y Verena Ruprecht. En particular, me gustaría agradecer el apoyo de Gertru no solo en sus aportaciones y *feedback* en los diferentes comités de Tesis sino también por haberme dado la oportunidad de poder realizar una estancia en su laboratorio para aprender más sobre electrofisiología y astrocitos.

Me gustaría dar las gracias a mis compañeros y compañeras de laboratorio con los que he tenido la suerte de trabajar más estrechamente. De todos ellos he aprendido lecciones muy valiosas. A Eduardo Domínguez, por su supervisión en las primeras fases de esta Tesis y por su inestimable empeño por transmitirme sus conocimientos sobre el hipocampo y electrofisiología. A María Martínez, por su enorme sabiduría, por su calma y por su paciencia en la gestión diaria del laboratorio. Sin ella, este laboratorio sería un completo caos. A Miguel Sabariego, por su infinita sabiduría, por su gran rigor científico y por estar siempre dispuesto a echar una mano y dar consejo cuando las circunstancias lo han requerido. A Alfonsa, por su meticulosidad y organización a nivel científico. Por las innumerables horas de arduo trabajo en el *setup* de electrofisiología, por su

orden y por sus lágrimas cuando los experimentos no salían de la forma en la que esperábamos. A Cèsar, por su ayuda a la hora de planificar y diseñar experimentos clave para esta tesis. Por tener siempre la respuesta a mis preguntas. Por su inestimable ayuda en la realización y análisis de los experimentos de RNA-seq.

A special thanks to the entire Goshen lab at the ELSC in Jerusalem. One of my greatest PhD experiences was visiting their lab for 10 days just before the pandemic started. The great environment and the excellent scientists I had the pleasure to meet taught me a lot about neuroscience. I want to thank Ron Rafeli for teaching me to clear whole brains like in a factory and to Tirzah Kreisel for teaching me optogenetics. Thanks to Adi Kol for her invaluable feedback not only during my visit but also on posterior occasions. Of course, I thank Inbal Goshen for the opportunity to visit her lab and for the useful discussions we had as the project was being developed.

Me gustaría también agradecer a todas las personas con las que he tenido la fortuna de realizar proyectos en colaboración. A Sergi Bonilla por su gran paciencia y por su buen rollo. A Ana Gallego, por la gran ayuda que me brindó en los momentos más duros de esta Tesis, por todo lo que aprendí de ella sobre cirugías. A Candela González, por todo lo que me enseñó, por su gran esfuerzo y devoción en la realización de los experimentos y por siempre ver el lado positivo de las cosas. A Julio Esparza, por su valiosa ayuda en el análisis de la imagen de calcio. A Patryk Pólinski, por su soporte, disponibilidad y ayuda durante estos cuatro años. A Anna Vázquez y Lorena Galera, por asesorarme siempre con una sonrisa y por auxiliarme en los momentos más críticos.

Me gustaría agradecer el gran trabajo y *feedback* de las *facilities* del CRG. Sin ellas, esta tesis no hubiera sido posible. A Xavi Sanjuan, Raquel García y Arrate Mallabiabarrena, miembros de la Unidad Avanzada de Microscopía del CRG ya que siempre han resuelto mis dudas y me han aconsejado científicamente. A Alexis Ràfols, por realizar histología con una destreza y meticulosidad asombrosa. Trabajar con todos ellos ha sido todo un placer.

Fuera del CRG, otras personas han hecho posible la consecución de esta Tesis. A Susana Miravet, de la *Viral Vector Production Unit* en la Universidad Autónoma

de Barcelona, por su asesoramiento y trabajo en la generación de los vectores virales utilizados en esta tesis. A Domenica Marchese y Giulia Lunazzi, por su gran ayuda en la realización del experimento de single nucleus RNA-seq. I would also like to thank Laurent Meijer and Mattias Lindberg from *Perha Pharmaceuticals* for providing the Leucettinibs used in this Thesis.

A los responsables de las diferentes zonas del estabulario en las que he tenido la suerte de trabajar: Pep Moreno, Begoña Peñalba, Lucía Moure, Mireia Juan e Ivan Ortega. A las cuidadoras Carla Jarque y Yolanda, en Cuarentena y a Paco Porrón, cuidador en Ubiomex-UPF.

A Aitor, Marc y David, miembros de mantenimiento científico por estar siempre dispuestos a echarnos una mano, por su excelente trabajo y por su gran humor.

A Magalí, la secretaria del programa de Biología de Sistemas, por su inestimable ayuda y disponibilidad a la hora de organizar todos los detalles logísticos para asistir a las diferentes conferencias durante esta Tesis.

En el ámbito más personal, me gustaría agradecer a las personas del laboratorio con las que he tenido la fortuna de compartir estos cuatro últimos años. Sin duda alguna para mí, han sido los mejores hallazgos durante esta Tesis. Gracias a Cèsar, Miguel, Alfonsa, Juanlu, Adrián, María, René, Paulina, Khashayar, Nico y Karla. Me gustaría agradecer a los ex-miembros del laboratorio de los cuales tengo un afectuoso recuerdo: Júlia, Linus, Mireia, Ilario, Marcin, Marta, Marcos, Ibo, y Edu. También a las personas que pasaron por el laboratorio durante cortos pero inolvidables períodos de tiempo: Natalia, Diana, Siân, Gemma, Federica, Santi, Lorenzo, Natalia Glazman, Domitille, Erica y Pau.

También me gustaría agradecer a todas aquellas personas con las que durante estos años he compartido uno de mis deportes favoritos: el vóley playa. A Fede, Giani, Chiara, Ivano, Sonia, Xavi, Oguzhan, Marta, Moritz, July, Borja, Cristina, Andrea, Chelsea, José, Joao, Eva y Marcos.

Durante esta tesis he conocido a personas extraordinarias que me han ayudado en este viaje y con las que he compartido innumerables experiencias, así como penas y alegrías. Muchísimas gracias a Fede, Xavi, Queralt, Julia, Ludo, Sergi, Patryk, Leire, Ana y Cristina.

A mis padres y a mi hermana, por haberme apoyado en todas mis decisiones, incluida la de seguir recorriendo el camino científico.
Por último, agradecer a la persona que siempre estuvo a mi lado, apoyándome incondicionalmente en los buenos y en los malos momentos. Sin ella, este largo camino hubiera sido mucho más difícil y tortuoso, especialmente en su última etapa. Muchísimas gracias Laura.

Álvaro Fernández Blanco has been funded by the FPI-Severo Ochoa grant from Ministerio de Ciencia, Innovación y Universidades with reference PRE2018-084504.

The work has been supported by the Secretaria d'Universitats i Recerca del Departament d'Economia I Coneixement de la Generalitat de Catalunya (Grups consolidats 2017 SGR 926). We also acknowledge the support of the Agencia Estatal de Investigación (PID2019-110755RB-I00/AEI/ 10.13039/501100011033), H2020 SC1 Gene overdosage and comorbidities during the early lifetime in Down Syndrome GO-DS21- 848077, Jerôme Lejeune Foundation #2002, 2002_2020B. NIH (Grant Number: 1R01EB 028159-01), Fundació La Marató-TV3 (#2016/20-30), JPND Heroes Ministerio de Ciencia Innovación y Universidades (RTC2019-007230-1 and RTC2019-007329-1).

ABSTRACT/RESUM

Abstract

Down syndrome (DS) is the most common genetic form of intellectual disability (ID). The partial or total trisomy of the *Homo Sapiens Autosome* 21 (HSA21) gives rise to complex pathological manifestations, including intellectual disability and increased prevalence of Alzheimer's disease (AD). Research on individuals with DS, and genetic mouse models has identified several pathogenetic mechanisms that contribute to the pathophysiology of the cognitive deficits of DS. However, the cellular and molecular mechanisms that contribute to learning and memory alterations are not completely understood. One of the main pitfalls is that until very recently, memory was understood as the changes that occurred at the neuronal population level, as a consequence of learning. However, in the last decade, methodological breakthroughs in the field have made it possible to identify and manipulate the concrete neurons storing a memory, known as engram cells. Research on engram cells has highlighted several cellular and molecular mechanisms that are indispensable for the proper encoding, consolidation and recall of memories. However, only few studies have addressed whether these mechanisms are altered in brain disorders associated with memory deficits.

Our previous work suggest that several mechanisms that are of paramount importance for engram formation and reactivation are impaired in DS. In this Thesis, we performed the first study of engrams in a mouse model of DS, Ts65Dn, using engram tagging techniques. We found a reduced number of engram cells in the Ts65Dn hippocampus, concretely in the dentate gyrus (DG), suggesting reduced neuronal allocation to engrams. Activation of engram cells did not overcome memory deficits in Ts65Dn, possibly due to the functional deficits we identified, since trisomic engram cells presented a lower number of mature spines than WT engram cells and the excitability of trisomic engram cells was not transiently enhanced during memory recall. In fact, we identified Kir3.2 as a promising candidate that might contribute to the sparser neuronal activation during learning and also during memory recall.

Besides the neuronal component, it has recently been shown that astrocytes participate in synaptic transmission and in memory function and, trisomic astrocytes show structural and functional alterations. We show a mild to moderate astrogliosis in Ts65Dn hippocampus, alterations in the transcriptomic profile, and altered astrocyte Ca^{2+} oscillations all of which might impact synaptic neurotransmission in Ts65Dn mice. Importantly, astrocyte activation using chemogenetic manipulation before memory acquisition in CA1, was sufficient to promote neuronal ensemble allocation and recover memory deficits in Ts65Dn mice.

Altogether, our findings suggest that perturbations in engram neurons may play a significant role in memory alterations in DS and might be contributed by alterations in astrocytes. These two lines of research might help to better understand the cellular and molecular foundation of intellectual disability in DS.

Resum

La síndrome de Down (SD) és la causa més freqüent de discapacitat intel·lectual. La trisomia parcial o del cromosoma humà 21 (HSA21) dona lloc a manifestacions patològiques complexes, incloent-hi discapacitat intel·lectual i una major prevalença de la malaltia d'Alzheimer. La investigació en individus amb la SD i models genètics murins han identificat diversos mecanismes patogenètics que contribueixen a la fisiopatologia dels dèficits cognitius de la SD. No obstant això, els mecanismes cel·lulars i moleculars que contribueixen a les alteracions de la memòria no s'entenen completament. Una de les principals dificultats fins ara, és que fins fa relativament poc temps, la memòria s'entenia com els canvis que es produïen a nivell de la població neuronal a conseqüència de l'aprenentatge. Tanmateix, en l'última dècada, els avenços metodològics han permès identificar i manipular les neurones específiques que emmagatzemen la memòria, les conegudes com a cèl·lules engrama. La investigació sobre les cèl·lules engrama ha posat de manifest diferents mecanismes cel·lulars i moleculars que són indispensables per a la codificació i evocació dels records. Tot i així, els estudis que han abordat si aquests mecanismes estan alterats en els trastorns cerebrals associats amb dèficits de memòria són molt escassos. Els nostres estudis previs suggereixen que molts mecanismes que tenen una importància cabdal per a la formació i reactivació d'engrames estan alterats en la SD. En aquesta Tesi, hem realitzat el primer estudi d'engrames en un model de ratolí de la DS, mitjançant tècniques que permeten marcar i manipular les cèl·lules engrama. Vam trobar una reducció en el nombre de cèl·lules engrama a l'hipocamp trisòmic, concretament al gir dentat (DG), cosa que suggereix una assignació neuronal reduïda als engrames. L'activació de les cèl·lules engrama no va rescatar els dèficits de memòria als ratolins trisòmics, possiblement a causa dels dèficits funcionals que hem identificat, ja que les cèl·lules engrama trisòmiques presenten un menor nombre d'espines madures que les cèl·lules engrama WT i l'excitabilitat de les cèl·lules engrama trisòmiques no augmenta de manera transitòria durant l'evocació dels records. De fet, hem identificat Kir3.2 com un candidat prometedor que podria contribuir a la reducció d'activació neuronal durant l'aprenentatge i el record.

A més del component neuronal, recentment s'ha demostrat que els astròcits participen en la transmissió sinàptica i en processos de memòria. També s'ha descrit que els astròcits trisòmics presenten alteracions estructurals i funcionals. Mostrem una astrogliosis moderada a l'hipocamp a ratolins trisòmics, canvis en el perfil transcriptòmic així com alteracions en les oscil·lacions de calci dels astròcits que podrien afectar a la transmissió sinàptica en ratolins trisòmics. És important destacar que l'activació dels astròcits mitjançant una manipulació quimiogenètica abans de l'adquisició de memòria a CA1 va ser suficient per promoure una major activació neuronal i recuperar els dèficits de memòria en ratolins trisòmics.

En conjunt, les nostres troballes suggereixen que les alteracions a les neurones engrama poden tenir un paper rellevant en les alteracions de la memòria en la SD i poden estar afavorides per alteracions a la població d'astròcits. Aquestes dues línies d'investigació poden ajudar a entendre millor els fonaments cel·lulars i moleculars de la discapacitat intel·lectual en la SD.

PREFACE

Preface

In order for learning to occur, an experience must result in enduring changes in anatomical connections and physiological processes within the brain, which allow efficient recall of this experience (e.g., an episodic memory). The sparse ensemble of neurons manifesting these learning-induced changes is called an engram. Over the last decade, the integration of novel technologies has enabled researchers to describe, examine and manipulate the neurons that are responsible for specific memories, known as engram cells. Engram cells have attracted a lot of attention because they allow us to study memory from a cellular perspective. Research on engram cells have delineated several features that are important for engram formation and reactivation. Few, though relevant studies have demonstrated that alterations in engram cells contribute to memory deficits in brain disorders such as Alzheimer's disease and Fragile X syndrome. However, whether DS can be considered as a model of defective engrams has not yet been explored. Previous work from our group and others suggest that this is the case as most of the fundamental mechanisms for engram formation are altered in DS.

However, until very recently, the engram field has taken a mainly neurocentric view of the problem. Now, a myriad of studies investigated whether non-neuronal cells play a role in memory function. A number of reports show that astrocytes can impair neuronal communication and memory function under pathological conditions. In fact, manipulation of astrocyte activity by means of chemo- and optogenetics has evidenced that astrocytes play a relevant role in memory function due to its ability to sense and respond to neuronal activity, thus acting as a third player in synaptic transmission. Of interest for DS, a recent study has underscored that alterations in the function of trisomic astrocytes negatively affect neuronal excitability, a feature that is fundamental for engram formation.

This Thesis arose from the interest of the Cellular and Systems Neurobiology group at the Center for Genomic Regulation to understand the molecular and cellular mechanisms contributing to memory alterations in DS.

In **Chapter I**, I applied memory engram cell identification and manipulation technology in Ts65Dn, a trisomic mouse model of DS, in order to characterize engram alterations and determine whether memory deficits could be restored using different strategies. By using this approach, we were able to detect that trisomic engram cells in the DG showed several alterations including changes in the number, structure and function that might contribute to alterations in memory encoding and consolidation. We were able to identify Kir3.2 as a major mechanism contributing to trisomic engram alterations in the DG. During my Thesis, I first attended a course in Venice on Learning and memory: cellular and molecular mechanisms, led by Sheena Josselyn and Susumu Tonegawa to get insightful knowledge on the state of the art in the field. I also had the opportunity to invite Inbal Goshen for a seminar in which we discussed my experimental work. Thereafter she invited me to her lab, and I presented and discussed my work on engrams and astrocytes at the Edmond and Lily Safra Center for Brain Sciences (ELSC) annual retreat.

In **Chapter II**, I explored the contribution of trisomic astrocytes to altered synaptic activity, plasticity and memory performance. I investigated trisomic astrocytes at different levels of complexity finding relevant alterations in their distribution and transcriptomic profile within the hippocampus. Using a chemogenetic approach to manipulate astrocyte activity, we were able to detect that trisomic astrocytes are able to influence synaptic transmission and enhance memory performance in Ts65Dn mice. In this Chapter, I visited the laboratory of Gertrudis Perea where I learned experimental approaches to investigate how the activation of Gq-pathway in trisomic astroglia influenced synaptic transmission at the single synapse level.

Finally, I participated and presented my work at the 3rd and the 4th International Conference of the Trisomy 21 Research Society, at the Spanish Society of Neuroscience (SENC) and at the Society for Neuroscience (SfN). During these four years, I also started my scientific network thanks to activities such as being a member of the organizing committee of the Early Career Research Committee of IBRO 2023.

Publications of this Thesis

Fernández-Blanco, Á., & Dierssen, M. (2020). “Rethinking intellectual disability: from neuro-to astro-pathology”. *International Journal of Molecular Sciences*, *21*(23), 9039. Impact Factor: 6.2; cited by 5.

- Review of the astroglial pathology in Down syndrome and other intellectual disability disorders. Served as background for the Thesis. I contributed to the conception of the paper and the figures and performed the bibliographic research. I contributed to writing the paper.

Bonilla-Pons, S. À., Nakagawa, S., Bahima, E. G., **Fernández-Blanco, Á.**, Pesaresi, M., D'Antin, J. C., ... & Cosma, M. P. (2022). Müller glia fused with adult stem cells undergo neural differentiation in human retinal models. *EBioMedicine*, *77*, 103914. Impact factor: 7.81; cited by 5.

- Collaboration that helped me to get familiar with some experimental techniques. I designed, performed and analyzed the electrophysiological recordings and Ca^{2+} imaging experiments.

Sabariego-Navarro, M., **Fernández-Blanco, Á.**, Sierra, C., & Dierssen, M. (2022). Neurodevelopmental disorders: 2022 update. *Free Neuropathology*, *3*, 8-8. Cited by 4.

- Related with the Thesis. Review of new findings on pathology of Down syndrome and related intellectual disability disorders. I conceived part of the paper and performed part of the bibliographic research.

Sierra, C., Sabariego, M., **Fernández-Blanco, Á.**, & Dierssen, M. (2022). The lncRNA Snhg11 is required for synaptic function, neurogenesis and memory and is downregulated in the dentate gyrus of Down syndrome mouse models *Nature Communications* (under revision). Impact Factor: 15.41.

- Collaboration. I designed and conducted *in vivo* animal experiments.

De Toma I., Ortega-Crespo M., **Fernández-Blanco Á.**, Calderón A., Barahona L., Trullas R., Sabidó E., Dierssen M. (2022). Proteomic profiling reveals the impact of DYRK1A overexpression, a Down syndrome candidate gene, on mitochondrial dysfunction in the cerebellum. *Frontiers in Molecular Neuroscience* (in press). doi: 10.3389/fnmol.2022.1015220. Impact Factor: 5.83.

- Collaboration. I prepared the figures and conducted the validation experiments.

Polinski P., Miret Cuesta M., Zamora-Moratalla A., Mantica F., Cantero-Recasens G., Normanno D., Iñiguez Rabago L., Morenilla-Palao C., Ordoño P., Bonnal S., Gómez Riera R., Martínez De Lagrán M., **Fernández-Blanco Á**., et al. (2022). A novel regulatory mechanism of actin cytoskeleton dynamics through a neural microexon in DAAM1 is necessary for memory formation. *Nature Neuroscience* (Submitted). Impact Factor: 19.85.

- Collaboration. I provided support for the *in vivo* animal studies performed.

Fructuoso M., **Fernández-Blanco Á**., Gallego-Román A., Martínez de Lagrán, De Toma I., Langohr K., Martín-García E., Maldonado R., Dairou J., Janel N., Dierssen M (2022). Overeating in a mouse model carrying a partial trisomy of Mmu 17 and Mmu16 is associated with dopaminergic neurotransmission deficit in the prefrontal cortex. *Cellular and Molecular Life Sciences* (Submitted). Impact Factor: 9.78.

- Collaboration that helped me to get familiar with some experimental techniques with viral vectors and circuit-specific manipulations. I designed some of the experiments and discussed results, conducted part of the *in vivo* animal experiments, analyzed the data and prepared the figures.

Fernández-Blanco, Á., Zamora-Moratalla A., Sabariego Navarro M., & Dierssen, M. (2022). “Defective engrams as a cellular mechanism of cognitive impairment in Down syndrome. *To be submitted to eLife. Deposited in bioRxiv.*

- Main paper of the Thesis. I designed experiments, conducted the *in vivo* animal experiments, analyzed the data, prepared the figures, and wrote the manuscript.

Fernández-Blanco, Á., Zamora-Moratalla A., González-Arias C., Perea G & Dierssen, M. (2022). “Exploring the role of astroglia in circuit and memory alterations in Down syndrome”. *To be submitted to Nature Neuroscience. Deposited in bioRxiv.*

- Main paper of the Thesis: I designed experiments, conducted the *in vivo* animal experiments, part of the *ex vivo* experiments, analyzed the data, prepared the figures, and wrote the manuscript.

Fernández-Blanco, Á., Sierra C., & Dierssen, M. (2022). “Single nuclei RNAseq suggest the loss of syncytial coupling into the glial network of Down syndrome astrocytes” *To be submitted to Cellular and Molecular Life Sciences. Will be deposited in bioRxiv.*

- Main paper of the Thesis: I designed experiments, conducted the *ex vivo* experiments, analyzed part of the data and prepared the figures. I will be responsible of the validation experiments and of writing the manuscript.

INDEX

Index

GENERAL INTRODUCTION

GENERAL INTRODUCTION

In Down syndrome and other intellectual disability disorders, studies on learning and memory have relied on basic neural functions, such as synaptic transmission, biochemical aspects, ionic channel malfunction, or synaptic plasticity. However, in the last decades, the conceptualization of memory has dramatically changed, incorporating new aspects, such as memory storage related to the inter-cell signaling in small assemblies of neurons called engrams. An important frontier for the DS community is to address those issues at the integrative neuroscience level, in order to understand the impact of the trisomy on emergent functions of cells in learning and memory circuits, and how new players such as glial-neuronal signaling are involved in cognitive disturbances. In this Thesis, we show that consideration of such important aspects may broaden our knowledge of DS pathophysiology, and help understand the physiological processes of information storage in an integrative way.

The historical context of the engram concept

Our memories define us as human beings and guide our behavior and emotional responses. The fact that memory persists long after the event occurred means that the learning experience induces permanent changes in the brain and creates an internal representation of the experience that can be reconstructed in the future. Synaptic plasticity is one of the main cellular mechanisms that has been proposed to explain learning and memory. Donald Hebb was the first to propose a mechanistic conception about how learning and memory would work [1]. He developed the neural ensemble theory that proposes that learning produces associations between neurons by means of synaptic plasticity. This concept is often summarized as “neurons that fire together, wire together”. Hebb’s central postulate claims that the simultaneous activation of neurons by a learning experience induces long-lasting changes that reinforce the connections between those cells. In other words, he proposed the existence of a coincidence detector that allows the plastic changes to occur only when the pre- and postsynaptic neurons are active at the same time. Thus, the co-activation of specific neurons

by a particular experience would leave behind a set of interconnected neurons that would be in charge of representing this memory in the brain. Hebb named those functionally intertwined neurons as “cell assemblies”. Thus, memory is a brain property that emerges from the coordinated and dynamic association of neurons.

Even though Hebb's ideas were revolutionary at his time, he was influenced by several authors before him. In fact, the concept of cell assemblies was probably inspired, directly or indirectly, by the mnemonic theory of Richard Semon. Semon’s work was largely ignored until his book The Mneme (1921) was re-discovered years later [2]. Semon proposed that memory representations are experience-dependent and that, as a result of a given experience, a specific population of brain cells are activated suffering persistent modifications to support the subsequent memory in the future. Consequently, the reactivation of these cells would recall the originally formed memory. He coined this group of cells responsible for a specific memory trace as “engram” or engram cells. It is remarkable that Semon’s conceptualizations were incredibly precise considering the lack of molecular and functional techniques available at his time.

Very recently, it has been demonstrated that the artificial reactivation of engram cells elicits memory recall [3,4]. The experimental demonstration of Semon’s conceptualizations was possible due to the development of activity-dependent tagging techniques [5]. These advances demonstrated that the activation of the learning-activated cells by means of optogenetics was sufficient to elicit memory [3,4,6]. Conversely, the inactivation of these same neuronal ensembles prevented memory recall [7,8]. These studies suggest that engram cells are both sufficient and necessary for memory recall and that engram ensembles are the physical representation of memories in the brain.

Other studies have also contributed to the understanding of the engrams. For instance, it has been described that the number or proportion of neuronal ensembles that “allocate” to an engram is region-specific. For instance in the dentate gyrus, engram cells encoding a particular memory comprise 2-8% of granule cells [3,4,6] while in the amygdala the proportion is around 15% [9]. Excitability is noted to be important during the process of neuronal allocation to

an engram [9]. As a matter of fact, it has been demonstrated that the relative cAMP-response element binding protein (CREB) activity at the time of learning, influences the probability that individual neurons are recruited into a fear memory trace [9]. As such, those cells with increased relative excitability during a particular learning event are more prone to be allocated to an engram compared to neighboring cells [9,10]. It has also been suggested that engram size is quite stereotyped and that deviations from the optimal size might prevent engram networks to reactivate in the exact pattern as when memory was encoded [11]. Besides the engram size, there are other molecular and cellular mechanisms that are of paramount importance to engram formation, consolidation and reactivation. For instance, during memory acquisition, engram cells undergo long-lasting chemical and plastic changes that enable them to reactivate upon recall cues. For instance, engram cells increase their spine density compared to non-engram cells [4,6] and undergo synaptic potentiation as noted by increased excitatory postsynaptic currents (EPSC) amplitude and higher AMPA/NMDA ratio [4]. It has been also reported that specifically between engram cells, there is an enhanced interconnectivity [12]. Moreover, it was shown that memory recall induced a transient increase in engram cell excitability that is mediated by Kir2.1 channel internalization [13]. Remarkably, enhanced excitability of engram cells promotes an enhanced context recognition, while the upregulation of Kir2.1 channels, which leads to reduced excitability, impairs it [13]. These studies have provided invaluable pieces of evidence to better understand how memory works in the healthy brain from a cellular perspective, uncovering mechanisms that are fundamental for memory acquisition, consolidation and recall.

Engram pathology

Even though the engram is a widely accepted mechanism of memory formation and consolidation, only few studies have investigated how engram defects can lead to memory impairment in different neurological disorders [6,14,15]. These scarce, yet relevant studies have provided valuable findings that indicate that defective memory engrams contribute to memory alterations in different

neurological disorders. For example, the upregulation of CREB function prior to learning in a mouse model of AD was sufficient to recover impaired neuronal allocation, restore dendritic spine alterations and recover memory deficits [14]. A different study showed that engram cells in a mouse model of AD failed to increase their dendritic spine density and showed a lower number of active neurons both during memory acquisition and recall compared to age-matched controls [6]. Moreover, those mice exhibited a long-term memory impairment that was restored when engram cells were optogenetically stimulated during memory recall, indicating that retrieval, rather than storage, is impaired [6]. It was shown that under retrograde amnesia, engram cells did not experience an increase in synaptic strength nor an enhanced dendritic spine density, all of which contributed to an impaired memory retrieval [4]. Research on a mouse model of FXS detected that the efficiency of hippocampal engram reactivation was reduced while performing contextual fear memory recall [15]. The exposure of mice to environmental enrichment (EE) prior to learning enhanced engram reactivation and rescued memory recall in a mouse model of FXS. Although the specific mechanisms responsible for these findings were not explored in this study, the authors claimed that EE possibly enhanced neurogenesis, increased dendritic density and complexity and promoted functional plasticity, thus restoring memory consolidation deficits.

Down syndrome as a model of defective engrams

Down syndrome (DS) is the most prevalent cause of intellectual disability (ID) of genetic origin affecting around 1 in about 700-1000 live births worldwide [16,17]. It is due to the partial or total trisomy of the Homo Sapiens Autosome 21 (HSA21) that results in a deregulated gene expression scenario. This extra gene dosage gives rise to a plethora of heterogeneous developmental alterations that affects multiple organs with different degrees of penetrance, being the brain one of the most affected areas. The most common clinical manifestations are intellectual disability along with neuroanatomical changes, heart or thyroid defects among others. Virtually every individual with DS develops AD-related neuropathology by

the age of 40 due to the deposition of amyloid-β(Aβ) in neuritic plaques and neurofibrillary tangles in the brain [18,19].

Even though the clinical manifestations were already detailed in 1866 by the physician John Langdon Down [20], the presence of an extra copy of HSA21 was not described until 1959 by Jérôme Lejeune and Marthe Gauthier [21]. Although the genetic cause of DS has been known for several years, the cellular and molecular mechanisms that lead to the wide range of phenotypes observed in individuals with DS are not completely understood. ID is the most prevalent and limiting feature of individuals with DS and negatively influences their independence and quality of life. Individuals with DS also present higher prevalence of neurological, psychiatric disorders and age-related comorbidities when compared to the general population.

Neuroanatomical alterations in cognitive-related brain regions in DS

Cognitive deficits of individuals with DS arise during neurodevelopment and are possibly related to several alterations in the DS brains. In DS individuals, the volume of the brain is reduced, beginning at early developmental stages, and in adults, the reduction in size reaches approximately 20%. Particular brain areas that are related with cognitive processes such as the prefrontal cortex, entorhinal, frontal, prefrontal, and temporal cortices, hippocampus and cerebellum are reduced in volume in individuals with DS [22–25]. Reduced volumes have also been reported in the amygdala, cerebellum, brain stem nuclei, and mammillary bodies of the hypothalamus in children and adults with DS. Along with neuroanatomical changes, several brain regions exhibit anomalies in their connectivity and functionality [26–28].

Remarkably, the proliferation of neural progenitor cells have been reported to be reduced in DS fetuses [29–32] while apoptosis is increased [30], so that neuron number is reduced in late gestation (after weeks 19–23). The number of neurons in the neocortex, hippocampus, parahippocampal gyrus and cerebellum is reduced in fetuses, and newborns with DS, and hypocellularity persists to adulthood in different areas of the brain [33–36]. Therefore, reduced brain

volumes and decreased neuronal number would be in part explained by defects in neurogenesis during neurodevelopment [31,32,37,38]. Moreover, DS fetuses showed fewer cells expressing neuronal markers and a similar number of astrocytes compared to euploid fetuses [39].

Preclinical mouse models of DS have recapitulated some of the alterations found in humans with DS. The brain volume of Ts65Dn, Ts1Cje, and Ts2Cje, Ms1Rhr, and Ts1Rhr mice is reduced during the embryonic period, but not after birth or during adulthood. Thus, most DS mouse models do not show changes in total brain volume during adulthood. Similar to individuals with DS, the Ts65Dn mouse model of DS presents impaired functional connectivity between the prefrontal cortex and the hippocampus [40]. As in humans, the hippocampus and the cerebellum appear to be the most affected structures in Ts65Dn, with the hippocampal granule cell layer and hilus showing reduced volume [41]. Instead, the hippocampal area is not reduced in Ts1Cje mice [42], and the Ts1Rhr mice show greater volume of the posterior hippocampus [43].

A reduction in the number of neurons has been observed in the hippocampus and cerebral cortex of different mouse models of DS [41,44]. Ts65Dn mice show reduced cell density during prenatal (E18.5) and early postnatal stages in the neocortex (P8) [45], and in the hippocampal DG [32], while in Ts1Cje mice, the thickness of the granule cell layer and molecular layer of the DG is not affected [42]. As expected from the reduced cerebellar volume of DS and trisomic mice, the cerebellum of Ts65Dn [46] Ts1Cje, Ms1Rs65, and Tc1 mice present a lower number of granule and Purkinje cells from early postnatal stages to adulthood [47]. Impaired neurogenesis was also found in different mouse models of DS [48–50]. In Ts65Dn mice, reduced neural precursor proliferation is found in the neocortical ventricular zone (VZ) during embryonic stages [45]. Neuronal architecture is also affected with a reduction in the dendritic arborization complexity together with decreased numbers of mature spines in different brain regions such as cortex [51] and hippocampus [52,53].

Candidate molecular mechanisms in DS

Two main mechanisms have been postulated to explain the molecular changes that contribute to DS phenotypic manifestations. First, increased dosage of individual HSA21 genes may have an effect on certain downstream pathways, resulting in the DS clinical manifestations. This first postulate is contributed by studies in mouse models overexpressing single dosage sensitive genes such as Dual specificity tyrosine-phosphorylation-regulated kinase 1A (*DYRK1A*) [54–56] or superoxide dismutase 1 (SOD1) [57,58] that replicate part of the DS phenotypes. Another example is the triplication of *APP*, a gene on HSA21 that encodes for amyloid precursor protein (APP) that explains why people with DS are more susceptible to early-onset Alzheimer's disease (AD) [59–61]. The second mechanism would be that the additional copy of HSA21 genes might disrupt molecular homeostasis by affecting the regulation of transcription across the genome. Indeed, HSA21 trisomy not only causes the overexpression of HSA21-encoded genes, it also causes a broad transcriptome disruption in a plethora of genes located in different chromosomes. In both scenarios, the resulting transcriptomic deregulation in the brain may affect cognition and possibly engram formation.

Engram related alterations in DS

Research on engram formation, maintenance and recall have underscored the importance of several molecular and cellular mechanisms. Our laboratory and others have provided several lines of evidence that suggest that DS is a model of defective engrams (Figure i). First, we found that the levels of phosphorylated CREB, a transcription factor directly regulating processes of memory consolidation and recruitment of neuronal ensembles to an engram [9], are reduced in Ts65Dn mice [62]. Similarly, Sierra et al. showed reduced levels of Arc, an immediate early gene (IEG), in the hippocampus right after a novel object recognition test (NORT), when compared to WT littermates [63]. Reduced excitability has also been described as an important factor in engram allocation

[9,64] and reactivation [13], and in DS there is overexpression of *KCNJ6* [65,66], the gene encoding for Kir3.2 (also named Girk2, the G protein-activated inward rectifier potassium channel 2), which probably leads to reduced excitability as shown in the Ts65Dn cortex [55] and hippocampus [67]. A more direct clue about engram alterations arise from the work of Smith-Hicks et al. who described that neuronal activation in the CA1 hippocampal region, an area important for the encoding and retrieval of contextual memories, during the exploration of novel environments is sparser in Ts65Dn mice [68]. Finally, deficits in dendritic spine density have also been extensively described in Ts65Dn mice [52,53,69] and in fetuses with DS [70–72], indicating deficits in structural plasticity, a mechanism related to engram stability. Other studies have also shown deficits in several forms of synaptic plasticity that are important for memory consolidation and engram consolidation such as deficits in long-term potentiation (LTP) [73–75] and exacerbated long-term depression (LTD) [76]. Altogether, all that evidence supports the notion that DS is a model of defective engrams.

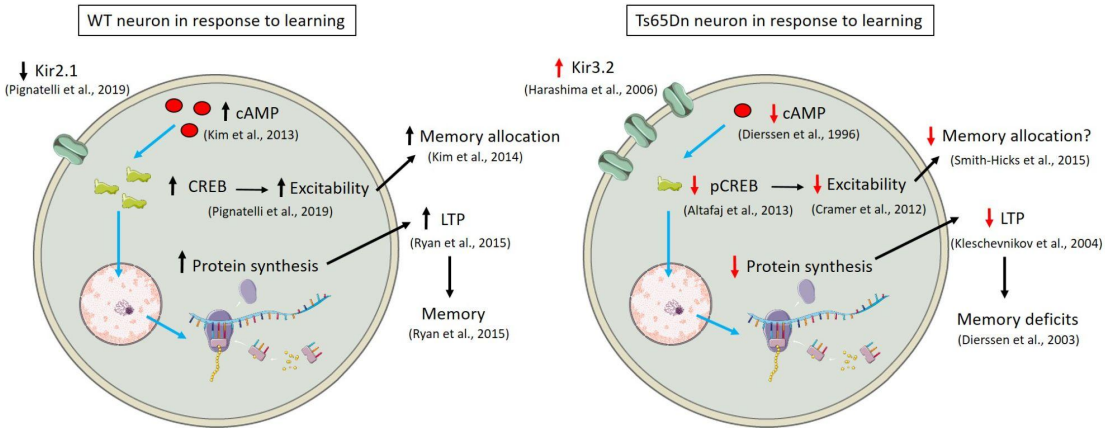

Figure i. The engram scenario in DS. Left panel: Proposed engram allocation and reactivation mechanisms. **Right panel:** Hypothesized scenario in DS.

Astrocyte involvement in memory function

The role of astrocytes has traditionally been limited to maintain brain homeostasis and provide metabolic and structural support to neurons, it has been recently shown that astrocytes play a role in synaptic physiology because they express a large number of functional neurotransmitter receptors that allow them to respond to a wide variety of neurotransmitters [77,78]. G-protein coupled receptors (GPCRs) are activated by neurotransmitters and are primarily responsible for neuronal to astrocyte communication. GPCRs and, specifically Gq GPCRs, are involved in the Ca^{2+} mobilization from internal stores through the activation of the canonical phospholipase C (PLC) pathway. Upon Gq GPCR activation, the membrane lipid phosphatidylinositol 4,5 bisphosphate (PIP_2) is hydrolyzed by Gq GPCR activation to generate diacylglycerol (DAG) and IP_3. IP_3 triggers Ca^{2+} release by binding to IP_3R in the endoplasmic reticulum (ER). This process leads to the release of several neurotransmitters and neuromodulators, such as glutamate, gamma-aminobutyric acid (GABA), ATP/adenosine and D-serine to the synaptic cleft by astrocytes in a Ca^{2+}-dependent manner [79–81]. This activity, known as gliotransmission, has received a lot of attention because it affects synaptic physiology in the short and long-term [79,82,83]. As a result, it is commonly believed that astrocytes constitute an essential component of the synapse (tripartite synapse [84]) that shapes synaptic transmission in the brain in tandem with neurons. The mechanisms by which astrocytes mediate these structural and functional responses, on the other hand, have been a hot topic of discussion [85–87].

The bidirectional connection between neurons and astrocytes is critical for neural plasticity [82,88] and, more particularly, for memory function [82,88–90]. Recently, genetic methods such as chemogenetics and optogenetics have made it feasible to selectively regulate astrocyte activity in the brain.

Transgenic mice overexpressing S100β provided one of the first pieces of evidence suggesting the astrocyte participation in memory given that the elevation of S100β mRNA and protein levels in astrocytes resulted in reduced LTP and increased LTD in hippocampal pyramidal neurons [91]. The Morris water

maze test (MWM), a hippocampal-dependent task, was significantly impaired as a result of S100β upregulation in astrocytes [91]. Contrarily, S100β-null mice displayed increased LTP and spatial memory in the MWM and in contextual fear conditioning [92]. S100β exhibits Ca^{2+} binding capabilities that lower extracellular Ca^{2+} levels and alter neuronal firing patterns [93]. S100β overexpression also influences neuronal excitability [94]. S100β has concentration-dependent effects: low concentrations protect the brain and promote central nervous system development and maturation [95] whereas high S100β concentrations are toxic, promote proinflammatory responses [96] and have negative consequences for neurons, including apoptotic cell death [97].

Recent investigations that modulated astroglial activity in a more mechanistic and time-constrained manner have shown that astrocytes play a role in memory function [82,88–90]. Transgenic animals that permitted the selective expression of tetanus toxin (TeNT1) in astrocytes had their Ca^{2+}-dependent neurotransmitter release abolished and their gamma oscillations, important for attention and learning [98], in the hippocampus *in vivo* [90]. TeNT expression caused a temporary blockade of astrocyte vesicular release, which resulted in a lower recognition memory. This work effectively illustrated in a mechanistic manner that gliotransmission is required for specific forms of memory, and it established the astrocyte as a sophisticated actor in memory function. It did, however, leave a few questions unanswered.

Part of these were answered in a recent work in which astrocytes in the CA1 area of the hippocampus were selectively activated during memory acquisition using chemogenetics (hM3Dq) or optogenetics (OptoGq) expressed under de glial fibrillary acidic protein (GFAP) before (but not after) learning [82]. By activating astrocytes before learning, fear conditioning (FC) memory was enhanced and an increase in the recruitment of activated neurons during memory acquisition was detected. This would imply that in this particular brain area, more neurons support this memory. Although this research implies that astrocyte activation is necessary for memory acquisition, it does not establish that astrocytes are active during memory processes under physiological circumstances in the brain.

The same research group found that activating the Gi pathway in astrocytes prior to learning reduced remote (but not recent) memory recall [89]. In the brain, Gi GPCRs play an important role in signal transduction [99]. In astrocytes, however, they have the complete opposite effect, raising intracellular Ca^{2+} levels and boosting glutamate release [100]. Because the activation and recruitment of cortical areas such as the anterior cingulate cortex (ACC) is required for recent-to-remote memory transition [101–103], the authors used the GFAP-hM4D(Gi) designer receptor to activate the Gi pathway in CA1 astrocytes. Even though both the CA1 and the ACC are involved in recent and remote memories, the activation of the Gi pathway in astrocytes by clozapine N-oxide (CNO), a hM4Di agonist, hindered neuronal activity (as measured by c-Fos+ neurons) in the ACC but not in the CA1. This implies that astrocytes affect functional connectivity between neurons in a projection-specific fashion. As a result, CA1 astrocytes would discriminate between different CA1 pyramidal neurons based on their projection target and control their activity differentially. It is worth noting that manipulating astrocyte activity using designer drugs during memory recall had no effect on memory performance, suggesting that astrocyte activity is required for memory acquisition but not for recent or remote memory recall [82,89].

Considering the involvement of astrocytes in synaptic transmission and memory function, only few studies have addressed whether astrocyte dysfunction can contribute to circuit and memory alteration in different brain disorders.

New players in Down syndrome engram research

Numerous glial genes are shown to be misregulated in neurodevelopmental disorders, suggesting that astrocytes might be involved in the pathogenesis of multiple cognitive disorders [104,105]. These genes encode proteins that have key roles in the brain, including neuronal differentiation, cell cycle progression, and neural injury repair. In various brain disorders, different degrees of astrocyte reactivity (or astrogliosis) are detected [106–108]. In addition, astrocytes exhibit abnormal structure [107,108] and physiology [94], both of which have been linked to synaptic deficits and changes in neuronal excitability [94], as well as neuronal

survival [109,110]. Astrogliosis describes alterations in the molecular, cellular and functional levels that occur as a result of brain trauma or genetic brain disorders [111]. Astrogliosis is characterized by morphological and physiological changes in the astrocytes, such as an increase in their number and size, as well as changes in the expression of astroglial proteins (GFAP and S100β [111]). Although upon an insult astrogliosis promotes an adaptive state that aids in dealing with the source of the brain insult (infection, hemorrhage, genetic perturbation, etc.), removing toxic debris, and promoting neuronal survival [111–113], in cognitive diseases such as DS, FXS, and AD they are in a chronic "reactive state" (or aberrant astrogliosis), a continuous malfunctioning mode that might be maladaptive and contribute to the advancement of neurodegeneration in these brain disorders [107,114]. In DS, the number of astrocytes is increased [107,114,115]. Astrocytes are more numerous, larger, and express increased levels of astroglial markers (S100β, GFAP). In the hippocampus, DS fetuses have a greater fraction of cells with an astrocytic phenotype [30], indicating a transition from neurogenesis to gliogenesis. The neurogenic-to-gliogenic switch was confirmed in induced pluripotent stem cells (iPSCs) from monozygotic twins discordant for trisomy 21, where increased expression of GFAP, S100β, and Vimentin indicated a shift towards the astroglial phenotype in DS-iPSC-derived cells [116]. Although the studies of astroglia in animal models of DS are more limited, hypertrophy, higher number of astrocytes and higher expression of GFAP have been reported in Ts65Dn mice [117].

HSA21 genes, such as *DYRK1A*, may play a role in inducing precocious astrogliogenesis by activating the astrogliogenic transcription factor signal transducer and activator of transcription (STAT), which then switches the neural progenitor fate to the astroglial phenotype [118].

Astrocytosis persists throughout life in people with DS, and is accompanied by an immature astroglial phenotype [119]. Furthermore, as evidenced by a more frequent spontaneous Ca^{2+} oscillations in DS astrocytes, astroglial physiology is also altered [94]. Because intracellular Ca^{2+} transients in astrocytes promote the release of gliotransmitters, this increased Ca^{2+} oscillations might have an influence on neuronal function in DS. In fact, astrocytes produced from DS-iPSCs

showed enhanced Ca^{2+} activity, which was proven to lower the excitability of co-cultured neurons [94]. S100β overexpression was implicated in this rise in Ca^{2+} oscillations, as normalizing S100β expression returned Ca^{2+} activity to normal levels [94]. There are few studies focusing on astrocyte pathology in DS, and even fewer have looked into the processes through which astrocytes may contribute to synaptic abnormalities in DS. Among them, co-cultures of rat hippocampal neurons on top of human DS astrocytes resulted in lower TSP-1 levels, resulting in fewer neuron spines and more immature (filopodia) spines than neurons cultured with control astrocytes [120,121] (Figure ii). Exploring the pathways that lead to astrocyte–synapse interactions might thus give new insights into how astrocyte dysfunction contributes to memory impairment in DS.

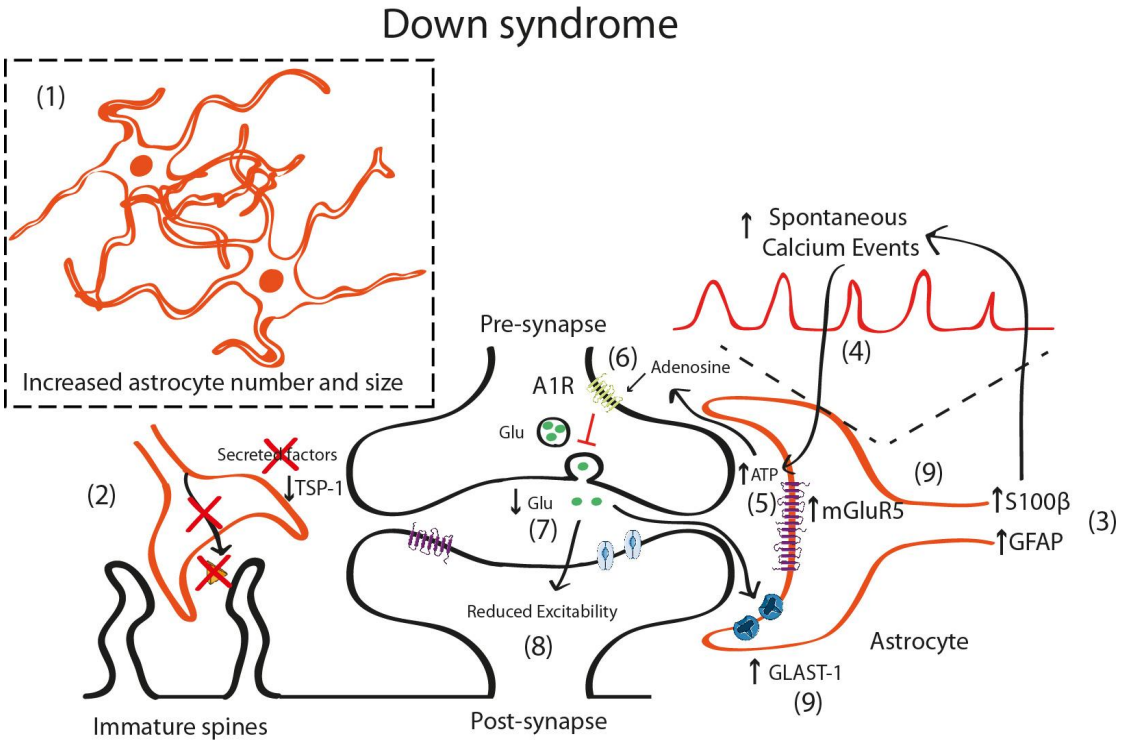

Figure ii: Schematic representation illustrating the astrocyte-synapse alterations in DS. (1) Astrocyte number and volume is increased in DS. **(2)** Reduced astrocyte secreted TSP-1 prevents spine maturation resulting in more frequent filopodia (immature) spines. **(3)** Increased S100β and GFAP expression has been described in astrocytes. S100β upregulation has been linked with increased astrocyte Ca^{2+} oscillations **(4)**. Increased astrocyte activity leads to adenosine triphosphate (ATP) release to the synaptic cleft **(5)** that is hydrolyzed to adenosine and activates A1 adenosine receptors (A_1R) **(6)**. A_1R activation prevents glutamate release from the presynaptic terminal and, consequently **(7)** depresses synaptic transmission **(8)**. Even though $mGluR_5$ is upregulated in astrocytes (and probably in neurons), no mechanistic studies have been performed

to uncover the contribution of $mGluR_5$ to DS pathophysiology. **(9)** Reduced glutamate concentrations can be contributed by increased expression of the glutamate transporter GLAST-1 that leads to increased astroglial glutamate uptake. (Figure from Fernández-Blanco et al., 2020 [122]).

Using mouse models to study Down syndrome

The understanding of molecular genetics in DS research would not have been possible without the development of animal models of DS. Even though DS mouse models have the limitation that DS is a human condition and cannot be replicated in other species, these mouse models of DS have provided extensive lines of evidence to better understand the complexity that arises from the gene regulation caused by the triplication of the HSA21.

Remarkably, among the 552 genes located in the long arm of the HSA21, only 166 are syntenically conserved in three principal regions of the mouse genome that are located on mouse chromosome 10 (Mmu10), Mmu16 and Mmu17 [123]. Due to the genetic differences in the distribution of genes in the murine chromosomes, creating animal models to investigate DS has been a challenging task. However, based on these homologies, a high number of mouse models of DS have been constructed (Figure iii). Some carry an additional copy of a chromosome segment orthologous to HSA21. Others present extra copies of HSA21 human genes, or their mouse orthologs or the full human HSA21. In this Thesis, we have focused on the Ts65Dn mouse model.

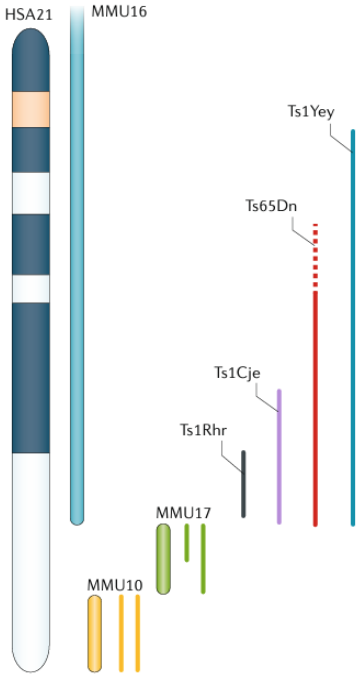

Figure iii. Representation of HSA21 and murine homologous components. Left: HSA21 genomic areas correspond to murine chromosomes 10, 16 and 17. Right: representation of the triplicated regions found in DS mouse models. (Adapted from Antonarakis et al., 2020 [124]).

Ts(17^{16})65Dn or Ts65Dn was the first viable trisomic mouse model of DS [125]. It was constructed from the Robertsonian translocation of the distal region of Mmu16 onto the Mmu17 centromere. This region of about 10 Mb comprises approximately 90 conserved protein-coding HSA21 gene orthologs [126], being trisomic for about two-thirds of the genes orthologous to HSA21. However it also contains 46 triplicated genes that are not syntenic to HSA21 [127]. Thus, this model does not present a perfect construct validity. Even so, Ts65Dn mice present high face-validity since it recapitulates many of the DS relevant phenotypes including craniofacial dysmorphology [128], neuroanatomic alterations and cognitive, motor and social deficits [129,130]. For this reason, Ts65Dn has been extensively used for testing new pharmacological interventions. At the neuroanatomical level, Ts65Dn mice present alterations at different macroscopic and microscopic levels as described above, showing better face validity than other DS mouse models that do not present changes in neuronal density, neuronal proliferation or brain volumes (see above). Ts65Dn mice also display learning defects in a broad span of cognitive tests.

Hippocampal-dependent tasks have been reported to be impaired including deficits in contextual-fear conditioning [73], NORT [74], MWM [129], Radial arm maze [131], Barnes maze [132] have been described. Working memory deficits such as in the spontaneous alternation task, have been also reported [133].

Regarding predictive validity, few therapies coming from preclinical investigations using different DS mouse models have failed to show efficacy in humans, questioning the credibility of mouse models. However, some examples such as epigallocatechin-3-gallate (EGCG), a green tea extract, as a potential pro-cognitive therapy, have demonstrated that Ts65Dn mice have predictive validity [134,135]. Similarly, results in Ts65Dn mice and in patients were published in 2022 in relation to the gonadotropin-releasing hormone (GnRH) [136]. Besides Ts65Dn, other segmental trisomic mouse models have been developed bearing different segments of Mmu16, 17 and 10 such as Tc1, Dp(16)1Yey and Ts66Yah. However, it is noteworthy to mention that even though these models show better construct validity than Ts65Dn, and present some of the DS-relevant phenotypes, none of them shows the high face-validity of Ts65Dn. This might be due to the presence of an extra freely segregating chromosome. In fact, an extra chromosome causes trisomic cells in DS and Ts65Dn to proliferate more slowly and have a longer cell cycle, which could have a significant impact on development [32].

The impact of possible dosage-sensitive genes have been studied using transgenic animals that overexpress a single gene. Transgenic mice models for *Dyrk1A* have indicated that this dosage-sensitive gene plays a central role in DS-related brain abnormalities [137], suggesting that its overexpression might be sufficient to produce some of the brain phenotypes in DS.

Taking into consideration not only the face-validity and the predictive-validity of Ts65Dn mice, but also that most of the more complete trisomic models were not available at the time of initiation of this Thesis, or present other problems such as increased prevalence of hydrocephalus [138] or increased perinatal mortality [139], and that the alterations in the mechanisms that are fundamental for engram formation and reactivation were found in Ts65Dn, we decided to use this model to study engram pathology in DS.

HYPOTHESIS AND OBJECTIVES

HYPOTHESIS AND OBJECTIVES

The etiology and pathophysiology of cognitive dysfunction in DS is exceedingly complex, with multiple cellular and molecular pathways and a number of HSA21 candidate genes that may contribute to learning and memory impairment. Studies until now have addressed alterations in basic neural functions, such as synaptic transmission, biochemical aspects, ion channel malfunction, or synaptic plasticity in the cerebral cortex and the hippocampus. However, in the last decades the conceptualization of memory has dramatically changed, incorporating new aspects, such as memory storage related to small assemblies of neurons, called engrams. Technological and conceptual advances in neuroscience have made it feasible to identify and manipulate these neurological correlates of memory, resulting in the concept of memory engrams, which are hypothetical storage places for acquired information in the brain. However, even though engrams are now widely regarded as the primary mechanism of memory consolidation, there is limited, yet compelling, evidence that engrams might be disrupted in cognitive disorders. Although DS is the most common form of genetic intellectual disability, the engram-specific alterations have not been examined.

In this Thesis, we have investigated in a DS mouse model, Ts65Dn, the engram formation and reactivation in the hippocampus, a critical region for memory formation and consolidation that is notably perturbed in DS, and the contribution of astrocytes to engram pathology.

Hypothesis

We propose that defective engram neuronal ensembles in DS would be unable to encode and reactivate memories adequately and would contribute to memory impairment. Engram disturbance would be explained by intrinsic deficits in excitatory neurons but also by changes in function and structure of trisomic astrocytes.

Objectives

To prove the hypothesis above, the specific aims of this Thesis are:

1. To identify the memory engram alterations in the Ts65Dn hippocampus.
2. To study the changes in engram formation/reactivation using engram tagging and manipulation techniques
3. To investigate whether astrocyte dysfunction is responsible for hippocampal circuit alterations and memory deficits in Ts65Dn mice.
4. To propose and test engram-specific therapies.

CHAPTER I. DEFECTIVE ENGRAMS AS A CELLULAR MECHANISM OF COGNITIVE IMPAIRMENT IN DOWN SYNDROME

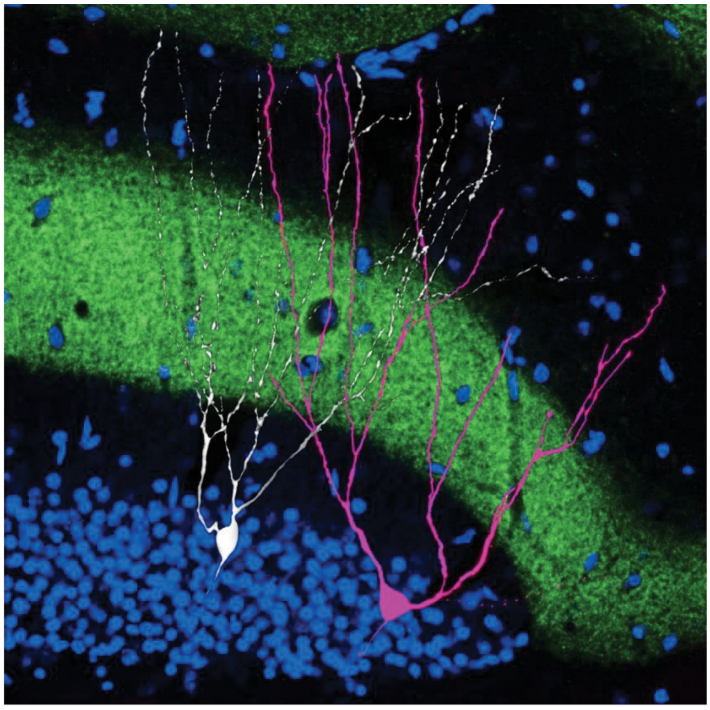

Image showing non-engram (white) and engram cell (purple) located in the upper blade of the granule cell layer of the hippocampus, depicted in blue (DAPI). Dendrites of these cells penetrate into the axons of the perforant path (green). Adapted from T. J. Ryan et al., Science ***348****, 1007 (2015)* [4].

Introduction

Down syndrome is the most common genetic cause of intellectual disability and results from the presence of an extra copy or major portion of the HSA21. Several pathophysiological changes in the brain of individuals with DS have been associated with intellectual disability including reduced volume and cellularity of different brain regions [31,140–142], reduced gray matter density and atypical connectivity patterns [40], among others. Hippocampal-dependent memory functions such as short-term and working memory are particularly affected in individuals with DS [135,143]. Even though research on animal models of DS have revealed extensive cellular and molecular mechanisms that might contribute to memory deficits, studies on learning and memory have relied on basic neural functions, such as synaptic transmission, biochemical aspects, ionic channel malfunction, or synaptic plasticity.

Recently, new molecular and genetic methods such as activity-dependent tagging along with chemo- and optogenetics have provided unprecedented opportunities to visualize and manipulate the neural correlates of memory [3,5]. With these new techniques, different research groups have demonstrated that a sparse assembly of neurons that activate at the time of contextual fear-conditioning (CFC) training are sufficient and necessary for subsequent memory retrieval [3,4,9]. These neurons, called engram cells, are thought to be the neural correlates of memory. Engram cells activate during learning and undergo molecular and structural changes that enable them to reactivate by recall cues [4,13]. Engrams have been extensively studied in the hippocampus [3,4,6,13], which is considered an essential region for the consolidation of short-term memories into stable long-term memories [144–146], and is mostly affected in DS.

Research on engram formation, maintenance and recall has uncovered several mechanisms and processes that are of paramount importance for memory function. Even so, only few studies have examined how engrams might be altered in cognitive disorders that are associated with memory deficits [6,14,15]. As a matter of fact, most of the critical mechanisms that contribute to adequate engram

formation and recall are altered in mouse models of DS. For instance, plasticity deficits including impaired hippocampal LTP [73,75], increased synaptic depression [76] and deficits in structural plasticity [52,53] have been widely described in Ts65Dn. Moreover, the excitatory/inhibitory balance, which is indispensable for engram formation, has been described to be altered in Ts65Dn mice and is thought to contribute to DS cognitive deficits [75,147,148]. Upregulation of CREB levels is one of the mechanisms that are described to enhance neuronal excitability at the time of memory acquisition and its active form (p-CREB) was described to be less abundant in the Ts65Dn hippocampus [62]. Similarly, it was found that *Kcnj6*, a gene that encodes for Kir3.2, an inwardly rectifying potassium channel, is triplicated in DS and on Ts65Dn and there is a 1.5-fold increase in the expression in the Ts65Dn hippocampus. The upregulation of this gene has been associated with decreased excitability and is sufficient to impair both synaptic plasticity and memory [65]. Decreased neuronal activation was reported in the CA1 region of Ts65Dn region during the exploration of novel environments [68]. Similarly, it was recently described a reduction of Arc expression in the hippocampus right after a NORT, when compared to wild type (WT) littermates [63]. Altogether, this body of mounting evidence supports that engrams are probably defective in DS.

Here, we have explored whether engrams can form and reactivate in the Ts65Dn hippocampus, a trisomic mouse model of DS. The hippocampus plays a critical role in the establishment of the contextual component of fear memories [149,150]. Specifically, the DG is involved in the discrimination between similar contexts [151]. The hippocampus of both in individuals with DS [22,23] and in mouse models of DS [44] is one of the most affected brain regions and hippocampal-dependent memories are impaired [73,74]. For this reason, we have tagged and manipulated engram cells and delineated the trisomic engram-specific alterations in the dorsal DG. Then, we have tested several strategies to revert engram-specific alterations to recover memory alterations in Ts65Dn mice.

Methods

Animals

Ts(17^{16})65Dn (Ts65Dn) mice were obtained through crossings of a B6EiC3Sn a/A-Ts (17^{16})65Dn (Ts65Dn) female to B6C3F1/J males purchased from The Jackson Laboratory (Bar Harbor, USA). Genotyping was performed by amplifying genomic DNA obtained from the mice tail as described in (Liu et al., 2003). Mice had access to food and water *ad libitum* in controlled laboratory conditions with temperature maintained at 22 ± 1ºC and humidity at 55 ± 10% on a 12h light/dark cycle (lights off 20:00 h). Mice were socially housed in numbers of two to four littermates. The colony of Ts65Dn mice was maintained in the Animal Facilities in the Barcelona Biomedical Research Park (PRBB, Barcelona, Spain).

According to Directive 63/2010 and Member States' implementation of it, all trials followed the "Three Rs" principle of replacement, reduction, and refinement. The investigation was conducted in accordance with the Standards for Use of Laboratory Animals No. A5388-01 (NIH) and local (Law 32/2007) and European regulations as well as MDS 0040P2 and the Ethics Committee of Parc de Recerca Biomèdica (Comité Ético de Experimentación Animal del PRBB (CEEA-PRBB)). A/ES/05/I-13 and A/ES/05/14 grant the CRG permission to work with genetically modified organisms. See the Ethics section for further information.

Experimental strategy

We have investigated engram-specific alterations using engram tagging techniques and chemogenetic intervention in Ts65Dn. In the first experiments using immunostaining and recombinant AAV_9-TRE-tight-hM3Dq-mCherry, we characterized neuronal activation pattern in Ts65Dn in 3 month old male mice both after learning and after recall. We quantified the number of cells expressing c-Fos and Arc IEGs in the dentate gyrus. For the behavioral experiments, all mice, unless otherwise specified, were males aged 10-12 weeks at the time of learning. For engram tagging and manipulation and CREB overexpression experiments, males were aged 8-10 weeks at the time of virus injection. For engram tagging experiments, mice treated with food containing 40 mg/kg

doxycycline (DOX) at least 7 days before the surgery. After surgery, mice remained on DOX except for the engram tagging time window. For *ex vivo* whole-cell patch clamp electrophysiology experiments mice were 11-13 weeks old at the time of the experiment. Engram tagging and manipulation was performed using chemogenetic intervention with clozapine N-oxide (CNO) to determine whether the trisomic engram was not properly formed, or not properly reactivated. We also evaluated whether EMD-173 treatment was effective to recover memory deficits in Ts65Dn mice (Figure 1).

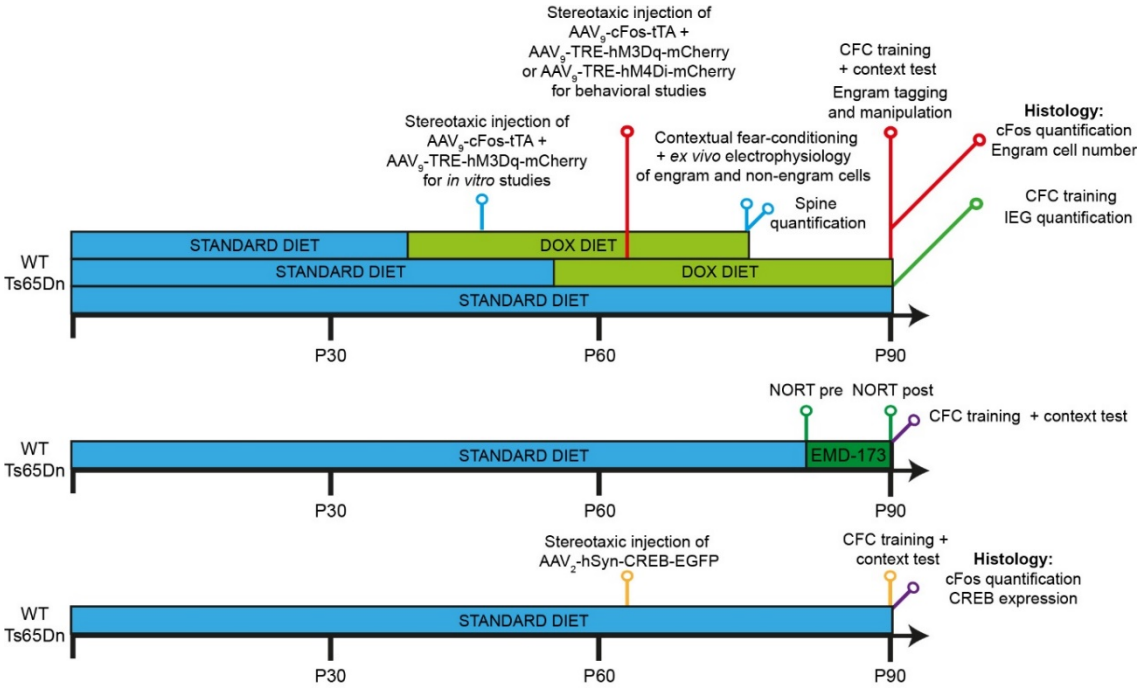

Figure 1. Overview of the experimental strategy.

Engram tagging and manipulation techniques

Viral constructs

In order to detect and to manipulate memory engram cells, we used a construct in which the excitatory DREADD hM3D(Gq) or the inhibitory DREADD hM4D(Gi) were fused to mCherry under the control of the tetracycline-responsive element (AAV_9-TRE-tight-hM3D(Gq)-mCherry). To allow the combination with AAV_9-cFos-tTA into the targeted zone, the dorsal DG, we used a double viral system.

For engram activation we combined (1:2) AAV_9-TRE-tight-hM3D(Gq)-mCherry and AAV_9-cFos-tTA. For engram inactivation we combined (1:2) AAV_9-TRE-tight-hM4D(Gi)-mCherry (diluted 1:5 in PBS) and AAV_9-cFos-tTA. pAAV-cFos-tTA-pA and pAAV-PTRE-tight-hM3Dq-mCherry were a gift from William Wisden (Addgene plasmid #66794 and #66795). AAV vectors were serotyped with AAV_9 coat proteins and packaged at the Viral Production Unit (UPV) at the Universitat Autònoma de Barcelona . Viral titers were 1.6 x 10^{13} genome copy (GC)/mL for AAV_9-cFos-tTA and AAV_9-TREtight-hM3Dq-mCherry. AAV_9-TREtight-hM4Di-mCherry was generated by replacing the hM3Dq-mCherry of #66795 for hM4Di-mCherry from #50479 (Addgene plasmid, gift from Bryan Roth). Viral titer was 1 x 10^{13} genome copy (GC)/ mL. AAV_2-hSyn-CREB-EGFP was constructed by substituting the CMV promoter for the hSyn from the AAV-CREB (Addgene plasmid #68550; gift from Eric Nestler), serotyped with AAV_2 coat proteins and packaged at Viral Production Unit at the UPV. Viral titer was 8 x 10^{12} genome copy (GC)/ mL for AAV_2-hSyn-CREB-EGFP.

Pharmacogenetics (DREADD)

For the inhibition or reactivation of the DREADDS we used CNO, an inactive form of clozapine drug. The synthetic ligand CNO binds to the modified human muscarinic receptor hM3D(Gq) or hM4D(Gi). CNO was dissolved in DMSO and diluted in 0.9% saline to yield a final DMSO concentration of 0.5%. Control animals received 0.5% DMSO saline solutions. For engram activation studies, 1 mg/kg CNO was intraperitoneally injected 30 min before the behavioral assays. For engram inactivation experiment, 3 mg/kg CNO dose was used. None of the doses of CNO induced any behavioral alterations or signs of seizure activity.

Stereotaxic surgery injection

Intracerebral injections in DG were performed bilaterally at Bregma -2.2 mm AP, ± 1.3 mm ML, -1.9 mm DV with the aid of a stereotaxic apparatus (Stoelting 51730). 8-10 weeks old male mice were anesthetized using ketamidol (7.5 mg/kg) and medetomidin (0.2 mg/kg). Fur was shaved from the incision site. Skin was wiped with ethanol 70% and small incisions were made along the midline to expose bregma and injection sites. Craniotomies were performed using a 0.45

mm diameter stereotaxic microdrill (RWD Life Science, model 78001). 150 nl of each virus (1:2) were injected per hemisphere at a rate of injection of 50 nl/min during 6 min through a 33-gauge cannula (Plastics One, C235I/Spc) attached to a Hamilton microsyringe (1701N; Hamilton) connected to a syringe pump (PHD 2000, Harvard Apparatus). Cannulas remained 10 min after injection to allow virus diffusion and were slowly withdrawn during 5 min. Skin was sutured and mice were treated with 0.03 mg/kg buprenorphine as analgesic. Mice were recovered from anesthesia by atipemazol (1 mg/kg) and maintained on a heating pad until fully recovered. Mice were allowed to recover for 3 weeks before experimentation to allow construct expression. After sacrifice, all injection sites were verified histologically. Only those mice in which virus expression was restricted to the dorsal DG were included in the analyses.

Behavioral assays

Contextual fear-conditioning (CFC) paradigm

CFC is a hippocampal-dependent test used to interrogate associative learning and to study engram formation and reactivation. Importantly fear memory is altered in trisomic mice. We adapted a training paradigm for contextual fear-conditioning (3 shocks; 0.6 mA, separated by 60 s) used in previous activity-dependent tagging studies (Figure 1A) [3,4]. Briefly, mice are introduced into a new environment and an aversive stimulus is delivered at different time points. The next day mice are reexposed to the same context without any shocks delivered. If mice recall and associate the context to the aversive stimuli, they will typically exhibit a freezing reaction when placed back in that setting. As a reaction to fear, freezing is described as "lack of movement other than breathing."

Two different contexts were employed in two different cages, one neutral not associated with fear-related learning (Context A) and a second one (Context B) that was paired to the unconditioned (shock) stimulus. Context A (neutral) consisted in a chamber (29 X 25 X 22 cm) with Perspex floors and transparent circular ceilings and Context B (30 X 25 X 33 cm) had grid floors, and opaque square ceilings. After each session, the apparatus was cleaned with 70% ethanol.

All mice were individually handled and habituated to the investigator during three days before the experiment. One day before conditioning (training) mice were habituated in Context A for 3 min. No shocks were delivered in this session. Immediately after the habituation, DOX diet was removed and mice switched to a standard diet for a period of 24h, to allow expression of the doxycycline sensitive tetracycline transactivator (tTA) under the control of the c-Fos promoter. After habituation mice were placed back in their home cages in the holding room.

After 24h, mice were trained in Context B during 300 s, with three 0.6 mA shocks of 2s duration delivered at 120 s, 180 s and 240 s, respectively [4]. After training, DOX diet administration was reestablished to restrict the expression of the construct to the learning period. After training mice were placed back to their home cages.

All testing sessions in Context B were 180 s in duration. Testing conditions were identical to training conditioning, except that no shocks were delivered. At the end of each session mice were placed in their home cages. Freezing behavior (>800 ms immobility) was automatically detected by Packwin 2.0 software (Panlab, Harvard Apparatus). Cages were calibrated according to manufacturer instructions each day of experiment.

Novel object recognition test (NORT)

The novel object recognition test (NORT) is a memory test that has been widely used to investigate the neurobiology of memory. Mice were habituated to a Plexiglas custom-made V-shaped maze for 5 min on day 1. On day two, the time that the mice spent exploring each of the two identical objects (familiar objects) that were placed at the ends of each corridor for nine min was measured. On day three, one of the familiar objects was replaced with one new object (novel object). Discrimination index was calculated as the difference between the time spent exploring the novel object minus the time exploring the familiar object divided by the total exploration time. Exploration of a given object was only considered when the mice nose was oriented towards the object and the distance was less than 2 cm. Mice that explored less than 10 s each object, were excluded from the analysis.

All the behavioral experiments were conducted in 11-13 weeks old male mice during the light cycle (7:30 am to 13:00 pm).

Histology

Immunohistochemistry

In order to quantify IEGs expression either after memory acquisition or memory recall, mice were transcardially perfused with ice-cold PBS followed by 4% paraformaldehyde (PFA) in PBS (pH 7.4). Brains were extracted and post-fixed in 4% PFA at 4ºC overnight. Brains were then transferred to PBS and 40 µm coronal consecutive brain sections were obtained employing a vibratome (Leica VT1200S, Leica Microsystems), collected in PBS and stored in cryoprotective solution (40% PBS, 30%, glycerol and 30% polyethylene glycol) for long-term storage. For immunofluorescence studies, 4-6 sections per mice were selected centered on the injection sites and according to stereotaxic coordinates Bregma, -1.54 to -2.54 mm, (mouse brain atlas; Franklin & Paxinos, 2012) with the aid of a bright-field microscope (Zeiss Cell Observer HS; Zeiss). Brain sections were washed with PBS (3 x 10 min). Then, sections were permeabilized with 0.5 % Triton X-100 in PBS (PBS-T 0.5 %) (3 x 15 min) and blocked with 10% of Normal Goat Serum (NGS) for two h at room temperature (RT). Sections incubated in PBS-T 0.5% and NGS 5 % with the primary antibodies overnight at 4ºC washed again (PBS-T 0.5 % 3x15 min) and incubated with the secondary antibodies (PBS-T 0.5 % + NGS 5 %) for two h at room temperature protected from light. Finally, samples were washed with PBS-T 0.5 % (3x15 min) followed by PBS washing (3x10 min) to remove the detergent and sections were mounted and coverslipped into a pre-cleaned glass slide with Fluoromount-G medium with DAPI (Thermo Fisher Scientific #00-4959-52). c-Fos was stained with rabbit anti-c-Fos (1:1000, Santacruz, #Sc-7202) and visualized with anti-rabbit Alexa-647 (1:500; Thermo Fisher Scientific, #A-21443). Ki-67 was stained with rabbit anti-Ki-67 (1:250; Abcam, #ab15580) and visualized with anti-rabbit Alexa-647 (1:500; Thermo Fisher Scientific, #A-21443). Arc was stained with mouse anti-Arc(C-7) (1:400; Santa Cruz, #sc-17839) and visualized with anti-mouse Alexa-488 (1:500; Thermo Fisher Scientific, #A-11001). CREB was stained with rabbit anti-CREB

(1:1000; Millipore, #06863) and visualized with anti-mouse Alexa-555 (1:500; Thermo Fisher Scientific, #A-32732). Prior to immunostaining, an optimization of the primary antibodies and PBS-T conditions was performed. Serial dilutions of primary antibodies ranging from 1:100 to 1:1000 were prepared while maintaining the secondary antibody concentration constant (1:500). By confocal microscopy, the best primary antibody concentration was selected taking into account the achievement of low background noise and the signal level obtained with the same laser configuration.

Biocytin immunohistochemistry protocol after whole-cell patch clamp recording

To visualize and quantify the dendritic spines of engram and non-engram cells that were subjected to electrophysiological recordings, 300 µm slices were first fixed in 4% PFA for 24h. Brain slices were washed with Tris-Buffered Saline (TBS) (3 x 10 min). Then, sections were permeabilized with 0.3% Triton X-100 in TBS (TBS-T) and blocked with 20% NGS for 1 h at RT. Then slices were incubated with Streptavidin, Alexa Fluor 488 conjugate (1:1000, Thermo Fisher; #S32357) in 0.3% TBS-T with 1% NGS overnight at 4ºC. Samples were washed with TBS (3 x 10 min) and sections were mounted and coverslipped intro pre-cleaned glass slice with Fluoromount-G medium with DAPI (Thermo Fisher Scientific #00-4959-52).

Cell counting

In order to quantify the number of engram cells in the DG (c-Fos and hM3D(Gq)-mCherry-expressing cells), 40 µm coronal sections were taken from the dorsal hippocampus centered in the coordinates where the viruses were injected (-1,54 to -2,54 mm AP; relative to bregma). Cell densities are expressed as cells/mm^2. Confocal fluorescence images were acquired on a Leica TCS SP5 inverted scanning laser microscope using a 20x/0.70 NA objective. Cell counting was performed using the Cell Counter plugin on ImageJ software (NIH, Bethesda) in a z-stack (3 µm step size). The somatic layer of the granule cell layer was selected as region of interest (ROI) and was manually delineated according to the DAPI signal in every section.

Alexa 488 and Alexa 568 channels were filtered and combined to produce composite images. Equal cutoff thresholds were applied to remove signal background from images. The number of double positive (hM3Dq-mCherry and c-Fos) and single positive (c-Fos) cells were counted in the DG in 3-6 consecutive coronal sections (spaced 200 µm between them) per mouse. The same procedure was used to quantify c-Fos, Arc, and Ki-67, the only difference being the channels used to create composite images. Data was analyzed using R studio. Imaging and quantifications were performed blind to experimental conditions.

Spine density analysis

Engram cells were labeled by the c-Fos-tTA-driven induction of hM3Dq–mCherry (see Viral Construct section). mCherry-expressing (engram) and mCherry non-expressing (non-engram) cells both in WT and in Ts65Dn DG cells were labeled with biocytin during whole-cell patch clamp recordings. Slices were fixed in 4% PFA for 24 h and immunofluorescence protocol against biocytin was performed. mCherry signal was also amplified using immunohistochemistry procedures. Fluorescence Z-stacks of dendritic spines were taken by confocal microscopy (Leica SP5 inverted, Leica Microsystems), using 63x glycerol immersion objective. Images were deconvoluted using Huygens essential software. To minimize quenching of fluorescence, z-stacks were rapidly scanned at 0.2 µm increments. We only included dendrites for analysis if the labeling was bright and continuous throughout its course. Primary dendrites were not included in the analysis. All images were processed in batch using the same template (available upon request). Deconvoluted images were imported into NeuronStudio and were semi-automatically analyzed blind to experimental conditions. 5-7 granule cells were analyzed for dendritic spine quantification (n = 5-7 cells per group; n = 4 groups). For spine density, we analyzed different fragments of each cell quantifying at least 100 µm of secondary dendritic spines. All dendritic spines were at least 50 µm apart from the neuronal soma primary dendrites were not counted. The density of spines was calculated as the number of spines in every dendritic fragment were divided by the fragment's length.

CREB fluorescence intensity measurements

In order to quantify the fluorescence intensity of CREB in euploid and trisomic granule neurons, confocal fluorescence images were acquired at 20x magnification on a Leica TCS SP5 inverted scanning laser microscope (Leica Microsystems) creating a composite image of the entire dorsal hippocampus at 16 bits. Confocal acquisition settings were maintained constant for all the samples and all images were taken the same day. Tissue was only exposed to the lasers during the moment of image acquisition to prevent photobleaching. The mean intensity of granule cell somas was performed by manually delineating the somas in accordance with the CREB signal using ImageJ software (NIH, Bethesda). Signal background was subtracted for every region and image.

Kir3.2 fluorescence intensity measurements

In order to quantify the fluorescence intensity of Kir3.2 channels in engram and non-engram cells in the DG, confocal fluorescence images were acquired at 40x magnification (oil immersion) on a Leica TCS SP5 inverted (Leica Microsystems) scanning laser microscope centered on the injection site in the dorsal hippocampus at 16 bits. Confocal acquisition settings were maintained constant for all the samples and all images were taken the same day. Tissue was only exposed to the lasers during the moment of image acquisition to prevent photobleaching. Mean intensity of Kir3.2 was measured both in hM3Dq-mCherry+ cell and in a contiguous (less than 20 μm) hM3Dq-mCherry- cell localized in the same focal plane using ImageJ (NIH, Bethesda). Background fluorescence was measured in consecutive hippocampal sections from the same animals without primary Kir3.2 antibody and subtracted from the data. Paired analysis was used considering engram vs. non-engram neuronal expression of Kir3.2 and paired *t*-test was used to test statistical significance.

Electrophysiology

Ex vivo whole-cell patch clamp recordings

Engram was tagged as previously mentioned and mice were decapitated 5 min after natural recall in Context B and the brain was quickly removed. Coronal slices (300 µm thick) were cut with a vibratome (Leica VT1200S, Leica Microsystems) in artificial cerebrospinal fluid (aCSF) rich in sucrose (aCSF sucrose) containing (in mM): 2 KCl, 1.25 NaH_2PO_4-H_2O, 7 $MgSO_4$, 26 $NaHCO_3$, 0.5 $CaCl_2$, 10 glucose and 219 sucrose) at 4°C, saturated with a 95% O_2, 5% CO_2 mixture and maintained at pH 7.32-7.4. Then, slices were transferred to recovery chamber with a heated (35ºC) oxygenated aCSF that contained (in mM) 124 NaCl, 2.5 KCl, 1.25 NaH_2PO_4-H_2O, 1 $MgSO_4$, 26 $NaHCO_3$, 2 $CaCl_2$ and 10 glucose for 15 min and incubated for > 1 h at room temperature (22 ± 2°C) and pH 7.32-7.4. Slices were transferred individually into an immersion-recording chamber and oxygenated aCSF was perfused at a rate of 2 mL/min (22 ± 2°C).

Whole-cell intracellular recordings in current clamp (CC) mode were performed in granule cell neurons in DG granule cell layer (upper horn). Cells were visualized with a water-immersion 40x objective. Patch electrodes were made from borosilicate glass capillaries (Sutter P-1000, Sutter Instruments) with resistance ranging from 4 to 6 MΩ when filled with the internal solution that contained (in mM): 130 K-$MeSO_4$, 10 HEPES, 0.5 EGTA, 2 $MgCl_2$, 4 Mg-ATP, 0.4 Na-GTP, 10 phosphocreatine disodium salt hydrate and 0.3 % biocytin, for membrane properties experiments in CC. KOH were used to adjust the pH of all pipette solutions to 7.2-7.3. Membrane currents and voltages were measured using Multiclamp 700B amplifiers, digitized using Digidata 1550B, and controlled using pClamp 10.7 (Molecular Devices Corporation, California, USA). Membrane intrinsic properties of granule cells were determined by applying hyperpolarizing and depolarizing current steps (1 s, with 10 pA increments from -100 to 140 pA) in CC.

Pharmacology

EMD-173 and EMD-478 drug preparation and administration

In order to dissect the possible involvement of DYRK1A in engram formation we used a DYRK1A inhibitor EMD-173, and a kinase death control molecule, EMD-478 (Perha Pharmaceuticals). Both formulations were daily dissolved at 0.4 mg/kg dose in carboxymethylcellulose sodium (0.5% in distilled water) protected from light. EMD-173 or EMD-478 formulations were daily administered by oral gavage during 10 consecutive days.

Statistical analysis

When two conditions were compared, the Shapiro-Wilks test was conducted to check the normality of the data and Fisher's F test was used to assess the homogeneity of variances between groups. When data met the assumptions of parametric distribution, results were analyzed by unpaired student's *t*-test. Paired *t*-tests were employed to compare paired variables. Mann-Whitney-Wilcoxon test was applied in cases where the data did not meet the requirements of normal distribution. Statistical analyses were two-tailed.

For comparison between more than two groups, two-way ANOVA with different levels was conducted followed by Tukey HSD multiple comparison test. Bartlett test was used to assess the homogeneity of variances between groups. If the data distribution was non-parametric, the Kruskal-Wallis test was used followed by Mann Whitney-Wilcoxon test. All statistical analyses were two-tailed.

The statistical test used is indicated in every Figure.

Differences in means were considered statistically significant at $p < 0.05$.

Data analysis and statistics were performed using R studio (Version 1.1.463).

Key resources

Table 1. Antibodies

Reagent	***Source***	***Identifier***
Rabbit anti-c-Fos	Santa Cruz	Sc-7202
Mouse anti-Arc	Santa Cruz	Sc-17839
Rabbit anti-CREB	Millipore	06-863
Rabbit anti-Kir3.2	Alomone Labs	APC-006
Rabbit anti-Ki67	Abcam	ab15580
Rabbit anti-RFP	Thermo Fisher Scientific	600-401-379-RTU
Goat anti-rabbit (Alexa Fluor 488)	Thermo Fisher Scientific	A-11008
Goat anti-rabbit (Alexa Fluor 555)	Thermo Fisher Scientific	A-32732
Goat anti-mouse (Alexa Fluor 555)	Thermo Fisher Scientific	A-32732
Chicken anti-rabbit (Alexa Fluor 647)	Thermo Fisher Scientific	A-21443
Streptavidin (Alexa Fluor 488)	Thermo Fisher Scientific	S32357

Table 2. Bacterial and Virus Strains

Resource	*Source*	*Identifier*
pAAV-PTRE-tight-hM3Dq-mCherry	Addgene	66794
pAAV-cFos-tTA-pA	Addgene	66795
pAAV-PTRE-tight-hM4Di-mCherry	Custom made	NA
AAV-CREB	Addgene	68550

Table 3. Chemicals, peptides and recombinant proteins

Reagent	*Source*	*Identifier*
Ethylene glycol	Sigma	107-21-1
PBS	CRG facility	NA
Glycerol	Sigma	G5516
Triton X-100	Sigma	9036-19-5
Clozapine N-oxide (CNO)	Tocris	4936
Biocytin	Sigma	B44261
Fluoromount	Thermo Fisher Scientific	00-4959-52

Results

1. Increased sparsity of behaviorally induced neuronal activity upon learning in Ts65Dn in the Dentate Gyrus (DG)

Cellular IEGs are transcriptionally induced by patterned synaptic activity and may reveal alterations in neuronal assembly recruitment upon learning. Cognitive deficits have been extensively described in Ts65Dn mice, especially deficits in hippocampal-dependent tasks such as NORT [63,74] and CFC [73,152]. During the training session, Ts65Dn mice showed normal performance along the training session, with increasing freezing behavior during the training session to levels similar to the WT (ANOVA repeated measures; $F(3,18) = 0.88$; genotype effect N.S.; Figure 2BC). We next studied the pattern of neuronal activation during memory acquisition. We focused on the dentate gyrus (DG) since it is the input hippocampal gate and it is important for pattern separation [153], which is crucial in contextual fear-conditioning paradigms [154]. We quantified the expression of c-Fos (Figure 2D) and Arc (Figure 2F) 90 min after learning. In non-trained controls (home cage), the number of c-Fos and Arc positive cells was similar between genotypes (Post-hoc Tukey HSD; N.S., Figure 2E; N.S.; Figure 2G). However, upon learning Ts65Dn mice displayed a reduced number of active neurons in the DG compared to WT mice, as shown by the significantly reduced number of c-Fos positive cells (Post-hoc Tukey HSD; $p = 0.005$; Figure 2E) and Arc+ cells (Post-hoc Tukey HSD; $p = 0.007$ Figure 2FG), indicating sparser neuronal activation upon learning.

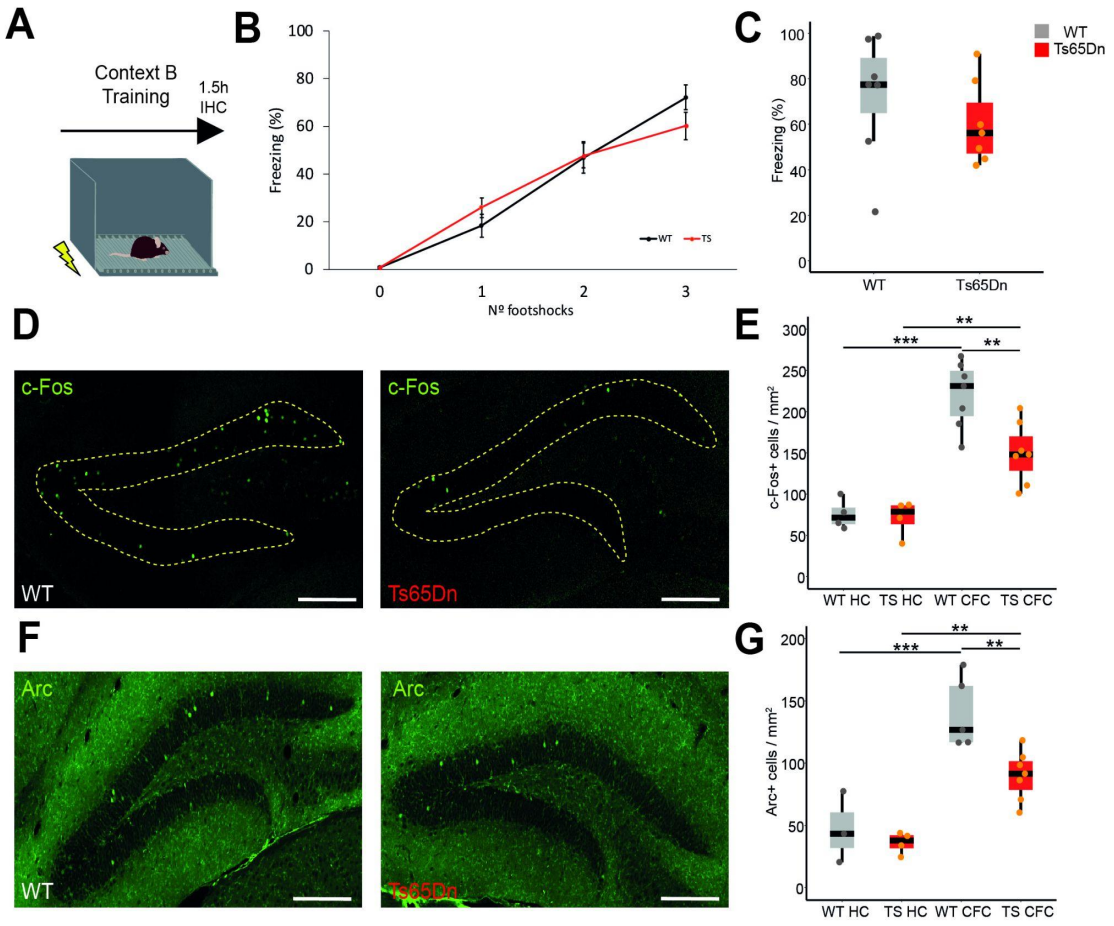

Figure 2. Sparse neuronal activation immediately after learning might contribute to defective engram allocation in Ts65Dn mice. (A) Behavioral schedule. Mice were trained in Context B. After 90 min, mice were sacrificed and the brain was extracted for IEG quantification. **(B)** Freezing behavior during the training session. Freezing was quantified before shock delivery (T 0), and after each shock (WT CFC = 7 mice, Ts65Dn CFC = 7 mice). **(C)** Freezing behavior after the last shock. **(D)** Representative images showing c-Fos expression (green) in the dorsal dentate gyrus. Yellow dashed lines delineate the granule cell layer of the dentate gyrus. Scale bars represent 100 µm. **(E)** Quantification of c-Fos positive cells in the DG in non-trained (home cage) controls (HC) and in mice that underwent contextual fear-conditioning (CFC) (WT HC = 4 mice, Ts65Dn HC = 4 mice, WT CFC = 7 mice, Ts65Dn CFC = 7 mice). **(F)** Representative images showing Arc expression (green) in the dorsal dentate gyrus. Scale bars represent 100 µm. **(E)** Quantification of Arc positive in the DG in HC controls and in mice that underwent CFC. (WT HC = 3 mice, Ts65Dn HC = 4 mice, WT CFC = 5 mice, Ts65Dn CFC = 7 mice). Two-way ANOVA, TukeyHSD as post hoc. On the boxplots, the horizontal line indicates the median, the box indicates the first to third quartile of expression and whiskers indicate 1.5 × the interquartile range. *$P < 0.05$, ** $P < 0.01$, *** $P < 0.001$.

2. Reduced engram size in Ts65Dn mice

The reduction in the number of active neurons during memory acquisition in Ts65Dn mice suggested that engram size was also reduced in Ts65Dn mice.

However, to determine the actual engram cells, those should be activated during learning and reactivated during recall, so, we used an activity-dependent engram tagging viral system (AAV_9-cFos-tTA and AAV_9-TRE_{tight}-hM3Dq-mCherry) [155,156]. Temporal control over the activity-dependent expression of hM3Dq-mCherry was achieved by the removal of the doxycycline (DOX) diet (Figure 3A). With this system, cells activated during learning were labeled with hM3Dq-mCherry in the CFC training session and memory was tested 24h after neuronal ensemble tagging (Figure 3B). Cells activated during learning were tagged specifically in the DG as shown in Figure 3C. After the training session, constant DOX administration was reinitiated to prevent non-specific neuronal labeling with hM3Dq-mCherry (Figure 3D). 24h after, contextual-fear memory was tested. Ts65Dn showed a significant reduction of freezing behavior compared to WT mice (Two-tailed T test; $p < 0.001$; Figure 2E) indicating a defective fear memory. To determine the actual engram size, brains were collected 90 min after memory recall and processed for IEG immunofluorescence to label memory recall activated cells (Figure 3F). In this experiment, the number of c-Fos+ cells was significantly reduced in Ts65Dn mice (Two-tailed T test; $p = 0.032$; Figure 3G). However, as engram cells are those activated during learning and reactivated during memory recall, we also quantified the number of c-Fos+ cells that co-expressed hM3Dq-mCherry. We found that the number of engram cells in Ts65Dn were reduced compared to WT mice (Two-tailed T test; $p = 0.017$; Figure 3H), indicating reduced engram size in Ts65Dn mice. We also found a weak positive correlation between the freezing behavior and the number of engram cells, although it did not reach statistical significance (Spearman; Figure 2I). To discard that AAV injection could influence neurogenesis, as it has been recently suggested [157], we quantified the number of Ki-67+ cells in non-injected and AAV-injected WT and Ts65Dn mice. We found that stereotaxic AAV injection did not modify the number of proliferating cells (Ki-67+) in the subgranular zone of the DG either in WT or in Ts65Dn mice (Post-hoc Tukey HSD; WT no AAV vs. Ts65Dn no AAV $p = 0.023$; WT AAV vs. Ts65Dn AAV $p = 0.028$; Figure 3J).

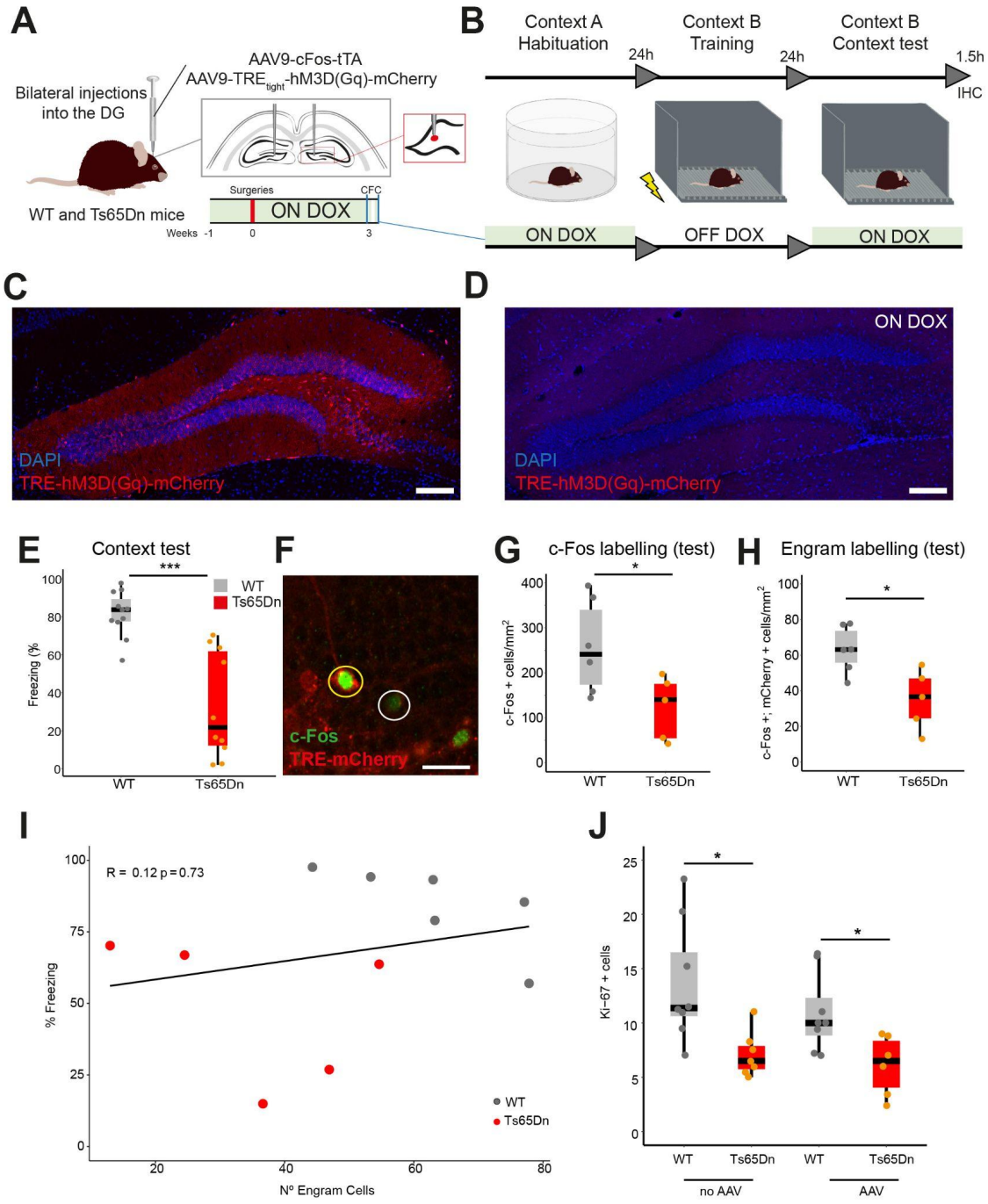

Figure 3. Reduced engram size and fear memory deficits in Ts65Dn mice. (A) AAV$_9$-cFos-tTA and AAV$_9$-TREtight-hM3D(Gq)-mCherry viruses were injected into the dorsal DG of WT and Ts65Dn mice. **(B)** Mice were chronically ON DOX including habituation in Context A. After habituation, DOX was removed and mice were trained in Context B 24h after. Then the DOX diet was resumed and mice were tested in Context B after 24h. Brains were extracted after 1.5h and processed for IEG quantification. **(C)** Image showing mCherry+ cells in a DG section 24h after engram-tagging procedure (OFF DOX). Scale bar = 100 µm. **(D)** Image showing DG section 24h after engram-tagging procedure keeping DOX diet (ON DOX) during the whole experiment. Scale bar = 100 µm. **(E)** Memory recall in Context B. Ts65Dn mice froze significantly less than WT mice upon reexposure to Context B (WT saline = 11, Ts65Dn saline = 10). Two-tailed T test. **(F)** c-Fos (green) and mCherry expressing cells 1.5h after memory recall test in the DG. **(G)** Density

(cell/mm^2) of c-Fos cells in the DG 1.5h after memory recall test (WT = 6, Ts65Dn = 5). Two-tailed T test. **(H)** Density (cell/mm2) of double c-Fos+/mCherry+ cells in the DG 1.5h after memory recall test (WT = 6, Ts65Dn = 5). Two-tailed T test. **(I)** Correlation between the number of engram (c-Fos+/mCherry+) cells and freezing behavior showing WT (black) and Ts65Dn (red). Spearman; R = 0,12, *p* = 0.73. **(J)** Number of Ki-67+ cells in WT and Ts65Dn animals with or without injection of AAVs in the DG (WT no AAV = 8 mice, Ts65Dn no AAV = 7 mice, WT AAV = 8 mice, Ts65Dn AAV = 6 mice). Two-way ANOVA, TukeyHSD as post hoc. On the boxplots, the horizontal line indicates the median, the box indicates the first to third quartile of expression and whiskers indicate 1.5 × the interquartile range. *P < 0.05, ** P < 0.01, *** P < 0.001.

3. Manipulation of training-activated granule neurons demonstrates their sufficiency and necessity for contextual fear memory expression

One important question when studying engram cells is their sufficiency and necessity to retrieve a specific memory [158]. To demonstrate necessity, we utilized in WT mice the engram tagging protocol with the inhibitory DREADD construct, AAV_9-TREtight-hM4Di-mCherry (Figure 4A). With this strategy, we were able to tag the learning-activated cells impede their activation during memory recall using CNO. Engram cells in WT mice were tagged with hM4Di during the training session and 24 h after, CNO (3 mg/kg) was administered before re-exposure to the trained context (Figure 4BC). We observed a significant reduction in freezing levels in WT animals treated with CNO compared to saline injected controls (Two-tailed T test; p = 0.0107; Figure 4D), that would indicate that engram cells are necessary for proper memory retrieval.

To demonstrate sufficiency, we used the activity-dependent tagging protocol (AAV_9-cFos-tTA and AAV_9-TRE_{tight}-hM3Dq-mCherry) to tag with mCherry and insert the excitatory DREADD (hM3Dq-mCherry) in those cells activated during acquisition (Figure 4E). In this case, 24h after training, mice were administered (i.p.) with CNO (1 mg/kg) and 30 min later were exposed to the neutral Context A, in which mice did not receive electric shocks (Figure 4F). The expression of hM3Dq-mCherry was restricted to the DG (Figure 4G).

In the contextual fear conditioning test, the neutral context (context A) did not produce freezing, as expected (Two-tailed T test; N.S.; Figure 4H). By administering CNO, both WT and Ts65Dn mice showed freezing levels comparable to the ones observed in the conditioned context (B), indicating the

successful activation of the fear memory engram. However, Ts65Dn mice froze significantly less than WT mice (Two-tailed T test; p = 0.04; Figure 4I), indicating that the activation of engram cells in a neutral context is sufficient to elicit memory recall in WT but, to a lesser extent in Ts65Dn, suggesting that the reduced engram size detected in trisomic mice might contribute to memory deficits.

Recent studies have also shown a reduced engram size both in mouse models of AD [6] and FXS [15]. In both cases, the exposure to recall cues is not sufficient to elicit a memory expression comparable to WT mice. However, the artificial reactivation of engram cells by optogenetics was sufficient to rescue memory deficits in a mouse model of AD [6]. This would indicate that an adequate engram reactivation is of paramount importance for memory recall. For this reason, we tagged learning activated cells with hM3Dq-mCherry and 24 h later, we activated the engram cells with CNO (1 mg/kg) 30 min before re-exposing mice to the conditioned-context (Context B) (Figure 4J). Compared to the saline-injected group, the artificial activation of engram cells by CNO showed similar freezing values both in WT and in Ts65Dn mice (Pairwise Wilcox comparisons; p = N.S.; Figure 4K). However, in Ts65Dn mice, engram cell activation by CNO was not sufficient to overcome the memory deficits when compared to o WT mice (Pairwise Wilcox comparisons; p = 0.02; Figure 4K). This would indicate that a reduced engram size cannot be bypassed by artificially reactivating the engram in Ts65Dn.

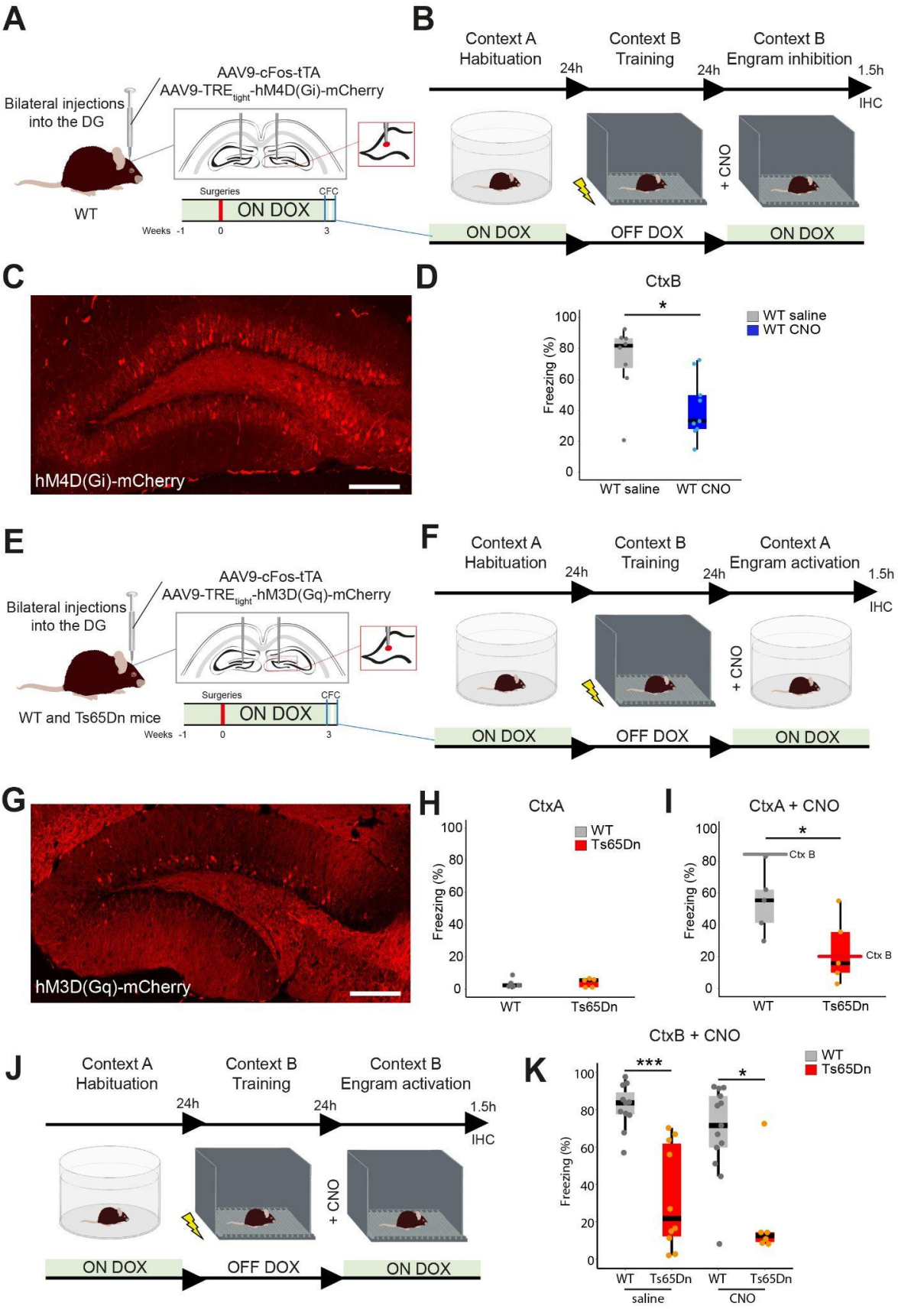
A
Bilateral injections into the DG
AAV9-cFos-tTA
AAV9-TRE$_{tight}$-hM4D(Gi)-mCherry
WT
Surgeries
CFC
ON DOX
Weeks -1 0 3
B
Context A Habituation
24h
Context B Training
24h
Context B Engram inhibition
1.5h
IHC
+ CNO
ON DOX
OFF DOX
ON DOX
C
hM4D(Gi)-mCherry
D
CtxB
*
WT saline
WT CNO
Freezing (%)
100
80
60
40
20
0
WT saline
WT CNO
E
Bilateral injections into the DG
AAV9-cFos-tTA
AAV9-TRE$_{tight}$-hM3D(Gq)-mCherry
WT and Ts65Dn mice
Surgeries
CFC
ON DOX
Weeks -1 0 3
F
Context A Habituation
24h
Context B Training
24h
Context A Engram activation
1.5h
IHC
+ CNO
ON DOX
OFF DOX
ON DOX
G
hM3D(Gq)-mCherry
H
CtxA
WT
Ts65Dn
Freezing (%)
100
80
60
40
20
0
WT
Ts65Dn
I
CtxA + CNO
*
Ctx B
Ctx B
Freezing (%)
100
80
60
40
20
0
WT
Ts65Dn
J
Context A Habituation
24h
Context B Training
24h
Context B Engram activation
1.5h
IHC
+ CNO
ON DOX
OFF DOX
ON DOX
K
CtxB + CNO
***
*
WT
Ts65Dn
Freezing (%)
100
80
60
40
20
0
WT
Ts65Dn
WT
Ts65Dn
saline
CNO

Figure 4. Engram manipulation reveals that engram allocation is probably defective in Ts65Dn mice. (A-B) Behavioral schedule used to test the inhibitory DREADD in WT. hM4D(Gi)-mCherry was expressed during training in Context B as previously described. CNO was administered 30 min before memory recall. **(C)** Representative image showing a DG section 24 h after engram-tagging procedure with hM4D(Gi)-mCherry. Scale bar = 100 μm **(D)** Engram inactivation in WT mice by CNO led to a memory impairment as evidenced by lower freezing levels when compared to saline injected controls (WT saline = 8, WT CNO = 9). Two-tailed T-test. **(E)** AAV_9-cFos-tTA and AAV_9-TREtight-hM3D(Gq)-mCherry viruses were injected into the dorsal DG of WT and Ts65Dn mice. **(F)** Mice were habituated in the neutral context (Context A) while ON DOX. After habituation, DOX was removed and mice were trained in Context B 24 h after. Then, the DOX diet was resumed and mice were tested again in the trained Context B after 24 h. Mice were sacrificed after 1.5 h and brains were extracted and processed for IEG quantification. **(G)** Representative image showing a DG section, 24 h after engram-tagging with hM3D(Gq)-mCherry. Scale bar = 100 μm. **(H)** Percentage of freezing of WT and Ts65Dn in Context A (WT= 5, Ts65Dn = 5). Two-tailed T-test. **(I)** Percentage of freezing of WT and Ts65Dn upon CNO (1 mg/kg) administration 30 min before the exposure to neutral Context A. Ts65Dn mice froze significantly less than WT mice (WT= 5, Ts65Dn = 5; Two-tailed T-test) Horizontal lines indicate the freezing values of WT and Ts65Dn, respectively, in CtxB (trained context). **(J)** Behavioral schedule used for testing engram activation. Engram was tagged in during the training session in Context B. CNO was administered 30 min before reexposing the mice to the trained context (B) 24 h after the training. **(K)** Percentage of freezing of WT and Ts65Dn (saline-injected) and WT and Ts65Dn mice (CNO-injected). Memory deficits in Ts65Dn were not rescued by CNO as evidenced by the reduced freezing levels compared to WT mice (WT saline = 11, Ts65Dn saline = 10, WT CNO = 13, Ts65Dn = 6). Horizontal lines indicate the freezing values of WT and Ts65Dn, respectively, in CtxB injected with saline. On the boxplots, the horizontal line indicates the median, the box indicates the first to third quartile of expression and whiskers indicate 1.5 × the interquartile range. $*P < 0.05$, $** P < 0.01$.

4. Trisomic engram cells do not display enhanced excitability after memory recall

Engram cells have been reported to undergo synaptic potentiation [4] after memory acquisition and their excitability is transiently enhanced after natural retrieval [13]. Because both synaptic potentiation [73,75] and neuronal excitability [159,160] are known to be impaired in Ts65Dn mice, we investigated whether trisomic engram cells are potentiated and increase their excitability to levels comparable to WT engram cells. Previous studies described a transitory increase in engram excitability state 5 min after memory recall that remained until 3 h [13]. Since the neurons activated during the training session were tagged with hM3Dq-mCherry, we could identify those fluorescent cells in the DG. Mice were sacrificed mice 5 min after memory recall [13] to examine the electrophysiological profile of

engram (hM3Dq-mCherry+) and non-engram (hM3Dq-mCherry-) cells by *ex vivo* whole-cell patch clamp recordings in the DG (Figure 5AB).

We found that action potential (AP) threshold was similar comparing hM3Dq-mCherry- and hM3Dq-mCherry+ both in WT and in Ts65Dn mice (Two-tailed T test; p = N.S.; Figure 5C). Resting membrane potential was also similar between engram and non-engram cells in WT mice (Two-tailed T test; p = N.S.; Figure 5D), but it was higher in trisomic engram cells comparing to non-engram cells (Two-tailed T test; p = 0.03; Figure 5D). Membrane resistance showed a non-significant increase (Mann-Whitney; p = 0.079; Figure 5EG) in WT engram cells compared to non-engram cells. We also found reduced rheobase in WT engram cells compared to non-engram cells (Mann-Whitney; p = 0.012; Figure 5H). However, in trisomic engram cells, we did not detect differences either in the membrane resistance or in the rheobase (Two-tailed T test; p = N.S.; Figure 5H). Interestingly, when plotting the rheobase against membrane resistance we could clearly see a higher mean difference between engram and non-engram cells in WT but not in Ts65Dn (Figure 5I). These results indicate that WT engram cells enhance their excitability during memory recall. However, this was not the case of trisomic engram cells. We did not detect differences in the firing rate of both engram and non-engram cells either in WT (Figure 6AB) or in Ts65Dn mice (ANOVA repeated measures = N.S.; Figure 6CD).

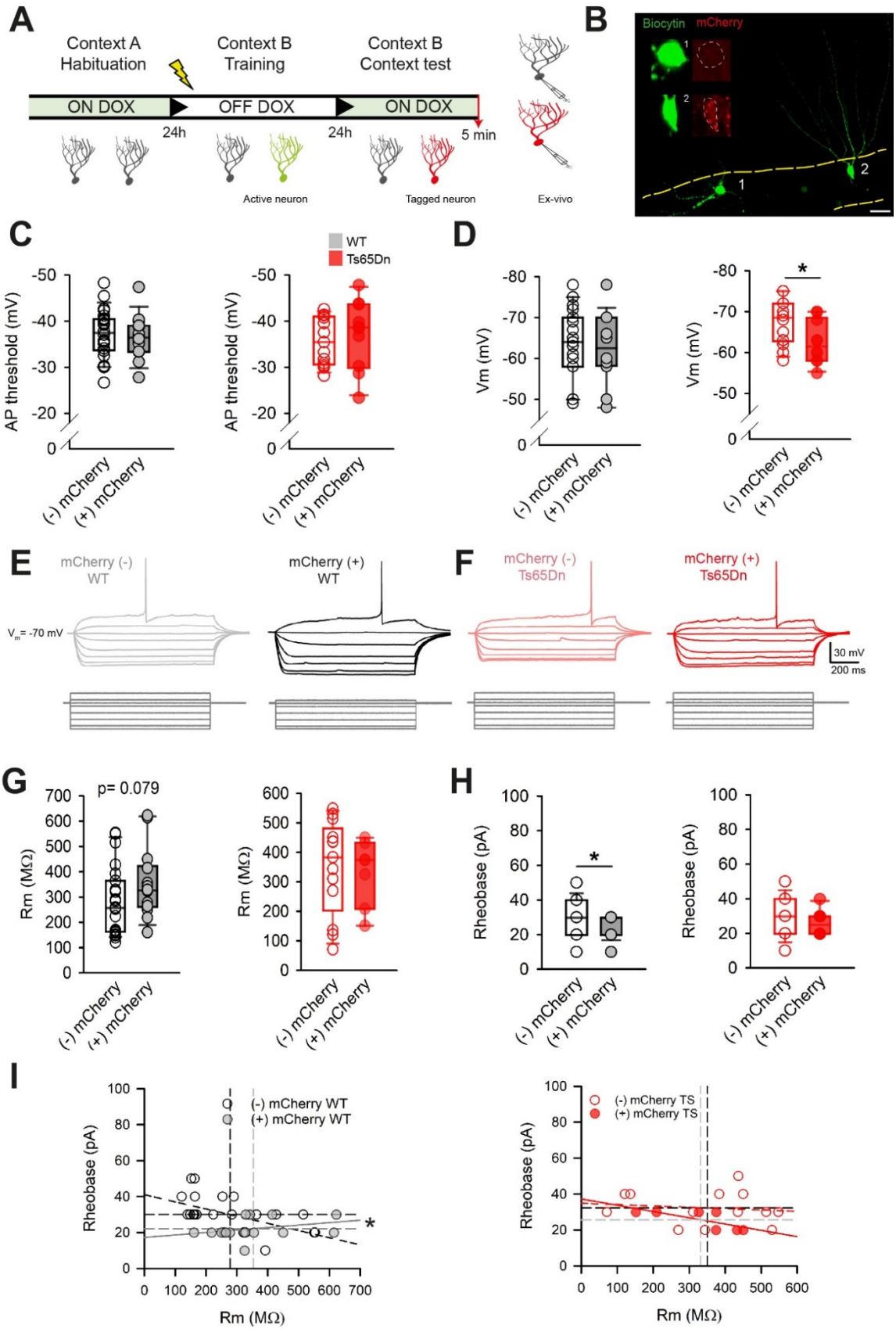
A
Context A
Habituation
Context B
Training
Context B
Context test
ON DOX
OFF DOX
ON DOX
24h
24h
5 min
Active neuron
Tagged neuron
Ex-vivo
B
Biocytin
mCherry
1
2
C
WT
Ts65Dn
AP threshold (mV)
(-) mCherry
(+) mCherry
D
Vm (mV)
*
E
mCherry (-)
WT
mCherry (+)
WT
Vm = -70 mV
F
mCherry (-)
Ts65Dn
mCherry (+)
Ts65Dn
30 mV
200 ms
G
p= 0.079
Rm (MΩ)
H
Rheobase (pA)
*
I
(-) mCherry WT
(+) mCherry WT
(-) mCherry TS
(+) mCherry TS
Rheobase (pA)
Rm (MΩ)
*

Figure 5. Electrophysiological profiling of DG engram cells. (A) Mice injected with the AAVs were habituated in the neutral Context A while ON DOX. After habituation, DOX was removed and mice were trained in Context B 24 h after to allow tagging of active cells (in green). Then the DOX diet was resumed and mice were tested again in Context B after 24 h. Brains were extracted and processed for electrophysiological studies. **(B)** mCherry expressing cells (hM3Dq-mCherry+), were considered as engram cells while non-mCherry expressing cells (hM3Dq-mCherry-) as non-engram cells. Image of non-engram (1) and engram (2) cells in the DG granule cell layer. Scale bar = 30 µm **(C)** Left: AP threshold of non-engram (black non-filled dots) and engram (gray filled dots) in WT mice (WT non-engram = 25 cells from 8 mice, WT engram = 16 cells from 8 mice). Right: AP threshold of non-engram (red non-filled dots) and engram (red filled dots) in Ts65Dn mice (Ts65Dn non-engram = 14 cells from 6 mice, Ts65Dn engram = 10 cells from 6 mice). **(D)** Left: resting membrane potential of non-engram (black non-filled dots) and engram (gray filled dots) in WT mice. (WT non-engram = 25 cells from 8 mice, WT engram = 16 cells from 8 mice). Right: resting membrane potential of non-engram (red non-filled dots) and engram (red filled dots) in Ts65Dn mice. (Ts65Dn non-engram = 14 cells from 6 mice, Ts65Dn engram = 10 cells from 6 mice). Mann Whitney. **P* >0.05. **(E)** Representative traces of the first action potential elicited by increasing depolarizing pulses in non-engram (gray) and engram (black) in WT mice. **(F)** Representative traces of the first action potential elicited by increasing depolarizing pulses in non-engram (pink) and engram (red) in Ts65Dn mice. **(G)** Left: membrane resistance (Rm) of non-engram (black non-filled dots) and engram (gray filled dots) in WT mice. (WT non-engram = 23 cells from 8 mice, WT engram = 14 cells from 8 mice). Right: membrane resistance (Rm) of non-engram (red non-filled dots) and engram (red filled dots) in Ts65Dn mice. (Ts65Dn non-engram = 13 cells from 6 mice, Ts65Dn engram = 7 cells from 6 mice). **(H)** Left: rheobase of non-engram (black non-filled dots) and engram (gray filled dots) in WT mice. Right: rheobase of non-engram (red non-filled dots) and engram (red filled dots) in Ts65Dn mice. Mann Whitney. **P* >0.05. **(I)** Left: rheobase vs. membrane resistance of non-engram (black non-filled dots) vs. engram (dark gray filled dots) in WT mice. (WT non-engram = 25 cells from 8 mice, WT engram = 16 cells from 6 mice). Right: rheobase vs. membrane resistance of non-engram (red non-filled dots) vs. engram (red filled dots) in Ts65Dn mice. (Ts65Dn non-engram = 14 cells from 8 mice, Ts65Dn engram = 10 cells from 5 mice). In every plot, horizontal and vertical black lines indicate the mean rheobase and Rm values, respectively of non-engram cells. Gray lines indicate the mean rheobase and Rm values of engram cells. Mann Whitney. **P* >0.05. On the boxplots, the horizontal line indicates the median, the box indicates the first to third quartile of expression and whiskers indicate 1.5 × the interquartile range.

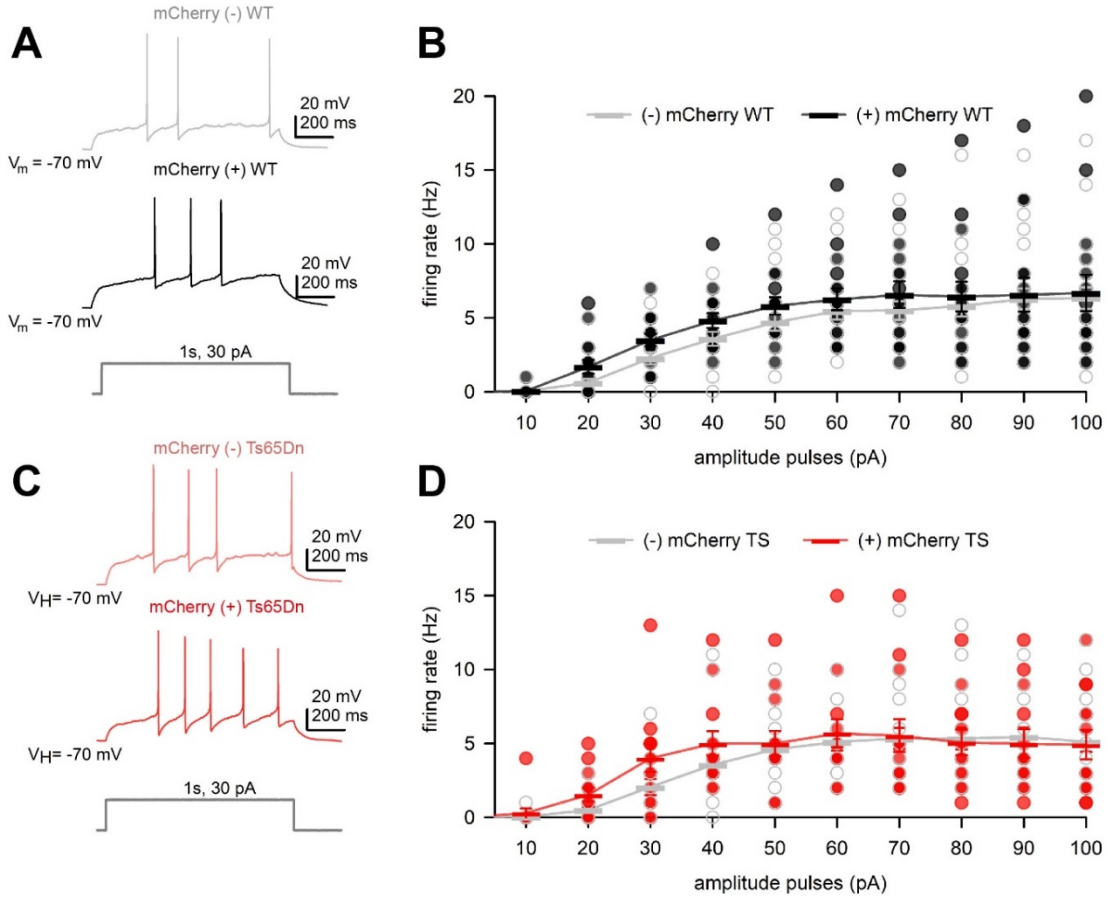

Figure 6: Firing rate is preserved between engram and non-engram cells both in WT and Ts65Dn mice. (A) Representative traces showing the voltage response of non-engram (gray) and engram (black) to a depolarizing current pulse in WT mice (WT non-engram = 26 cells from 8 mice, WT engram = 16 cells from 8 mice). **(B)** Current injection vs. firing rate recorded in non-engram (gray non-filled dots) and engram cells (black filled dots) in WT mice. **(C)** Representative traces showing the voltage response of non-engram (pink) and engram (red) to a depolarizing current pulse in Ts65Dn mice. (Ts65Dn non-engram = 18 cells from 7 mice, Ts65Dn engram = 13 cells from 6 mice). **(D)** Current injection vs. firing rate recorded in non-engram (gray non-filled dots) and engram cells (red filled dots) in Ts65Dn mice. ANOVA repeated measures. Data expressed as mean ± SEM.

5. Trisomic engram cells undergo structural plasticity

Among the chemical and molecular changes that occur in engram cells during memory consolidation, it has been reported that the number of dendritic spines increase in engram cells [4]. Numerous neurodevelopmental disorders including DS have been associated with abnormal dendritic spines [51]. To quantify dendritic spines of engram and non-engram cells, hM3Dq-mCherry- and hM3Dq-mCherry+ neurons were filled with biocytin during electrophysiological recordings both in WT and in Ts65Dn mice (Figure 7AB). In accordance with previous reports, we found that spine density of hM3Dq-mCherry+ was significantly higher compared to hM3Dq-mCherry- cells (Post-hoc Tukey HSD; $p < 0.001$; Figure 7C) in WT mice. This increase was mainly accounted for by the mushroom and stubby spines (Post-hoc Pairwise Wilcoxon test; $p < 0.001$; Figure 7D). Trisomic hM3Dq-mCherry+ cells also exhibited an increased number of dendritic spines compared to hM3Dq-mCherry - neurons (Post-hoc Tukey HSD; $p < 0.001$; Figure 7D). There was a non-significant tendency to an increase in mushroom and stubby spines compared to trisomic hM3Dq-mCherry - cells (Post-hoc Pairwise Wilcoxon test; $p = 0.056$; Figure 7D), but the number of mature spines was significantly lower when compared to WT hM3Dq-mCherry+ neurons (Post-hoc Pairwise Wilcoxon test; $p = 0.018$; Figure 7D).

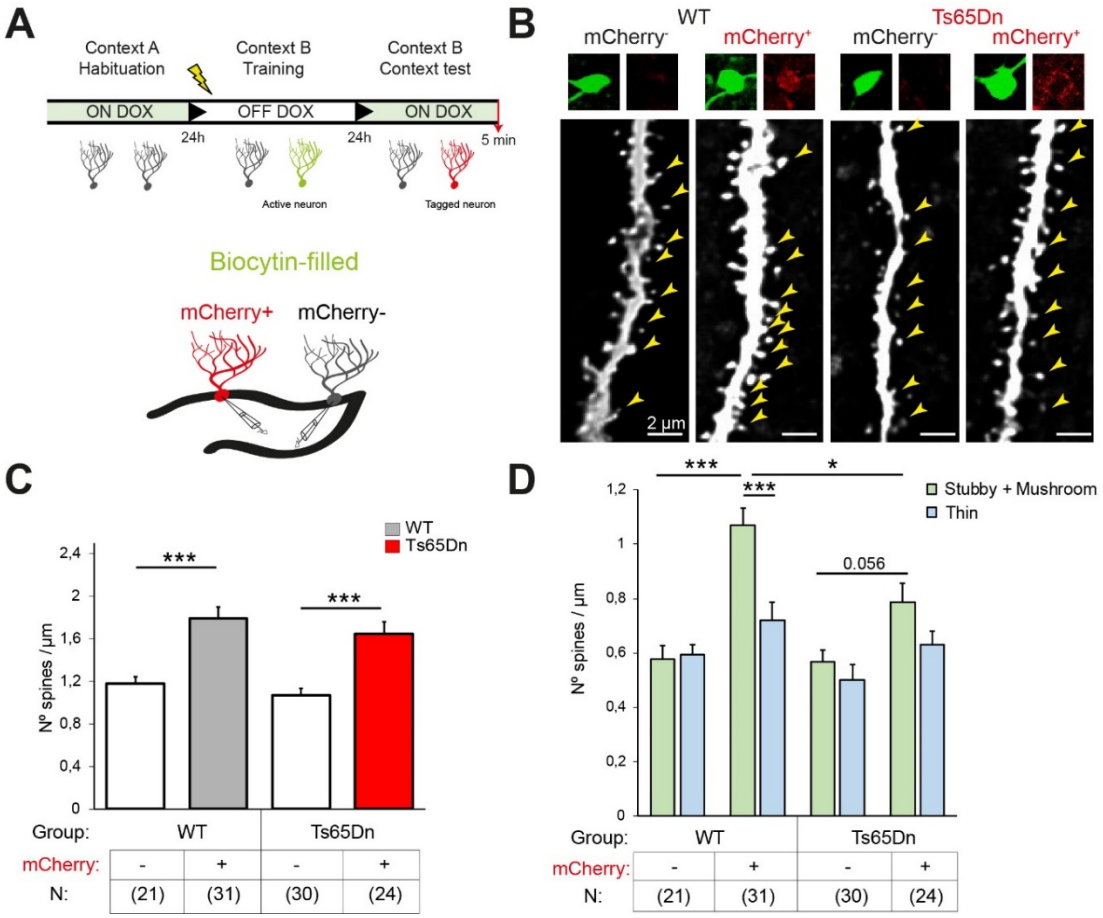

Figure 7. Trisomic engram cells undergo synaptic potentiation but present a fewer number of mature spines. (A) Mice injected with the AAVs were habituated in the neutral Context A while ON DOX. After habituation, DOX was removed and mice were trained in Context B 24 h after to allow tagging of active cells (in green). Then the DOX diet was resumed and mice were tested again in Context B after 24 h. Brains were extracted and processed for electrophysiological studies. During electrophysiological recording, granule cells were filled with biocytin for posterior reconstruction. **(B)** Representative images of mCherry- and mCherry+ cells both in WT and in Ts65Dn mice (arrow heads: dendritic spines). Scale bar = 2 µm. **(C)** Average dendritic spine density showing an increase in mCherry+ cells (WT non-engram = 21 dendritic fragments from 6 cells, WT engram = 31 dendritic fragments from 6 cells, Ts65Dn non-engram = 30 dendritic fragments from 7 cells, Ts65Dn engram = 24 dendritic fragments from 5 cells). Two-way ANOVA, Tukey HSD as post hoc. **(D)** Average dendritic spine density divided by spine type. (WT non-engram = 21 dendritic fragments from 6 cells, WT engram = 31 dendritic fragments from 6 cells, Ts65Dn non-engram = 30 dendritic fragments from 7 cells, Ts65Dn engram = 24 dendritic fragments from 5 cells). Two-way ANOVA, Tukey HSD as post hoc.*$P < 0.05$, ** $P < 0.01$. Data are expressed as mean ± SEM.

6. EMD-173, a DYRK1A kinase inhibitor, does not rescue memory deficits in CFC nor improves sparse neuronal activation in Ts65Dn mice

We hypothesized that *DYRK1A,* a major candidate of DS pathophysiology, might contribute to defective engram formation. As a matter of fact, treatment of DS mouse models with the DYRK1A inhibitor leucettine L41 rescued the novel object cognitive impairment in Ts65Dn, Dp(16)1Yey and TgDyrk1A mice [161]. Thus, we used a derivative of this compound, leucettinib-21 (also named EMD-173) in order to test whether DYRK1A kinase activity normalization could correct CFC memory deficits and sparser neuronal activation in Ts65Dn mice.

We treated WT and Ts65Dn mice with EMD-173 for 10 days (Figure 8A) before the CFC test (daily oral gavage administration; 0.4 mg/kg; Figure 8B). EMD-173 had no effects in WT mice and was not able to recover contextual fear-conditioning Ts65Dn memory deficits compared to Ts65Dn vehicle controls (Post-hoc Tukey HSD; N.S.; Figure 8C). Likewise, the sparser neuronal ensemble reactivation in Ts65Dn mice during memory recall was not recovered by EMD-173 treatment (Post-hoc Tukey HSD; N.S.; Figure 8D).

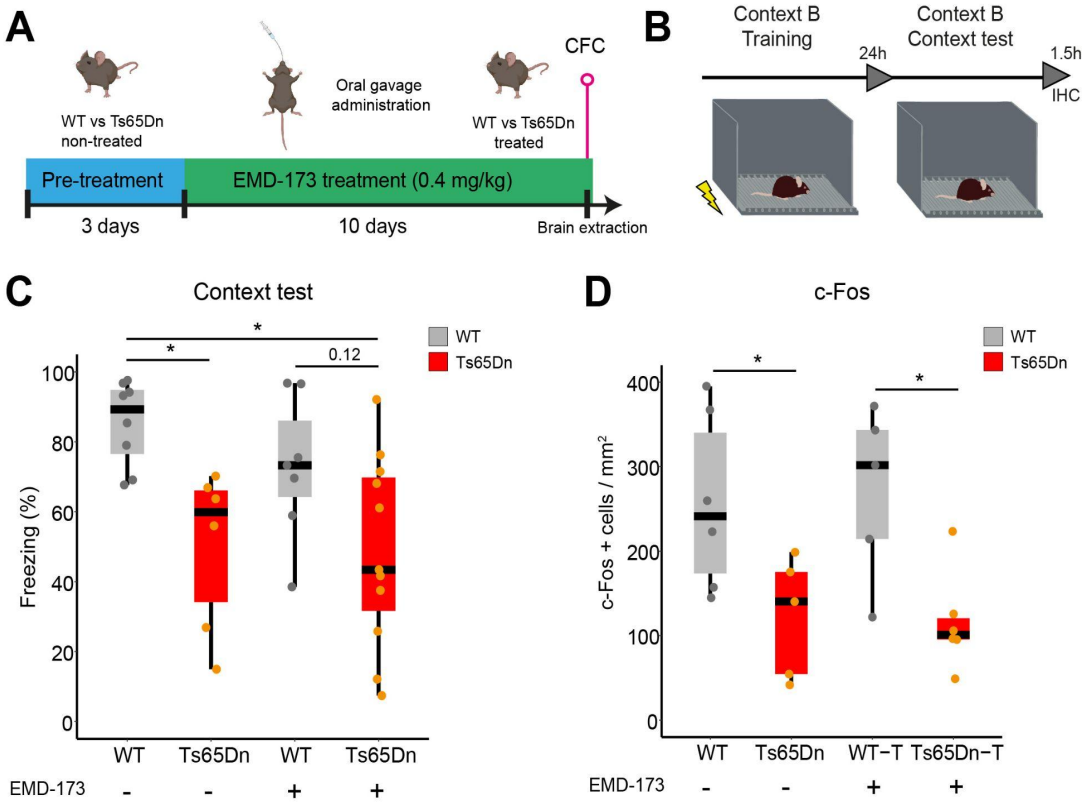

Figure 8. Inhibition of Dyrk1A activity by EMD-173 does not recover CFC memory deficits in Ts65Dn mice. (A) Experimental design of treatment with leucettinib-21 (EMD-173). Mice were daily treated with EMD-173 (0.4mg/kg) by oral gavage for 10 consecutive days. Control group received a vehicle solution by oral gavage. On the 10th day of treatment, mice were submitted to the CFC protocol. **(B)** Experimental design of contextual-fear conditioning paradigm. Mice were trained in Context B and memory was tested 24 h later in Context B. **(C)** Percentage of freezing in the trained context (B) during the test session (WT non-treated = 8, Ts65Dn non-treated = 6, WT + EMD-173 = 7, Ts65Dn + EMD-173= 11). Two-way ANOVA, Tukey HSD as post-hoc. **(D)** c-Fos+ cell density in the dorsal DG 1.5h after context test (WT non-treated = 6, Ts65Dn non-treated = 5, WT + EMD-173 = 5, Ts65Dn + EMD-173= 6). Two-way ANOVA, Tukey HSD as post-hoc. On the boxplots, the horizontal line indicates the median, the box indicates the first to third quartile of expression and whiskers indicate 1.5 × the interquartile range. *P < 0.05.

Next, we explored whether EMD-173 treatment was effective to recover recognition memory in Ts65Dn mice using the Novel Object Recognition test (NORT). We used EMD-478, a kinase inactive isomer, as a control. We performed a NOR before and after EMD-173 treatment in WT and in Ts65Dn mice (Figure 9A). EMD-173 treatment did not modify exploration time neither in Ts65Dn nor in WT (Post-hoc Tukey HSD; N.S.; Figure 9B). Ts65Dn littermates showed a clear deficit in recognition memory (Post-hoc Tukey HSD, p = 0.012; Figure 9C). Remarkably, we found that EMD-173 treatment was able to rescue memory performance in Ts65Dn mice to WT levels (Post-hoc Tukey HSD; p = 0.002; Figure 9C). In a different cohort of animals, we evaluated memory performance before and after the treatment with the kinase-death inactive isomer EMD-478 (Figure 9D). EMD-478 did not altered exploration time during the discrimination test (Post-hoc Tukey HSD; N.S.; Figure 9E). Likewise, EMD-478 was not able to recover recognition memory in Ts65Dn mice (Post-hoc Tukey HSD; WT before treatment vs. Ts65Dn before treatment p = 0.009; WT after treatment vs. Ts65Dn after treatment p = 0.0011; Figure 9F).

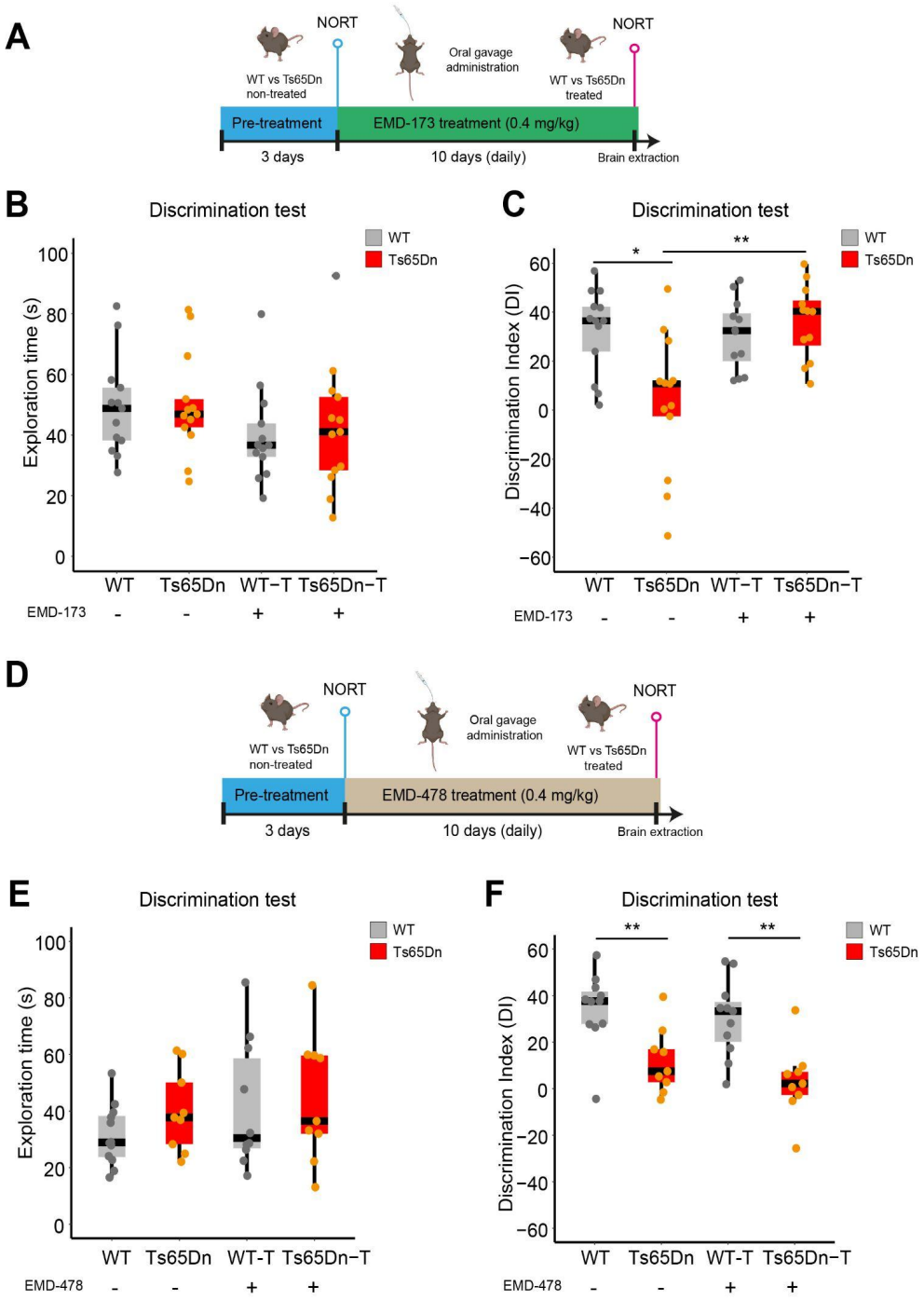

Figure 9. Inhibition of Dyrk1A kinase activity by EMD-173 recovers Ts65Dn NOR memory deficits. (A) Experimental design of treatment with leucettinib-21 (EMD-173). After a first NOR (pre-treatment) was performed, mice were daily treated with EMD-173 (0.4mg/kg) by oral gavage for 10 consecutive days. Then, mice were tested again in the NOR. **(B)** Exploration time during the discrimination test before and after receiving the EMD-173 treatment (WT = 13, Ts65Dn = 13). Two-way ANOVA, Tukey HSD as post-hoc. **(C)** Discrimination index (DI) before and after receiving the EMD-173 treatment (WT = 13, Ts65Dn = 13). Two-way ANOVA, Tukey HSD as post-hoc. **(D)** Experimental design of treatment with the kinase inactive iso-leucettinib-21 (EMD-478) as in (**A**). **(E)** Exploration time during the discrimination test before and after treatment with EMD-478 (WT = 12, Ts65Dn = 9). Two-way ANOVA, Tukey HSD as post-hoc. **(F)** DI before and after receiving the EMD-478 treatment (WT = 12, Ts65Dn = 9). Two-way ANOVA, Tukey HSD as

post-hoc. On the boxplots, the horizontal line indicates the median, the box indicates the first to third quartile of expression and whiskers indicate 1.5 × the interquartile range. *$P < 0.05$,**$P < 0.01$.

7. Overexpression of CREB in the DG does not rescue engram size and memory deficits in Ts65Dn mice

Several lines of evidence suggested that CREB plays a key role in neuronal ensemble allocation to an engram [9]. Previous studies from our laboratory found that the levels of phosphorylated CREB was reduced in Ts65Dn mice [62]. In our experiments, levels of CREB in granule cells were reduced in Ts65Dn right after the CFC training session compared to WT mice (Two-tailed T test; $p < 0.001$; Figure 10AB). Thus, we decided to upregulate CREB expression in the DG prior to the acquisition of contextual fear conditioning memory to determine whether we could rescue engram size and memory in Ts65Dn. We injected AAV_2-hSyn-CREB-EGFP into the dorsal DG 3 weeks before CFC training (Figure 10C). CREB-EGFP expression was restricted to the granule cell layer of the dorsal hippocampus (Figure 10D). Compared to our previous findings, WT mice showed similar freezing levels despite the upregulation of CREB expression, indicating no effect on memory. Similarly, the overexpression of CREB did not enhance memory performance in Ts65Dn mice (Two-tailed T test; $p = 0.0273$; Figure 10EF). Indeed, the number of c-Fos+ neurons during the context test was reduced in Ts65Dn compared to WT mice (Two-tailed T test; $p = 0.0277$; Figure 10G). AAV-CREB-EGFP was effective in elevating CREB expression levels in neurons expressing CREB-EGFP both in WT and in Ts65Dn mice (Post-hoc Tukey HSD; $p < 0.001$; Figure 10HI). Remarkably, Ts65Dn granule cells that expressed CREB-EGFP showed a lower upregulation of CREB levels than WT granule cells (Post-hoc Tukey HSD; $p < 0.001$; Figure 10I).

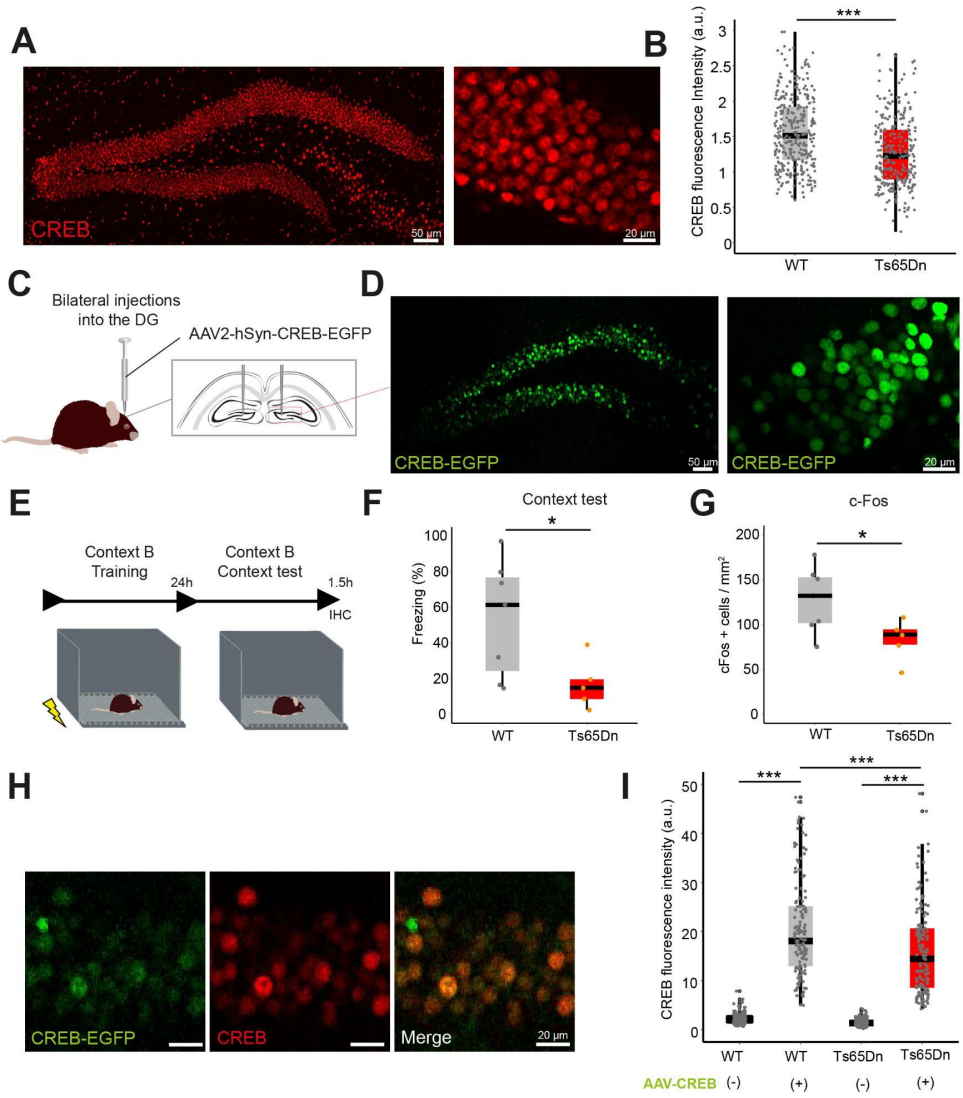

Figure 10. CREB overexpression does not rescue memory deficits in Ts65Dn mice. (A) Left: representative images showing CREB expression in the dorsal DG. Scale bar = 50 µm. Right: Image magnification showing CREB expression. Scale bar = 20 µm. **(B)** Fluorescence intensity granule cells in the DG in arbitrary units (WT = 328 granule cells from 6 mice, Ts65Dn = 280 granule cells from 7 mice). Two-tailed T test. **(C)** AAV_2-CREB-EGFP was injected into the DG of WT and Ts65Dn mice. **(D)** Left: Representative image showing CREB-EGFP expression in the dorsal DG. Scale bar = 50 µm. Right: Magnification showing the pattern of CREB-EGFP expression. Scale bar = 20 µm. **(E)** Experimental schedule of CFC. **(F)** Percentage of freezing of WT (gray) and Ts65Dn (red) in the context B during the test session (WT = 7, Ts65Dn = 5). **(G)** c-Fos density in the DG 1.5h after memory recall test (WT = 7, Ts65Dn = 5). Two-tailed T test. **(H)** Representative image showing expression of AAV-CREB-EGFP (green), CREB (red) and the merged image in the granule cell layer of the hippocampus. Scale bar = 20 µm **(I)** CREB fluorescence intensity on CREB-EGFP negative and positive cells both in WT and Ts65Dn mice (WT AAV-CREB negative = 158 cells from 3 mice , WT AAV-CREB positive = 149 cells from 3 mice, Ts65Dn AAV-CREB negative = 143 cells from 3 mice , Ts65Dn AAV-CREB positive = 149 cells from 3 mice). Two-way ANOVA, Tukey HSD as Post-hoc. On the boxplots, the horizontal line indicates the median, the box indicates the first to third quartile of expression and whiskers indicate 1.5 × the interquartile range. *** $P < 0.001$, * $p < 0.05$.

8. Inward Rectifier Potassium Channel Kir3.2 might impair cell excitability state of trisomic engram cells

Recently, it has been shown that the inward rectifier potassium channel Kir2.1 contributes to an increased excitability state in engram cells [13] by their internalization immediately after memory recall. Of interest for DS, it is known that Kir3.2 is overexpressed in the hippocampus of Ts65Dn and its normalization recovers LTP deficits and memory impairment in Ts65Dn mice [65]. For this reason, we decided to investigate whether the upregulation of Kir3.2 levels in the Ts65Dn hippocampus might be causative of engram alterations.

In order to measure Kir3.2 levels in engram and non-engram cells in the DG, we tagged training activated cells using the double virus system previously described in both WT and Ts65Dn mice, (Figure 11AB). We found that Kir3.2 was upregulated in the DG molecular cell layer of Ts65Dn mice by approximately 1.5-fold compared to WT (Two-tailed T test; $p = 0.028$; Figure 11CD). Confocal analysis of pairs of hM3Dq-mCherry+ and hM3Dq-mCherry- cells revealed that in WT, Kir3.2 expression was downregulated in engram cells (Paired T test; $p = 0.0108$; Figure 11EF). However, this was not the case in Ts65Dn engram cells (Paired T test; N.S.; Figure 11EF). Remarkably, the expression of Kir3.2 in Ts65Dn was significantly higher both in engram (Post-hoc Tukey HSD; $p < 0.001$; Figure 11G) and non-engram cells (Post-hoc Tukey HSD; $p = 0.006$; Figure 11G) compared to WT engram vs non-engram pairs.

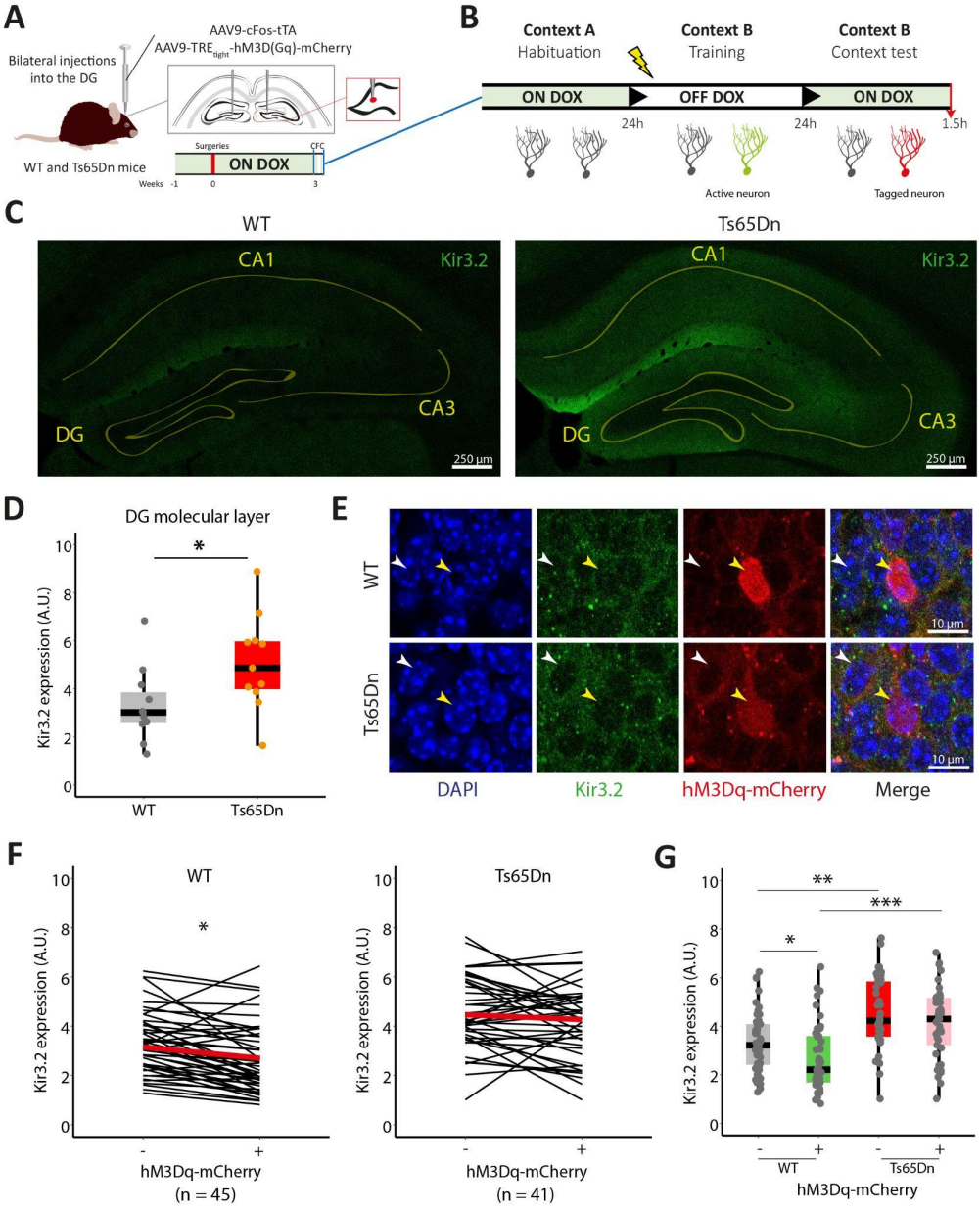

Figure 11. Kir3.2 overexpression might contribute to reduced neuronal excitability and might hinder neuronal allocation to an engram. (A) AAVs were injected into the DG of WT and Ts65Dn mice. **(B)** Experimental design for engram tagging previously described. Brains were extracted and processed for Kir3.2 immunofluorescence staining 90 min after recall. **(C)** Representative images showing the expression of Kir3.2 (green) in the dorsal hippocampus of WT (left) and Ts65Dn mice (right). Yellow lines delineate CA1, CA3 and DG. **(D)** Expression of Kir3.2 in the molecular layer of the DG both in WT (gray) and in Ts65Dn (red). (WT = 11 sections from 3 mice, Ts65Dn = 11 sections from 3 mice). Two-tailed t test, * $p < 0.05$. **(E)** Confocal images of DG granule cells stained with Kir3.2. DG granule cells hM3Dq-mCherry- (white arrowhead) and hM3Dq-mCherry+ (yellow arrowhead). **(F)** Paired analysis of Kir3.2 expression, hM3Dq-mCherry- vs hM3Dq-mCherry+ in WT (left) and in Ts65Dn mice (right). Mean in red (WT hM3Dq-mCherry- = 45 cells from 3 mice, WT hM3Dq-mCherry+ = 45 cells from 3 mice, Ts65Dn hM3Dq-mCherry- = 41 cells from 3 mice, Ts65Dn hM3Dq-mCherry+ = 41 cells from 3 mice). Two-tailed paired t test, * $p < 0.05$. **(G)** Expression of Kir3.2 in hM3Dq-mCherry- and hM3Dq-mCherry+ in WT and

Ts65Dn granule cells. (WT hM3Dq-mCherry- = 45 cells from 3 mice, WT hM3Dq-mCherry+ = 45 cells from 3 mice, Ts65Dn hM3Dq-mCherry- = 41 cells from 3 mice, Ts65Dn hM3Dq-mCherry+ = 41 cells from 3 mice). Two-way ANOVA, TukeyHSD as post-hoc. On the boxplots, the horizontal line indicates the median, the box indicates the first to third quartile of expression and whiskers indicate 1.5 × the interquartile range. *** $P < 0.001$, ** $p < 0.01$, * $p < 0.05$.

Discussion

In this Chapter, we provide new insights of the cellular mechanisms that might be responsible for cognitive impairment in DS and explore several strategies to revert these alterations.

Previous work in the laboratory showed that memory deficits in the Ts65Dn mouse models may arise from a failure to convert transitory learning-induced neuronal activity into long-term memory traces [51], as trisomic mice did not undergo structural plasticity four months after environmental enrichment, and the rescuing effects on learning and memory obtained in the MWM also faded. Given that most studies on engram formation have used the CFC paradigm, and that previous reports showed impairment in CFC in the Ts65Dn mice [73], in a first set of experiments, we studied the impact of the trisomy on this paradigm. Ts65Dn mice showed training-induced freezing levels similar to WT mice, indicating adequate learning. In agreement with our findings, also other groups reported no differences in the freezing behavior during the training session [162,163]. However, even though mice were able to learn, we found that the number of learning-activated neurons (c-Fos+ and Arc+ cells) were reduced in Ts65Dn DG, indicating that sparser learning-induced neuronal ensemble activity is not accompanied by learning deficits in Ts65Dn. Similar results were obtained in a mouse model of AD, in which, even though training-induced freezing levels were similar to WT mice, the number of activated neurons were reduced during training [6]. Altogether, these findings suggest that training-induced freezing does not predict the number of active neurons during memory acquisition and that alternative mechanisms might explain the reduced number of active neurons in Ts65Dn mice. A sparser neuronal ensemble activation was also detected in a previous study in the CA1 region of Ts65Dn, upon exposure to novel environments [68]. In addition, a recent study from our laboratory found a lack of upregulation of Arc levels immediately after learning in Ts65Dn mice while Arc levels did not differ in basal conditions [63]. It might be possible that cell-autonomous mechanisms, such as impaired intrinsic excitability [159,160,164] or non-autonomous factors such as hyperinnervation of basket cells into granule cells [165] might lower the number of active neurons in response to learning cues.

In Ts65Dn, some evidence supports that reduced neuronal activation could be explained by reduced neuronal excitability [159,160,164]. This reduced excitability might prevent trisomic granule neurons to respond to synaptic inputs from the entorhinal cortex (EC), therefore contributing to an increased sparsity of neuronal activation. As a matter of fact, primary hippocampal cultures from Ts65Dn mice exhibited decreased number of spikes and network bursts were significantly reduced compared to diploid controls [160]. Although we did not directly evaluate neuronal activity after learning, the reduced number of granule cells expressing c-Fos and Arc in Ts65Dn mice would be in line with a reduced neuronal activity. In fact, studies on animal models of AD also observed sparser neuronal activation during learning [6] along with plasticity defects [6,14] and engram size reduction [6,15].

Thus, and even though c-Fos is not a direct marker of the engram, our findings could be interpreted as a deficit in the allocation of stable and long-lasting neuronal ensembles during learning, as this depends on IEGs production [166,167]. To proof this assumption, we next used activity-dependent tagging with the fluorescent reporter mCherry to identify the neurons that were activated both during the acquisition of a contextual fear memory and reactivated during memory recall (c-Fos and mCherry expressing neurons), e.g. engram cells. Remarkably, the number of engram cells was significantly reduced in the Ts65Dn granule cell layer, and correlated with memory performance both in WT and in Ts65Dn mice. Although neuronal ensemble activation during learning is assumed to be relevant for the correct representation of memories in the brain [11,166,168], it has been suggested that engram size is quite stereotyped and that deviations from the optimal size might prevent engram networks to reactivate memory. For instance, larger engram size could lead to better discrimination due to a greater cellular reactivation in the conditioned context [11]. Considering the DG has a role in memory resolution [169,170], the greater the neuronal ensembles recruited during learning would promote an improved memory specificity. As such, it could be assumed that the degree of learning and memory specificity corresponds with neuronal activity in a subset of DG cells that were active during both learning and recall [11].

Reduced engram size, on the other hand, would make it more difficult to distinguish between comparable contexts since less contextual information would be encoded into the same the memory trace, resulting in memory instability and poorer discrimination [11]. In fact, Ts65Dn are impaired in a pattern separation task [171]. Although in our experiments engram size was not directly related to learning capability, it is commonly accepted that accessing the memory engrams is necessary for memory recall [172], and thus, engram size in the trisomic mice would affect recall. Indeed the engram studies on AD and in FXS also observed reduced engram size upon memory retrieval [6,14,15]. However, while in AD mouse models, engram size was restored and memory could be recalled by artificial reactivation of the engram using optogenetics, in the FXS model, memory deficits and impaired engram reactivation were rescued by promoting neuronal plasticity before learning by submitting mice to EE [15]. Based on these studies, we could speculate that impaired trisomic memory engram reactivation may be due to i) defective engram allocation, as suggested by the reduced c-Fos expression, or ii) impaired engram reactivation, as indicated by the reduced proportion of mCherry/c-Fos+ cells. In fact, chemogenetic inhibition of WT engram cells in the trained context (Cxt B) worsened memory performance to levels comparable to Ts65Dn littermates, reinforcing the concept that the number of active neurons during memory recall is important for memory expression.

In order to decipher this question, we decided to activate the engram neurons that were tagged with mCherry and inserted with an excitatory DREADD (hM3Dq-mCherry) in the trained context using CNO (1 mg/kg). However, and contrary to what was observed in the AD scenario, memory was not rescued in Ts65Dn. This result would suggest that memory deficits in Ts65Dn are not contributed by impaired engram reactivation since artificial engram activation by CNO does not rescue the reduced memory during natural recall in trisomic mice. Taken together, these results would indicate that reduced engram size in Ts65Dn is causative for reduced contextual fear memory recall.

Besides the number of engram cells, other critical factors such as engram excitability and connectivity have been found to be important for memory retrieval. Alterations in the capability of engram cells to form a stable engram network

and/or to properly reactivate under specific recall cues can hinder memories to be retrieved. For instance, a recent study found that engram cell excitability influences the efficacy of memory retrieval [13]. The authors found that recall cues induce a transient enhancement of engram cell excitability that leads to improved context recognition. This increase in excitability is mediated by the internalization of Kir2.1 potassium inwardly rectifying potassium channel. Remarkably, in Ts65Dn and in individuals with DS there is a significant upregulation of the Kir3.2 channel, encoded by *Kcnj6* gene [65,163,173]. The overexpression of Kir3.2 is associated with enhanced signaling through GABAB receptors in primary cultures of hippocampal neurons [174] and hippocampal slices [66] in Ts65Dn mice. In fact, GABAB receptor antagonists restored synaptic plasticity and memory deficits in Ts65Dn mice by inhibiting GABAB/Kir3.2 signaling [163].

In our experiments in WT mice, Kir3.2 expression was downregulated in engram cells compared to non-engram cells immediately after memory recall, in accordance with a recent study [13]. Internalization of Kir3.2 channels by recall cues would enable WT engram cells to temporarily enhance their excitability state, improve context recognition, and consequently, elicit freezing behavior. However, Kir3.2 expression was upregulated in trisomic non-engram cells and remained overexpressed in engram neurons after memory recall, suggesting that the increase in engram excitability required for memory retrieval is hampered by the trisomy of the *Kcnj6* gene [65,163,173]. Kir3.2 channels contribute to the resting membrane potential in dendrites [175], and can therefore influence how synaptic potentials are amplified by voltage-gated channels [176]. Moreover, the expression of Kir3 channels in glutamatergic synapses has been reported to shunt excitatory synaptic currents and hyperpolarize neurons in order to attenuate excitatory postsynaptic responses [177]. In Ts65Dn mice, basal upregulation of Kir3.2 both in engram and in non-engram cells and lack of internalization after memory recall would have two consequences for neuronal ensembles. (i) Kir3.2-mediated hyperpolarization of granule cells in Ts65Dn would reduce their probability to activate during memory acquisition thus reducing the number of cells able to form a neuronal ensemble. (ii) The inability of trisomic

engram cells to downregulate Kir3.2 channels upon recall cues would prevent the transitory enhancement of neuronal excitability that is needed to boost context recognition and would impede memory to be entirely recalled. Altogether, this data encouraged us to specifically downregulate Kir3.2 expression in Ts65Dn using AAV_9-CaMKIIa-miRNA-Kcnj6-GFP. Unfortunately, these results could not be included in this Thesis because the production of the viral vector was not completed before submission. Further analysis will help to elucidate whether this mechanism can be a promising strategy to recover engram-specific alterations in DS.

Thus, we next studied the intrinsic properties of engram and non-engram cells to detect possible alterations in neuronal excitability and neuronal plasticity [3,4,6]. By means of whole-cell patch clamp recordings, we were able to determine the passive and active electrical properties of both WT and trisomic mCherry- and mCherry+ cells, as a proxy of non-engram and engram cells. In WT mice, we confirmed the reduced rheobase in mCherry+ compared to mCherry- cells that Pignatelli et al. found in engram cells immediately after memory retrieval [13]. This enhancement of neuronal excitability of mCherry+ cells was not observed in Ts65Dn reinforcing the concept that reduced excitability might prevent memory to be entirely recalled.

Although this reduced engram cell excitability might be explained by the lack of internalization of Kir3.2 channels, as discussed before, other factors could also contribute to the engram dysfunction in trisomic mice. It is well known that CREB-mediated mechanisms increase excitability by reducing voltage-gated K^+ currents [178,179]. These currents are important as they serve as a molecular break on neuronal firing by hyperpolarizing the neurons by a short time-period named refractory period. Remarkably, upon CREB upregulation, these molecular breaks are released and, therefore, excitability is increased [7], which is crucial in the engram allocation process. Previously in the lab, we showed altered levels of p-CREB in the Ts65Dn hippocampus [62]. Thus, the next obvious aspect to investigate was whether alterations in CREB signaling could account for the smaller engram size in Ts65Dn mice. We found that in Ts65Dn, CREB levels were reduced after memory acquisition in the DG compared to WT littermates. In

light of the key role of CREB on the engram allocation process, and given its reduced levels in trisomic mice, we decided to upregulate its expression in the DG using a custom-made AAV_2-hSyn-CREB-EGFP. CREB-EGFP was expressed in granule cells and was effective to upregulate CREB expression both in WT and Ts65Dn mice. Neither in WT mice nor in Ts65Dn, CREB upregulation was able to improve memory performance or neuronal activation after memory recall.

Our results may seem contradictory to previous work showing that increasing the function of CREB in principal lateral amygdala neurons increased the likelihood to become part of a fear memory engram [9]. It could be argued that WT mice already perform at very high levels, thus possibly indicating a ceiling effect. However, a result similar to our finding was observed in a previous study, in which CREB upregulation did not enhance neuronal activation nor memory performance in WT mice [14]. Importantly, in that work it increased the number of active neurons and rescued memory deficits in a mouse model of AD [14]. Instead, we show that this is not the case in Ts65Dn mice, in which the upregulation of CREB alone might not be sufficient to increase the number of active neurons suitable for being allocated to an engram at the time of learning. As our construct CREB-EGFP is under the hSyn promoter, CREB is upregulated in interneurons, so it is also conceivable that elevated interneuron excitability could lead to a greater inhibition of excitatory trisomic granule cells. In order to exclude this possibility, it would be interesting to investigate whether enhancing CREB expression exclusively in excitatory granule cells might be effective to overcome sparser neuronal activation in Ts65Dn mice.

Our work by now showed reduced neuronal excitability in Ts65Dn mice possibly related to Kir3.2 overexpression but not CREB deficiency. It is important to bear in mind that the connectivity of neural subnetworks activated by learning depends on the strength and numbers of synapses between neurons, which influences the neuronal activation and, thereby, determines the way engrams stabilize and reactivate. It has been demonstrated that engram cells undergo structural and functional plasticity [4,6,13]. Previous studies on retrograde amnesia [4] and AD [6] have described that the lack of memory retrieval originates from a disruption

of the consolidation phase that occurs during the transition from a fragile and recently encoded memory engram to a stable and mature memory engram. During this consolidation process, engram cells persistently increase their synaptic strength and spine density. It was thus important given the altered structural plasticity detected in trisomic mice [51] to study dendritic spine density of engram and non-engram cells in WT and in Ts65Dn mice. In accordance with previous results, WT spine density was increased in engram compared to non-engram cells [4,6]. However, spine density was also slightly, although not significantly enhanced in trisomic engram cells. Interestingly, engram cells the increased spine number was contributed by mature spines, in both genotypes. Even so, the number of mature spines was higher in WT engram cells compared to Ts65Dn engram cells. Our results do not confirm previous findings of reduced number of spines in the trisomic DG [52,53,69,180], as we did not detect differences in spine density between WT and Ts65Dn granule cells. It is possible that differences in the quantification methods and the age of the animals might account for these variations. For instance, some studies were performed at P15 [52,53] while others at 6 months-old Ts65Dn mice [69]. Moreover, most of these studies used Golgi staining [52,53,180] or electron microscopy [69] that might allow a higher resolution of spines and, therefore, to detect smaller differences in spine number. In our case, the method used to identify engram (mCherry+) cells using stereotaxic injection of the activity-dependent tagging system along with the whole-cell patch clamp recordings, might add some degree of variability that might prevent us from detecting differences in spine number in granule cells. Even so, we were able to reproduce previous results of increased spinogenesis in WT engram cells [4].

Again, the trisomic case is different from both anterograde amnesia and AD. Whilst in anterograde amnesia and AD, structural plasticity is not detected in engram cells [4,6], Ts65Dn engram cells showed a slight increase in dendritic spine density. These results suggest that, as shown in Ts65Dn mice, the reduced structural plasticity is not sufficient to support engram stabilization. This finding may relate to the reduced neuronal ensemble activation during memory acquisition, as one would expect reduced activity to impair structural plasticity.

Taking all this evidence into consideration, and given the role of Dyrk1A in neuronal excitability and synaptic transmission, we designed several strategies to recover engram-specific alterations in Ts65Dn mice. We first tested whether leucettinib-21 (also named EMD-173), a DYRK1A kinase inhibitor, would be effective in rescuing memory deficits and sparser neuronal activation in Ts65Dn mice. DYRK1A inhibitors have been extensively used in DS research since they have been effective in recovering dendritic alterations, plasticity and memory deficits in different mouse models of DS [161,181,182]. On that account, we treated WT and Ts65Dn mice with EMD-173 (0.4 mg/kg) for 10 days and tested memory using CFC. EMD-173 was not able to recover CFC memory deficits, nor the number of active cells during memory recall in Ts65Dn mice. Intriguingly, EMD-173 was effective in recovering recognition memory in Ts65Dn mice using the NORT. The memory type (recognition memory for NORT vs. associative and emotional memory for CFC) along with memory strength (moderate for NORT vs. strong for CFC) differ between these two tests. It might be possible that the tested dose of EMD-173 was effective in specific brain regions involved in certain tasks but not others. As a result, it was possible to specifically rescue recognition memory but not associative memory, even though the reasons for this task-dependent efficacy of EMD-173 are still under investigation.

In conclusion, to the best of our knowledge, herein, we have performed the first characterization of the trisomic engram cells in the hippocampus, thereby identifying key cellular and molecular changes that might lead to defective engrams in DS. The identification of engram dysfunction in DS along with several candidate mechanisms will open new research avenues to explore DS from a completely different perspective.

CHAPTER II. EXPLORING THE ROLE OF ASTROGLIA IN CIRCUIT AND MEMORY ALTERATIONS IN DOWN SYNDROME

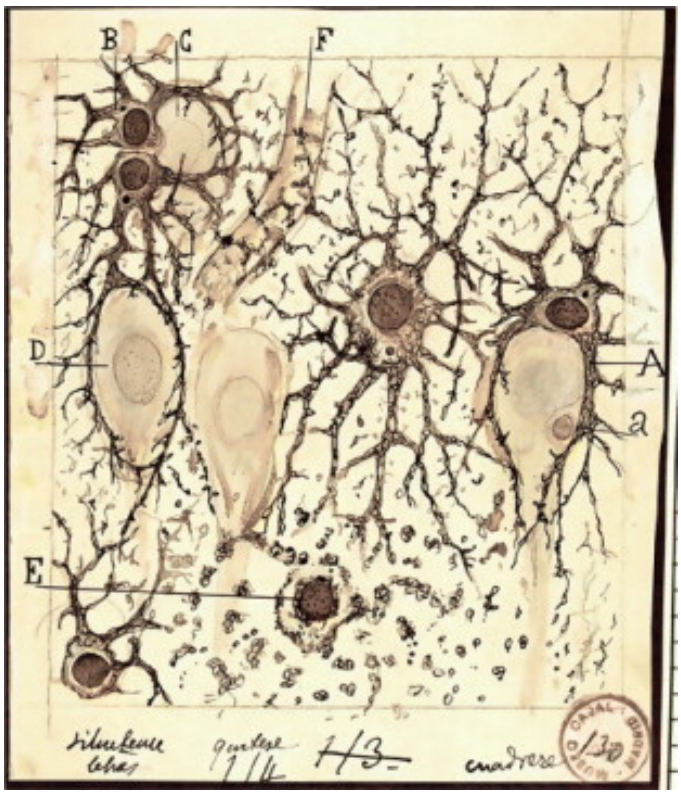

Drawings from Santiago Ramón y Cajal illustrating astrocytes and their processes (a), dividing astrocytes (B) embracing neuronal somas (C and D) and dendrites along with blood capillaries (F) in the human hippocampus using the gold chloride-sublimate staining. Image from [183].

Introduction

Learning and memory were once believed to be uniquely controlled by neurons. However, this vision has evolved into a more integrative conception in which astroglia, rather than just acting as metabolic supply and structural anchoring for neurons, interacts at distinct levels modulating neuronal communication. Compelling evidence including the discovery of astrocyte excitability and the existence of a bidirectional neuron-astrocyte communication led to coin the concept of tripartite synapse that suggests that astrocytes would interact at the synaptic level with neurons, modulating synaptic physiology [84,184]. Astrocytes integrate and respond to neuronal inputs, by triggering intracellular Ca^{2+} signals, which induce the release of gliotransmitters to the synaptic cleft, and modulate synaptic transmission [79,184].

Recently, genetic tools have made it possible to specifically manipulate astrocyte activity, unraveling novel functions that involve astrocytes in memory function in the healthy brain [82,89,185]. For instance, it was recently shown that the role of astrocytes do translate at the behavioral and cognitive level, since specifically blocking the vesicular release from astrocytes not only resulted in reduced ɣ brain oscillations, that are strongly correlated with memory storage and retrieval [186], but also in major impairments in memory consolidation [90]. On the contrary, astrocyte activation by Gq-DREADDs increased neuronal activation during memory acquisition induced *de novo* synaptic potentiation in CA1 and enhanced memory performance in control mice [82]. On the contrary, the Gi-pathway activation in astrocytes impaired remote, yet not recent, memory recall [89]. A recent study also found that astrocyte activation had anxiolytic effects and increased exploratory behavior [187]. Conversely, astrocyte manipulation has also underscored potential mechanisms by which defective astrocytes could contribute to memory deficits in a number of neurodevelopmental disorders revealing new pathogenic mechanisms in intellectual disability [122,188,189].

In DS, besides the alterations in the neuronal component, astrocytes are also affected at structural and functional levels [94,104,107,117]. However, the potential implications of astrocyte dysfunction on cognition are still unexplored. In

individuals with DS, the astroglial population is affected at different levels [190]. Astrogliosis is reported in several brain areas of individuals with DS and includes hypertrophy, proliferation and increase of astrocytic proteins such as GFAP and S100β [107,115]. In fact, the astroglial population is more abundant and mature than in age-matched controls [107,115]. Remarkably, in patient-derived iPSCs, S100β overexpression has been linked not only with impaired Ca^{2+} oscillations but also with reduced neuronal excitability [94]. Indeed, reduction in neuronal excitability was rescued by S100β gene expression normalization meaning that probably neuron-astrocyte crosstalk is impaired in DS [94]. Basal Ca^{2+} levels in astrocytes are elevated in Ts65Dn and Ts16 mouse models [191,192]. In spite of all the data suggesting that astroglial alterations in DS might affect astrocyte to neuron communication and possibly cognitive processes, hardly any studies have delved into this issue.

Although several anatomical and functional alterations have been described in trisomic astrocytes, how these alterations are distributed within the Ts65Dn hippocampus has not been explored. Therefore, we systematically studied astrocyte distribution, number and volume within the Ts65Dn hippocampus, detecting a sub-region specific mild to moderate astrogliosis. We also investigated whether the transcriptional profile of trisomic astrocytes was different from WT astrocytes in the hippocampus, underscoring potential signaling pathways and mechanisms that contribute to defective astrocyte-neuron crosstalk. We also found aberrant Ca^{2+} oscillations in trisomic astrocytes in CA1. We next studied whether the manipulation of astrocyte activity in Ts65Dn could influence neuronal activation, synaptic activity and memory function using chemogenetic tools. We found that the activation of the Gq pathway in trisomic astrocytes in CA1 increased neuronal ensemble allocation and enhanced memory performance in Ts65Dn when astrocytes were activated during memory acquisition. Herein, we present novel results that suggest that astrocytes can act as a dual player in the trisomic engram scenario: contributing to engram pathology but also as potential star-players capable of restoring memory deficits in Ts65Dn mice.

Methods

Animals

Ts(17^{16})65Dn (Ts65Dn) mice were obtained through crossings of a B6EiC3Sn a/A-Ts (17^{16})65Dn (Ts65Dn) female to B6C3F1/J males purchased from The Jackson Laboratory (Bar Harbor, USA). Genotyping was performed by amplifying genomic DNA obtained from the mice tail as described in (Liu et al., 2003). Mice had access to food and water *ad libitum* in controlled laboratory conditions with temperature maintained at 22 ± 1ºC and humidity at 55 ± 10% on a 12h light/dark cycle (lights off 20:00h). Mice were socially housed in numbers of two to four littermates. The colony of Ts65Dn mice was maintained in the Animal Facilities in the Barcelona Biomedical Research Park (PRBB, Barcelona, Spain).

According to Directive 63/2010 and Member States' implementation of it, all trials followed the "Three Rs" principle of replacement, reduction, and refinement. The investigation was conducted in accordance with the Standards for Use of Laboratory Animals No. A5388-01 (NIH) and local (Law 32/2007) and European regulations as well as MDS 0040P2 and the Ethics Committee of Parc de Recerca Biomèdica (Comité Ético de Experimentación Animal del PRBB (CEEA-PRBB)). A/ES/05/I-13 and A/ES/05/14 grant the CRG permission to work with genetically modified organisms. See the Ethics section for further information.

Experimental strategy

In the first set of experiments, we combined immunostaining, stereology, electrophysiology and single nuclei RNA-seq in adult WT and trisomic mice to identify possible changes in the number and size, and transcriptomic profile of Ts65Dn astrocytes in the hippocampus as shown in Figure 1. We next manipulated astrocyte activity *ex vivo* or *in vivo* by utilizing a chemogenetic approach that expressed a Gq-DREADD under the GFAP promoter. For *ex vivo* electrophysiology and calcium imaging experiments, mice were 5-7 weeks old at the time of the surgery while for behavioral experiments males were aged 8-10 weeks at the time of surgery. With this strategy, we first studied astroglial calcium dynamics and interrogated whether astrocyte-neuron crosstalk was impaired

combining electrophysiology and chemogenetics. Finally, in order to test whether memory alterations were contributed by astrocyte activity in trisomic mice, we manipulated astrocyte activity while mice learned to associate a particular context with fear.

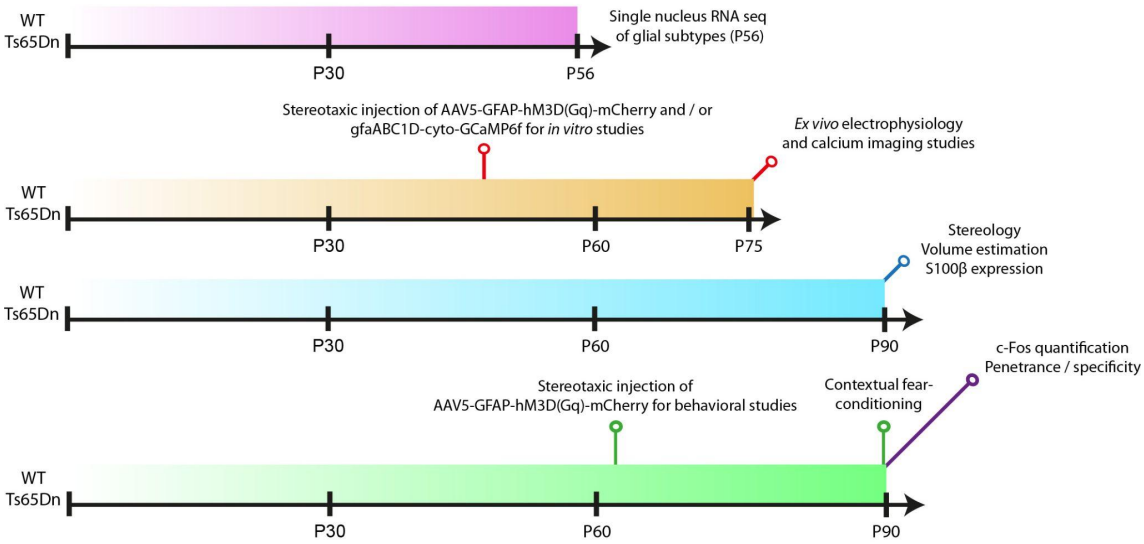

Figure 1. Overview of the experimental strategy.

Astrocyte tagging and manipulation techniques

Viral constructs

In order to identify and manipulate astrocytes, we used a construct that expressed the excitatory DREADD hM3D(Gq)-mCherry under the GFAP promoter. AAV_5-GFAP-hM3D(Gq)-mCherry was a gift from Bryan Roth (Addgene Viral prep # 50478-AAV5; RRID:Addgene_50478). We also used a construct to express a genetically encoded calcium indicator (cyto-GCaMP6f) under the gfaABC1 promoter. AAV_5-gfaABC1D-cyto-GCaMP6f was a gift from Baljit Khakh (Addgene viral prep #52925-AAV5; RRID: Addgene 52925-AAV5) [193]. Viral titers were 1.4 x 10^{13} genome copy (GC)/mL for AAV_5-GFAP-hM3D(Gq)-mCherry and 1.3 x 10^{13} GC/mL for gfaABC1D-cyto-GCaMP6f. For *ex vivo* calcium imaging studies, a 1:2 mixture of both AAV_5-GFAP-hM3D(Gq)-mCherry and AAV_5-gfaABC1D-cyto-GCaMP6f was used.

Pharmacogenetics (DREADD)

For the activation of the Gq-DREADD expressed in astrocytes we used CNO, an inactive form of clozapine drug. The synthetic ligand CNO binds to the modified human muscarinic receptor hM3D(Gq). CNO was dissolved in DMSO and diluted in 0.9% saline to yield a final DMSO concentration of 0.5%. Control animals received 0.5% DMSO saline solutions. For Gq-DREADD activation in the CA1 astrocytes, 3 mg/kg was intraperitoneally injected 30 min before the behavioral assays [82]. To activate Gq-DREADD in DG astrocytes, we modified the CNO dose to 1 mg/kg because the 3 mg/kg dose induced an extensive induction of granule cell activation. None of the CNO doses induced any behavioral alterations or signs of seizure activity.

Stereotaxic surgery injection

Intracerebral injections in CA1 were performed bilaterally at Bregma -2.5 mm AP, +/- 2.0 mm ML, -1.5 mm DV with the aid of a stereotaxic apparatus (Stoelting 51730). For *in vivo* studies 8-10 weeks old male at the time of surgery while for electrophysiology *ex vivo* studies, mice were 5-7 weeks at the time of surgery. Mice were anesthetized using ketamidol (7.5 mg/kg) and medetomidin (0.2 mg/kg). Fur was shaved from the incision site. Skin was wiped with ethanol 70% and small incisions were made along the midline to expose bregma and injection sites. Craniotomies were performed using a 0.45 mm diameter stereotaxic drill (RWD Life Science, model 78001). Viral vectors were injected at 60 nl/min through a 33-gauge cannula (Plastics One, C235I/Spc) attached to a Hamilton microsyringe (1701N; Hamilton) connected to a syringe pump (PHD 2000, Harvard Apparatus) for 10 min. AAV_5-GFAP-hM3D(Gq)-mCherry was injected with a volume of 500 nl/hemisphere for behavioral studies. For *ex vivo* calcium imaging studies, a volume of 600 nl/hemisphere of a 1:2 mixture of both AAV_5-GFAP-hM3D(Gq)-mCherry and AAV_5-gfaABC1D-cyto-GCaMP6f was used. Cannulas remained 10 min after injection to allow virus diffusion and were slowly withdrawn during 5 min. Skin was sutured and mice were treated with 0.03 mg/kg buprenorphine as analgesic. Mice were recovered from anesthesia by Atipemazol (1 mg/kg) and maintained on a heating pad until fully recovered. Mice

were allowed to recover for 3 weeks before experimentation to allow construct expression. After sacrifice, all injection sites were verified histologically. Only those mice in which virus expression was restricted to the dorsal CA1 were included for analysis.

In the experiment of astrocyte Gq-DREADD activation in the DG, only the stereotaxic coordinates (Bregma -2.2 mm AP, ± 1.3 mm ML, -1.9 mm DV) and the volume (200 nl/hemisphere) were changed. In this case, only those mice in which virus expression was restricted to the dorsal DG were included for analysis.

Behavioral assays

Contextual fear-conditioning (CFC) paradigm

CFC is a hippocampal-dependent test used to interrogate associative learning. Importantly, fear memory is altered in trisomic mice. We adapted a training paradigm for contextual fear-conditioning (3 shocks; 0.6 mA, separated by 60 s) used in previous studies (Figure 1A) [4]. Briefly, mice are introduced into a new environment and an aversive stimulus is delivered at different time points. The next day mice are reexposed to the same context without any shocks delivered. If mice recall and associate the context to the aversive stimuli, they will typically exhibit a freezing reaction when placed back in that setting. As a reaction to fear, freezing is described as "lack of movement other than breathing." Trained context was associated with fear-related learning since it was paired to the unconditioned (shock) stimulus. Trained context (30 x 25 x 33 cm) had grid floors and an opaque square ceiling. After each session, the apparatus was cleaned with 70% ethanol.

All mice were individually handled and habituated to the investigator for five min during three days before the experiment. Mice were trained in the trained context during 300 s, with three 0.6 mA shocks of 2 s duration delivered at 120 s, 180 s and 240 s, respectively. After training mice were placed back to their home cages. All testing sessions in Context B were 180 s in duration. Testing conditions were identical to training conditioning, except that no shocks were delivered. At the end of each session mice were placed in their home cages.

Freezing behavior (>800 ms immobility) was automatically detected by Packwin 2.0 software (Panlab, Harvard Apparatus). Cages were calibrated according to manufacturer instructions each day of experiment.

Histology

Immunohistochemistry

In order to quantify the expression of c-Fos 90 min after memory acquisition or memory recall, mice were sacrificed with CO_2 and transcardially perfused with ice-cold PBS followed by 4% PFA in PBS (pH 7.4). Brains were extracted and post-fixed in 4% PFA at 4ºC overnight. Brains were then transferred to PBS and 40 µm coronal consecutive brain sections were obtained employing a vibratome (Leica VT1200S, Leica Microsystems), collected in PBS and stored in cryoprotective solution (40% PBS, 30%, glycerol and 30% polyethylene glycol) for long-term storage. For immunofluorescence studies, 3-6 sections per mice were selected centered on the injection sites and according to stereotaxic coordinates Bregma, -1.74 to -3.24 mm, (mouse brain atlas; Franklin & Paxinos, 2019) with the aid of a bright-field microscope (Zeiss Cell Observer HS). Brain sections were washed with PBS (3 x 10 min). Then, sections were permeabilized with 0.5 % Triton X-100 in PBS (PBS-T 0.5 %) (3 x 15 min) and blocked with 10% of Normal Goat Serum (NGS) for two h, at RT. Sections incubated in PBS-T 0.5% and NGS 5 % with the primary antibodies overnight at 4ºC washed again (PBS-T 0.5 % 3x15 min) and incubated with the secondary antibodies (PBS-T 0.5 % + NGS 5 %) for two h at room temperature protected from light. Finally, samples were washed with PBS-T 0.5 % (3x15 min) followed by PBS washing (3x10 min) to remove the detergent and sections were mounted and coverslipped into a pre-cleaned glass slide with Fluoromount-G medium with DAPI (Thermo Fisher Scientific; #00-4959-52). c-Fos was stained with rabbit anti-c-Fos (1:500, Santacruz, #Sc-7202) and visualized with anti-rabbit Alexa-647 (1:500; Thermo Fisher Scientific, #A-21443). GFAP was stained with mouse anti-GFAP (1:250; Millipore, #MAB360) and visualized with anti-mouse Alexa-488 (1:500; Thermo Fisher Scientific, #A-11001). S100β was stained with rabbit anti-S100β (1:1000; Synaptic systems, #287003) and visualized with anti-rabbit 488 (1:500; Thermo

Fisher Scientific, #A-11008). NeuN was stained with mouse anti-NeuN (1:500; Millipore, #MAB377) and visualized with anti-mouse Alexa 555 (1:500; Thermo Fisher Scientific; #A-11001). Prior to immunostaining all the samples, an optimization of the primary antibodies and PBS-T conditions was performed with sections not needed for the estimations but sectioned with the same conditions. Serial dilutions of primary antibodies ranging from 1:100 to 1:1000 were prepared while maintaining the secondary antibody concentration constant (1:500). By confocal microscopy, the best primary antibody concentration was selected taking into account the achievement of low background noise and the signal level obtained with the same laser configuration.

Cell counting

In order to quantify the density of activated cells we used image analysis with the help of ImageJ (NIH, Bethesda) since c-Fos+ cells are easy to identify both in CA1 and DG. With this method, we were able to quantify the density of c-Fos+ cells, the co-localization of c-Fos and Gq-DREADDs and the specificity and penetrance of Gq-DREADDs in astrocytes. c-Fos density in CA1 and DG is expressed in cells/mm^3. 40 µm coronal sections were obtained from the dorsal hippocampus centered in the coordinates where the viruses were injected (-1,74 to -3,24 mm AP; relative to bregma) using a vibratome (Leica VT1200S, Leica Microsystems). Confocal fluorescence images were acquired on a Leica TCS SP5 inverted scanning laser microscope (Leica Microsystems) using a 20x/0.70 NA objective. Cell counting was performed using the Cell Counter plugin on ImageJ software (NIH, Bethesda) in a z-stack (3 µm step size). The somatic layer of the CA1 or DG layer was selected as a region of interest (ROI) and was manually delineated according to the DAPI signal in every section. Alexa 488, Alexa 568 and Alexa 647 channels were filtered and combined to produce composite images. Equal cutoff thresholds were applied to remove signal background from images. The number of double positive (hM3Dq-mCherry and c-Fos) and single positive (c-Fos) cells were counted in the CA1 or DG in 3-6 consecutive coronal sections (spaced 200 µm between them) per mouse. The same procedure was used to quantify GFAP, the only difference being the

channels used to create composite images. Data was analyzed using R studio (Version 1.1.463). Imaging and quantifications were performed blind to experimental conditions.

Estimation of astroglial volume

In order to estimate astroglia volumes, we utilized the S100β marker since it is mainly expressed in the astrocyte soma. Confocal fluorescence images were acquired at 20x magnification on a Leica TCS SP5 inverted scanning laser microscope creating a composite image of the entire dorsal hippocampus at 16 bits. Tissue was only exposed to the lasers during the moment of image acquisition to prevent photobleaching. To minimize quenching of fluorescence, z-stacks were rapidly scanned at 1 µm increments. After image acquisition, stitched images of the dorsal hippocampus were converted to binary masks using ImageJ (Figure 2AB). To estimate the size of astroglia, the somatic area was semi-automatically identified in every plane and the volume was calculated using the Cavalieri estimator (Figure 2C-E):

$$\mathbf{Volume} = \sum(\mathbf{A}) \times \mathbf{n} \times \mathbf{T}$$

Where:

- A = area of an astrocyte in a single plane (in μm^2)
- n = number of planes
- T = spacing between sections (in µm)

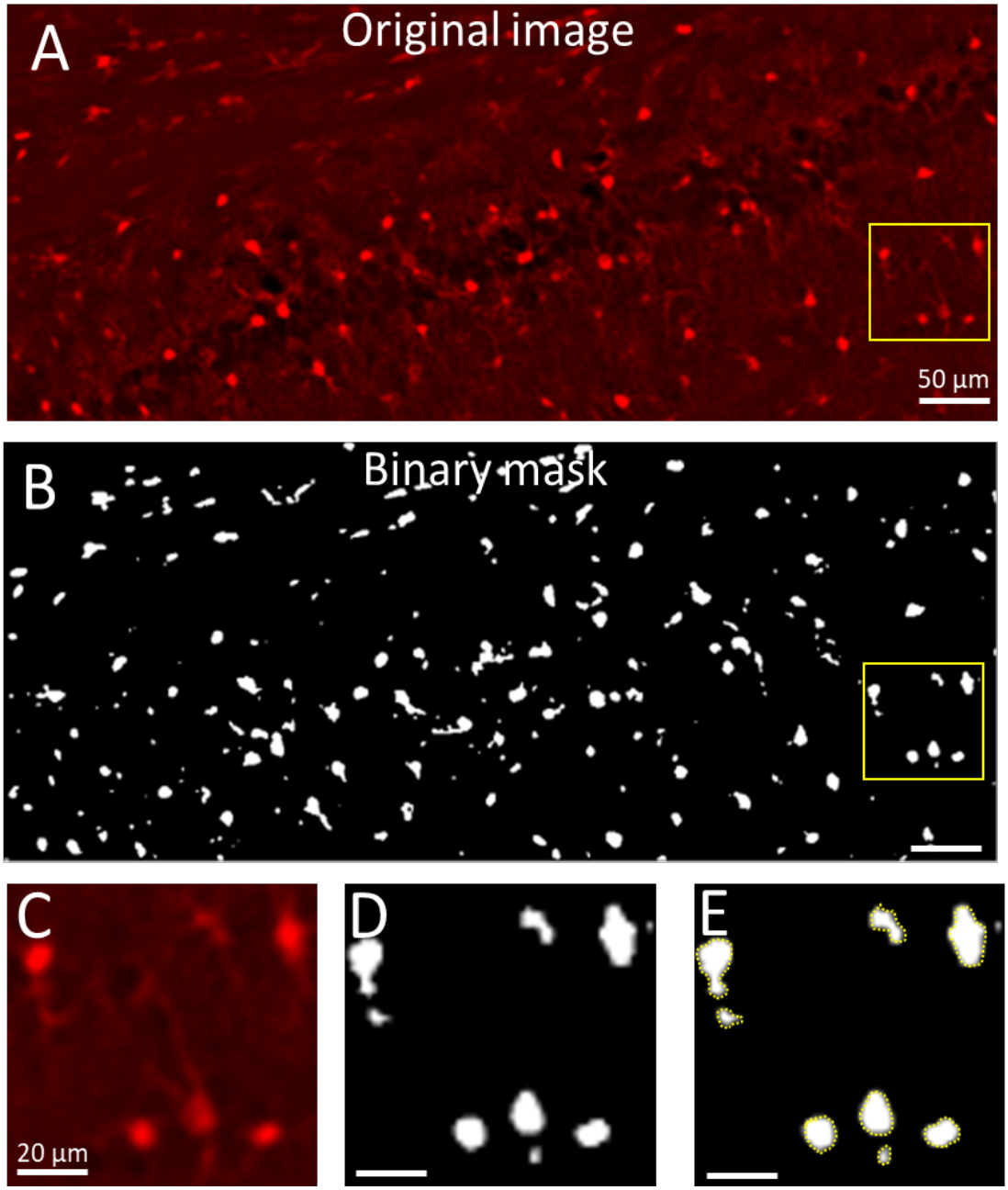

Figure 2. Unbiased technique used for astrocyte volume estimation. (A) Confocal image showing S100β immunostaining in the CA1 region of the hippocampus (in red). Scale bar = 50 µm. **(B)**. Same image processed to create a binary mask. Astrocytes somas are depicted in white while the background is completely black. Scale bar = 50 µm. **(C-D)** Zoomed image of A and B, respectively. Scale bar = 20 µm. **(E)** Semi-automatic detection of astroglial somatic area in the binary mask image. Scale bar = 20 µm.

Quantification of S100β fluorescence intensity

In order to quantify the fluorescence intensity of S100β in euploid and trisomic astrocytes, confocal fluorescence images were acquired at 20x magnification on a Leica TCS SP5 inverted scanning laser microscope creating a composite image of the entire dorsal hippocampus at 16 bits. Confocal acquisition settings were maintained constant for all the samples and all images were taken the same day. Tissue was only exposed to the lasers during the moment of image acquisition to prevent photobleaching. The mean intensity of astroglial somas was performed by manually delineating the somas in accordance with the S100β signal using ImageJ. Signal background was subtracted for every region and image.

Stereological estimates

Stereological estimates were performed using a Leica DMI6000B inverted microscope (Leica Microsystems) equipped with a motorized stage, a microcator and a digital camera connected to a PC was used to obtain microscopic captures. Images were analyzed with the newCAST software (Version: 5.3.0.1562) from Visiopharm Integrator System. All the estimations were performed single-blinded to avoid researcher bias.

Tissue sampling and stereological methods

In order to precisely quantify the number of neurons and astrocytes in the different regions of the dorsal hippocampus we used stereology, a technique that utilizes stringent sampling methods to obtain three-dimensional information about the entire tissue that is unbiased. Although 2D morphometry can provide quantitative information about the tissue sections being examined, it also makes several assumptions about the tissue, all of which are sources of bias, and can thus only be used in specific cases. Given the high neuronal density in CA1 and in the DG, stereological methods such as the Optical Disector prevent double-counting and precisely corrects for the tridimensional volume of the region of study. Mice were sacrificed with CO_2 and transcardially perfused with ice-cold PBS followed by 4% PFA in PBS (pH 7.4). Brains were extracted and post-fixed in 4% PFA at 4ºC overnight. Brains were then transferred to PBS and 40 µm coronal consecutive

brain sections were obtained using a vibratome (Leica VT1200S, Leica Microsystems), collected in PBS and stored in cryoprotective solution (40% PBS, 30%, glycerol and 30% polyethylene glycol) for long-term storage. Every 6th section was collected using the principle of systematic uniform random sampling. In total, six sections per mice were selected from bregma, -1.74 to -3.24 mm, (mouse brain atlas; Franklin & Paxinos, 2019) with the aid of a bright-field microscope (Zeiss Cell Observer HS). We next followed the immunohistochemistry protocol previously described to stain and visualize astrocytes and neurons.

Prior to starting any stereological quantification, a quality check was performed in every section based on our expectations for global hippocampal architecture and specific immunostaining patterns. All the estimations were performed in one side, randomly chosen. Stereological estimates were performed in concrete ROIs of the hippocampus. Regions of interest were manually delineated according to the Franklin & Paxinos, 2019 brain atlas [194] and the immunohistochemistry labeling (see below). For astrocytic and neuronal populations 63x Oil 1.4 numerical aperture (NA) lens objective was required to resolve fine details in order to be able to: (i) differentiate neurons inside a high density of cells (i.e CA1 and DG) and (ii) clearly distinguish between somatic and astrocytic processes when moving through the z-axis.

Volume estimation

Volume estimation of the selected ROIs was calculated according to the Cavalieri principle as it provides an estimate of the volume of any object when it is divided into parallel cross sections. At least 200 points of known area were required in each ROI to obtain accurate volume estimations. For this reason, a specific point configuration was configured to ensure that more than 200 points in total were counted for every ROI across all the selected slices. For the Cavalieri estimation, the area of each ROI was 100 % covered.

Volume estimation for the whole ROI and for every slice was calculated according to this formula:

$$\textbf{Volume} = T \times a(p) \times \Sigma P$$

Where:

- T = spacing between sections
- a(p) = area per point given by each specific configuration.
- Σ P = sum of points inside the ROI.

Estimation of the number of neurons and astrocytes

Optical Disector (OD) uses thick sections and a microcator that allows focusing through the z-axis of the section to count cells directly as they appear in an unbiased tridimensional counting frame (CF). For every region of interest, the percentage of the total sampling area was adjusted to obtain from 21-24 CFs. This range was established for two reasons: (i) fixing the same sampling area for every ROI can lead to biased results as hippocampal subregions vary across the anteroposterior axis and (ii) this CF range covers a representative area of each structure and is superior to the values found in the literature, which ensures a reliable estimation [195]. Real thickness of the planar sections was calculated for every section to avoid biased assumptions and adjusting the tridimensional CF accordingly, as tissue is usually shrinked after histological fixation. CFs were uniform and randomly sampled across each ROI. CF zero position was set when the first cell became clear to vision meaning the top view of the histological preparation. Cells were only counted if the nucleus was clearly visible inside the disector along the z-axis section or touching the inclusion lines (right and upper border), otherwise neurons were discarded.

Zero µm position was set when the first cell became clear to vision e.g. the top view of the histological preparation. Cells were only counted if the nucleus was clearly visible inside the disector along the z-axis section or touching the inclusion lines (right and upper border), otherwise neurons were discarded. Each time that the upper right corner of the CF was inside the delineated ROI, a corner point

(CP) mark was introduced to the counting meaning that the CF was hitting the reference tissue. Once a CF was quantified, the microscope returned to the zero position and the CF went to the next sampling position. To avoid potential double counting, the optical plane was moved throughout the whole thickness of the preparation section to ensure correct cell identification. Cell densities were calculated according the Nv formula [196]:

$$N_V := \frac{\overline{t_{Q^-}}}{BA} \cdot \frac{\sum Q^-}{h \cdot (a/p) \cdot \sum P}$$

Where:

- tQ-: is the number-weighted mean section thickness.
- BA: Block Advance: the cut thickness of the section on a calibrated cutting device.
- h: disector height.
- (a/p): a is the area of the CF and p the number of points associated to the frame (1 - using the upper right corner of the CF)
- Σ P: is the sum of corner points hitting reference tissue.

The total number of cells (N) was estimated by the product of the cell density (Nv) and the volume (Vref) obtained from Cavalieri estimations:

$$\mathbf{N = V_{ref} \times N_v}$$

CF dimensions were adjusted based on the lens objective used and the surface of a specific area to cover. For the somatic layers of the neuronal population the frame was adjusted to cover 5% of the area of the field of view given for the 63x Oil objective.

Calcium Imaging

To characterize spontaneous and evoked Ca^{2+} oscillations, coronal hippocampal slices (300 µm) were obtained from 8-10 weeks of Ts65Dn and WT littermates injected with AAV_5-GFAP-hM3D(Gq)-mCherry and AAV_5-gfaABC1D-cyto-GCaMP6f. Animals were sacrificed, brains were quickly removed and sliced using a vibratome (Leica VT1200S, Leica Microsystems) in ice-cold oxygenated low

Ca^{2+} ACSF (126 mM NaCl, 2.6 mM KCl, 26 mM $NaHCO_3$, 1.25 mM NaH_2PO_4, 10 mM Glucose, 1 mM $MgCl_2$, 0.625 mM $CaCl_2$). Slices were then incubated for 1h with oxygenated normal Ca^{2+}ACSF (126 mM NaCl, 2.6 mM KCl, 26 mM $NaHCO_3$, 1.25 mM NaH_2PO_4, 10 mM Glucose, 1 mM $MgCl_2$, 2 mM $CaCl_2$). Individual slices were transferred to a recording chamber in an Olympus BX51WI upright microscope at room temperature (20-22ºC) in the presence of picrotoxin (50 µM). Images were acquired at 1 Hz for 240 s having 6-15 astrocytes in the field of view using epifluorescence microscope (Olympus BX51 WI upright). In the first 120 s the spontaneous astrocyte calcium activity was measured. Between second 118 and 120, a 2 s pulse (1 bar) was applied using a patch pipette to locally apply CNO (1 mM) into the field of view. Then, astrocyte calcium activity post CNO administration was measured from 120 s to 240 s. Co-localization of GCaMP6f with hM3D(Gq)-mCherry was checked after the recording. Image acquisition and image analysis was performed using a cellSens software (Olympus). Ca^{2+} oscillations were recorded from the cell body. Background was subtracted for every image. Data was then fed into a second in-house code kindly provided by Dr. Gertudis Perea and Julio Esparza [197] that identified Ca^{2+} events when the signal showed maximum values above 2 times the standard deviation of the previous steady signal. Ca^{2+} variations were estimated as changes in the fluorescence signal (ΔF) over the baseline (F_0). Mean event frequency and amplitude values for each experimental group were obtained by averaging the mean amplitude and frequency over a 2 minute period. Astrocytes with no oscillations were not included in the analysis. Frames with movement artifacts were excluded for the analysis.

Electrophysiology

Minimal stimulation protocol

We used a minimal stimulation protocol to investigate whether astrocyte to neuronal communication is impaired in Ts65Dn mice. Coronal hippocampal slices (300 µm) were made from 8-10 weeks WT and Ts65Dn littermates previously injected with AAV5-GFAP-hM3D(Gq)-mCherry in CA1. Animals were decapitated, brains were quickly removed and sliced using a vibratome (Leica

VT1200S, Leica Microsystems) in NMDG solution (93 mM NMDG, 2.5 mM KCl, 30 mM $NaHCO_3$, 1.2 mM NaH_2PO_4, 20 mM HEPES, 5 mM sodium ascorbate, 2 mM thiourea, 3 mM sodium pyruvate, 25 mM Glucose, 10 mM $MgCl_2$, 0.5 mM $CaCl_2$). Slices were then incubated for 1h with oxygenated normal Ca^{2+}ACSF (126 mM NaCl, 2.6 mM KCl, 26 mM $NaHCO_3$, 1.25 mM NaH_2PO_4, 10 mM Glucose, 1 mM $MgCl_2$, 2 mM $CaCl_2$). Individual slices were transferred to a recording chamber in an Olympus BX51WI upright microscope. Electrophysiological recordings were acquired at 20kHz with Multiclamp 700B (Axon Instruments) and digitized at 16 bits (Axon 1550B Digidata, Molecular Devices). Patch pipettes of borosilicate glass were pulled (Sutter P-1000, Sutter Instruments), and filled with internal solution for whole-cell somatic current clamp recordings (135 mM $KMeSO_4$, 10 mM KCl, 10 mM HEPES, 5 mM NaCl, 2.5 mM ATP-Mg, 0.3 mM GTP-Na). The membrane potential was held at -70 mV while fast and slow whole-cell capacitances were neutralized and series resistance was compensated (by around 70%). Before and after the trials, electrophysiological parameters were monitored. Throughout the experiment, a -5 mV pulse was used to keep track of the series and input resistances. When the series and input resistances, resting membrane potential, and stimulus artifact duration did not fluctuate by more than 20%, recordings were considered stable.

Synaptic responses in CA1 were evoked by stimulating the Schaffer collateral fibers (SCs) with an extracellular bipolar tungsten filled with ACSF electrode delivering monophasic currents of 50 μs duration at 0.5 Hz. Recordings were performed in the presence of picrotoxin (50 μM). Stimulus intensity was set to stimulate single or very few synapses and was kept constant during the experiment. Stimulus intensity was also adjusted to achieve a 50% of failures and 50% of success of CA1 evoked synaptic responses. Basal evoked-responses were measured for 5 min. At min 5, CNO was locally applied at 1mM with a puff (2 s, 1 bar) and then activity was measured for 10 more min. The following synaptic parameters were examined: synaptic efficacy (mean peak amplitude of all responses, including failures); synaptic potency (mean peak amplitude of the successes); probability of release (Pr, ratio between number of successes versus total number of stimuli); and paired-pulse facilitation (PPF = [(2nd EPSC - 1st

EPSC)/ 1st EPSC]). Stimuli before and after astrocyte stimulation with CNO were used to evaluate synaptic parameters. Experiments were performed at room temperature (22 ± 2°C).

Single Nucleus RNA sequencing

Nucleus isolation

Mice were sacrificed by cervical dislocation and hippocampus were dissected and placed in cold Hanks' Balanced Salt Solution (Sigma #55021C). To obtain a nuclei suspension, the "Frankenstein" procedure was used [198]. Each hippocampus was placed in a fresh tube with 500 µL cold EZ lysis buffer (Sigma #3408) and a sterile RNase-free douncer (Mettler Toledo #K-749521-1590) was used to homogenize the buffer. To eliminate any leftover material fragments, the homogenate was filtered through a 70 µm-strainer mesh and centrifuged at 500 g for 5 min at 4 ºC. The nuclei pellet was resuspended in 1.5 mL EZ Lysis Buffer and centrifuged again. Supernatant was discarded and 500 µL of Nuclei Wash and Resuspension Buffer (NWRB, 1X PBS, 1% BSA and 0.2 U/µL RNase inhibitor (Thermo Scientific #N8080119) was added to the pellet. After incubation, the pellet was resuspended in 1mL of NWRB. The nuclei suspension was centrifuged once again, and the washing step with 1.5 mL of NWRB was repeated. Nuclei were then resuspended in 500 µL of 1:1000 anti-NeuN antibody conjugated with Alexa Fluor 647 (Abcam, #ab190565) in PBS and incubated in rotation for 15 min at 4 ºC. Nuclei were rinsed with 500 µL of NWRB and centrifuged again after incubation. To create a single-nuclei suspension, nuclei were resuspended in NWRB mixed with DAPI and filtered through a 35 µm cell strainer.

10x single-cell barcoding, library preparation and sequencing

NeuN negative neuronal nuclei were sorted using fluorescent activated nuclear sorting (FANS). 10.000 nuclei from each sample were sorted directly into a 96-well plate prefilled with 10X RT buffer prepared without the RT Enzyme Mix using a 70 µm nozzle to minimize the volume deposited. Following sorting, RT Enzyme C was added, and the volume of each well was increased to 80 µL with nuclease-

free water. The Chromium Single Cell Chip was loaded with 75µL of the nuclei plus RT mix. The manufacturer's instructions (10x Genomics Chromium Single Cell Kit Version 3) were followed for all downstream cDNA synthesis, library preparation, and sequencing. Libraries were prepared and sequenced. Libraries were sequenced on a NovaSeq 6000 S1 to an average depth of approximately 20.000 reads per cell.

10x data pre-processing

The readings were matched to the reference genome, including exons and introns, and transformed to mRNA molecule counts using the manufacturer's Cellranger pipeline (CellRanger v3.0.1). We counted the number of genes for which at least one read was mapped for each nucleus, then discarded any nuclei with fewer than 200 or more than 2500 genes, respectively, to eliminate low-quality nuclei and duplets. Genes found in fewer than six nuclei were discarded. To normalize for differences in coverage, expression values Ei,j for gene I in cell j were calculated by dividing UMI counts for gene I by the sum of UMI counts in nucleus j, multiplying by 10,000 to create TP10K (transcript per 10,000) values, and finally computing log2(TP10K + 1) (using the NormalizeData function from the Seurat package v.2.3.4 [199]).

Dimensionality reduction, clustering and visualization

Using the RunPCA method in Seurat (a wrapper for the irlba function), we computed the top 60 principle components using the scaled expression matrix restricted to the variable genes. UMAP (Uniform Manifold Approximation and Projection) used the scores from these principal components as input to downstream grouping and visualization (UMAP). The FindNeighbors and FindClusters functions in Seurat (resolution = 0.6) were used to cluster the data. After that, using UMAP, the clusters were visualized. Before integrating with the IntegrateData function, reference anchors between genotypes were found, and the combined data was analyzed using the same procedures.

Identification of marker genes within every cluster

The FindAllMarkers function was used to find cluster-specific marker genes using a negative binomial distribution (DESeq2). A marker gene was defined as having a detectable expression in > 20% of the cells from the related cluster and being >0.25 log-fold greater than the mean expression value in the other clusters. We were able to choose markers that were highly expressed within each cluster while still being restricted to genes unique to each individual cluster.

Identification of differentially expressed genes between WT and Ts65Dn

Using a hypergeometric test (function enrichGO from the de clusterProfiler package in R) [200], the differential expression profiles from each cellular subtype were evaluated for enriched Gene Ontology processes, and false discovery rate (FDR) was used to compensate for multiple hypotheses. Significantly enriched processes had a p adjusted value of less than 0.05. The universe for the hypergeometric test was the entire list of genes found in the dataset.

Diffusion map

Using the DiffusionMap function from the destiny package in R [201] (with k = 30 and a local sigma), the diffusion components were calculated using the cell embedding values in the top 15 principal components (generated either on the scaled expression matrix restricted to the variable genes in the 7-month-old mouse dataset or on the aligned canonical correlation analysis (CCA) subspace for the entire time-course data). For data visualization, we selected the top two diffusion components. This function allowed us to discover drivers of cell embedding at a global or subregion level using non-linear low-dimensional embeddings like UMAP or Diffusion Map.

Gene set enrichment

Using a hypergeometric test (shinyGO) [202], the differential expression signatures from each cellular subtype were examined for enriched Gene Ontology processes, and multiple hypothesis testing was adjusted for using FDR. Processes were classified as considerably enriched when their p-adjusted value

was less than 0.05. The universe for the hypergeometric test was the entire list of genes found in the dataset.

Cellular proportion

The proportional fraction of nuclei in each cell type was standardized to the total number of nuclei taken from each library to acquire insight into cell type variations in the trisomic hippocampus. We used single cell differential composition analysis (scDC) to bootstrap proportion estimates for our samples to see if any changes in cell-type proportion were statistically significant [203]. To see if there were any changes in cell-type proportion, we used a linear mixed model (random effect of subject).

Statistical analysis

When two conditions were compared, the Shapiro-Wilks test was conducted to check the normality of the data and Fisher's F test was used to assess the homogeneity of variances between groups. When data met the assumptions of parametric distribution, results were analyzed by unpaired student's *t*-test. Paired *t*-tests were employed to compare paired variables. Mann-Whitney-Wilcoxon test was applied in cases where the data did not meet the requirements of normal distribution. Statistical analyses were two-tailed.

For comparison between more than two groups, two-way ANOVA with different levels was conducted followed by Tukey HSD multiple comparison test. Bartlett test was used to assess the homogeneity of variances between groups. If the data distribution was non-parametric, the Kruskal-Wallis test was used followed by Mann Whitney-Wilcoxon test. All statistical analyses were two-tailed.

The statistical test used is indicated in every Figure.

Differences in means were considered statistically significant at $p < 0.05$.

Data analysis and statistics were performed using R studio (Version 1.1.463).

Key resources table

Table 1. Antibodies

Reagent	Source	Identifier
mouse anti-GFAP	Merck-Millipore	MAB360
rabbit anti-S100β	Synaptic systems,	287003
Mouse anti-NeuN	Merck-Millipore	MAB377
Rabbit anti-c-Fos	Santacruz	Sc-7202
Goat anti-mouse (Alexa Fluor 555)	Thermo Fisher Scientific	A-11001
Goat anti-rabbit (Alexa Fluor 488)	Thermo Fisher Scientific	A-11008
Chicken anti-rabbit (Alexa Fluor 647)	Thermo Fisher Scientific	A-21443
Streptavidin (Alexa Fluor 488)	Thermo Fisher Scientific	S32357
anti-NeuN conjugated (Alexa Fluor 647)	Abcam	ab190565

Table 2. Bacterial and Virus Strains

Resource	Source	Identifier
AAV_5-GFAP-hM3D(Gq)-mCherry	Addgene	50478-AAV5
AAV_5-GFAP104-mCherry	Addgene	58909-AAV5
AAV_5-gfaABCD-cyto-GCaMP6f	Addgene	52925-AAV5

Table 3. Chemicals, peptides and recombinant proteins

Reagent	Source	Identifier
Ethylene glycol	Sigma	107-21-1
PBS	CRG facility	NA
Glycerol	Sigma	G5516
Picrotoxin	Sigma	P1675
Fluoromount	Thermo Fisher Scientific	00-4959-52
Clozapine N-oxide	Tocris	4936
Triton-X	Sigma	9036-19-5

Results

1. Ts65Dn hippocampus display a subregion-specific increase of astrocyte number

Previous studies in individuals with DS and in DS mouse models reported an increase in the number and size of astrocytes in different brain areas [107,114,115,117]. However, a systematic study of the astroglial distribution in the hippocampus has not yet been fully delineated.

We systematically studied the number, volume and expression of astroglial proteins in the dorsal hippocampus. Both S100β and GFAP are specific immunohistochemical markers for astrocytes. In all hippocampal subregions, we detected GFAP and S100β, which typically exhibited a small soma with ramified processes. Microscopic examination of S100β and GFAP revealed reliable S100β immunofluorescent labeling of astroglial somas while GFAP targeted mainly the astroglial processes (Figure 3A). Since our aim was to count cell bodies of astroglia by means of the optical dissector principle (see Methods), we decided to count the S100β positive cells.

We quantified the total number of astrocytes and neurons corrected by the regional volumes of the dorsal hippocampus in young adult mice (3 months). Cellular densities were calculated by the systematic-random optical dissector method and the regional volumes were estimated using the Cavalieri estimator. Both in WT and in Ts65Dn hippocampus, the distribution of S100β positive cells was homogenous across all the dendritic layers. However, astrocytes were less abundant in the somatic layers of the hippocampus (CA1 pyramidal layer, CA3 pyramidal layer and DG granule cell layer) and in smaller areas such as the DG polymorphic layer and CA3 *stratum lacunosum*.

The number of astrocytes was quantified in the dendritic and somatic layers of the CA1, CA3 and DG regions of the dorsal hippocampus along with the number of neurons in the somatic layers as shown in Figure 3B. The number of NeuN+ cells did not differ between WT and Ts65Dn mice in CA1, CA3 and DG (Two-tailed T test; N.S.; Figure 3C). However, the number of S100β+ cells was significantly higher in CA1 *stratum lacunosum* (Two-tailed T test; $p < 0.001$ Figure

2D), CA1 *stratum oriens* (Two-tailed T test; $p < 0.05$ Figure 3D) and DG granule cell layer (Two-tailed T test; $p < 0.05$; Figure 3F). No differences were observed in the volumes of hippocampal subregions or layers between WT and Ts65Dn mice.

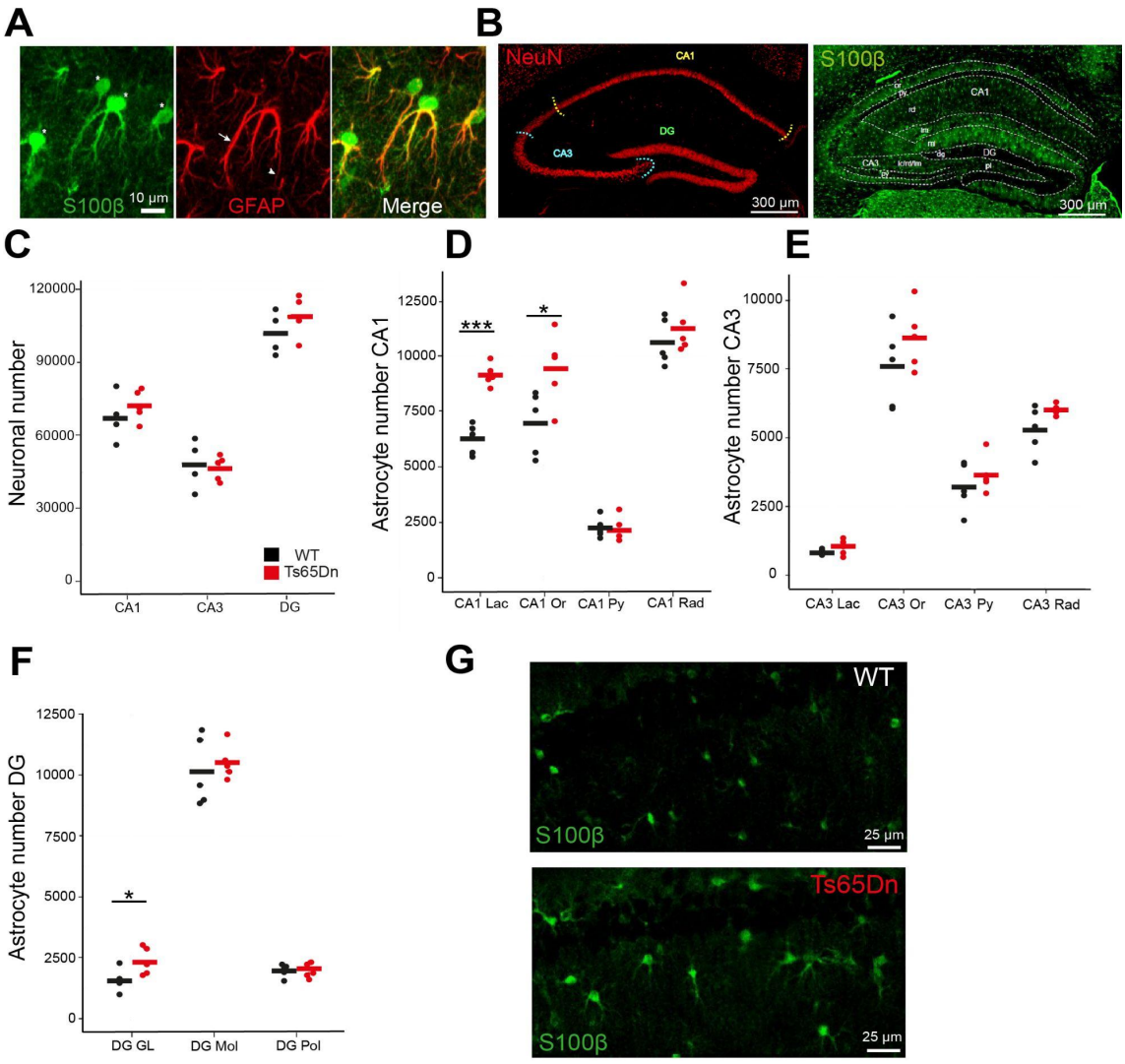

Figure 3: Subregion-specific astrogliosis in Ts65Dn hippocampus. (A) Representative Images showing different antibodies used against astroglial antigens. Left: S100β is mainly located in the astrocyte soma (*). Middle: GFAP is mainly distributed in the astroglial processes (arrows and arrowheads). Right: Merged image. Scale bar = 10 µm **(B)** Left: Image showing the neuronal distribution in the dorsal hippocampus using the NeuN neuronal marker (in red). Right: Image showing the astroglial distribution in the dorsal hippocampus using S100β (in green). Scale bar = 300 µm. **(C)** Stereological estimations of neuronal numbers (CA1, CA3 and DG) in the somatic regions of the hippocampus. Black dots indicate the estimations of every WT mouse while red dots indicate the estimations of Ts65Dn mouse. Each dot represents the mean of 6 different sections. Horizontal lines indicate the mean values for every group. **(D)** Stereological estimations of S100β+ cells in the CA1 somatic (CA1_py) and dendritic layers (CA1_Lac, CA1_Or and CA1_Rad). **(E)** Stereological estimations of S100β+ cells in the CA3 somatic (CA3_py) and

dendritic layers (CA3_Lac, CA3_Or and CA3_Rad). **(F)** Stereological estimations of astrocyte numbers in the DG somatic (DG_GL) and dendritic regions (DG_Mol and DG_Pol). All data are expressed as mean ± SEM. WT (n = 4-5 mice), Ts65Dn (n = 5 mice). **(G)** Representative image of WT (above) and Ts65Dn (below) showing the S100β expression in the CA1 region of the hippocampus. It is noticeable that Ts65Dn are larger than WT astrocytes. Scale bar = 25 μm. Two-tailed T test. Data are expressed as mean of every group *P < 0.05, **P < 0.01, ***P < 0.001.

2. Astrocyte volume is increased in Ts65Dn astrocytes

To further investigate whether the subregional increase in astrocyte number was also accompanied by an increased astroglial size, we systematically studied astrocyte volume in the dorsal hippocampus. The astroglial volume was estimated by the astrocyte cell bodies, using S100β. This study revealed that in all hippocampal regions, except for the CA3 pyramidal layer (Mann-Whitney; p = 0.12; Table 4), the astroglial volume was larger in Ts65Dn compared to euploid astrocytes (Mann-Whitney; p < 0.05; Table 4). Astroglial volumes and statistical significance comparing genotypes in the different hippocampal areas are summarized in Table 4.

Hippocampal region	**WT** (μm^3)	**Ts65Dn** (μm^3)	**p-value**
CA1 stratum oriens	697,13 ± 29,97 (106)	883,22 ± 37,79 (103) ***	5,3e-05
CA1 pyramidal layer	630,50 ± 24,74 (87)	817,13± 36,29 (103) ***	7,4e-06
CA1 stratum radiatum	496,86 ± 27,51 (70)	711,81 ±34,20 (80) ***	4,55e-07
CA1 lacunosum-moleculare	537,74 ± 24,99 (83)	689,16 ± 37,77 (100) *	0,013
CA3 stratum oriens	486,74 ± 23,52 (61)	602,05 ± 21,36 (58) *	0,016
CA3 pyramidal layer	567,24 ± 26,71 (61)	617,52 ± 23,93 (69) ns	0,12
CA3 stratum radiatum	465,17 ± 21,59 (65)	565,91 ± 17,52 (70) *	0,01618
DG molecular layer	649,48 ± 34,85 (75)	785,35 ± 33,05 (98) **	0,0013
DG granule cell layer	397,46 ± 20,18 (83)	616,72 ± 34,62 (98) ***	2,03e-07
DG polymorph layer	397,69 ± 26,78 (76)	577,83 ± 27,29 (88) ***	6,60e-08

Table 4. Astrocyte volume is increased compared to WT littermates in the different subregions of the hippocampus. Volumes of WT and Ts65Dn astrocytes are indicated for every hippocampal subregion. Parentheses indicate the number of astrocytes per region. WT (n = 4 mice), Ts65Dn (n = 4 mice). Mann-Whitney. Data are expressed as mean ± SEM of astrocyte volume (μm^3). *P < 0.05, **P < 0.01, ***P < 0.001.

3. S100β expression is upregulated in trisomic astrocytes

Astrogliosis also consists of the increase of astroglial proteins such as S100β and GFAP. To investigate whether this was also the case in the trisomic scenario, we used S100β to quantify the relative expression of this protein in both WT and in Ts65Dn astrocytes. Dorsal hippocampal sections were immunostained against S100β, astrocyte somas were manually delineated and signal intensity was measured. In accordance with previous studies [107,115,204], S100β levels in Ts65Dn astrocytes were significantly higher than in WT astrocytes in all the hippocampal regions (Mann-Whitney; p < 0.001; Figure 2G; Table 5) confirming that trisomic astrocytes have a higher expression of S100β compared to WT.

Hippocampal region	**WT** (a.u.)	**Ts65Dn** (a.u.)	**p-value**
CA1 stratum oriens	23885,18 ± 977,73 (94)	35872 ± 1001,22 (91) ***	2e-13
CA1 pyramidal layer	26813,90 ± 1317,81 (86)	45498,10 ± 995,90 (95) ***	2e-16
CA1 stratum radiatum	25392,44 ± 1124,57 (90)	38742,31 ± 1055,12 (92) ***	2,2e-13
CA1 lacunosum-moleculare	22689,92 ± 957,37 (92)	32343,01 ± 1120,13 (95) ***	1,3e-08
CA3 stratum oriens	26113,41 ± 886,82 (93)	35011,74 ± 906,14 (97) ***	4,3e-13
CA3 pyramidal layer	30392,78 ± 1142,61 (92)	40352,09 ± 885,00 (93) ***	3,7e-13
CA3 stratum radiatum	24119,93 ± 951,16 (92)	35531,92 ± 1106,62 (93) ***	2e-16
DG molecular layer	24771,44 ± 1058,85 (95)	33393,14 ± 1624,42 (87) ***	8,4e-10
DG granule cell layer	20967,98 ± 1150,94 (81)	30780 ± 1670,08 (81) ***	5,9e-14
DG polymorph layer	23882,27 ± 1101,58 (82)	34304,77 ± 1493,84 (91) ***	5,2e-10

Table 5: Astrocyte S100β expression is increased compared to WT littermates in the different subregions of the hippocampus. Astrocyte S100β expression measured as arbitrary units (a.u.) in the different hippocampal regions in WT and Ts65Dn mice. Background signal subtraction was performed for all the data. Parentheses indicate the number of astrocytes per region. WT (n = 4 mice), Ts65Dn (n = 4 mice). Mann-Whitney. Data are expressed as mean ± SEM of S100β fluorescence intensity (a.u.). ***$P < 0.001$.

4. Single-nucleus RNA sequencing identifies the main glial subtypes

To address whether the astroglial pattern of expression was affected in the Ts65Dn hippocampus, we performed single-nucleus (sn) RNA sequencing to compare astroglial transcriptomic profile in the mouse hippocampus in an unbiased and thorough manner in euploid and trisomic mice. To be able to compare our data with external gene expression databases such as the Allen Brain Atlas [205], we selected postnatal day 56 (P56). The NeuN negative population was isolated by fluorescent activated nuclear sorting (FANS) from one WT and one Ts65Dn animal. Immediately after FANS, 9973 and 9459 nuclei, respectively, were sequenced using 10X technology (Figure 4A).

Cells were embedded in a K-nearest neighbor graph that constructs cell clusters unbiasedly using single-cell feature-barcode matrices. The identification of every cluster was determined based on their unique differential expression pattern compared with the other clusters. Considering all the sequenced cells, we were able to identify that 46% of cells were classified as oligodendroglia, 19% as astroglia, 8% as microglia while the rest of cells (27%) were classified as vascular cells, ependymal cells and other minor cell types. No differences in cell proportion were observed between WT and Ts65Dn mice.

A uniform manifold approximation and projection (UMAP) plot was used to display nuclear transcriptomes. 17 clusters of cells sharing similar gene expression patterns were identified (Figure 4B). We selected the gene markers for every cluster based on their selective differential expression compared to the other clusters, to determine their identity (Figure 4B). These markers allowed us to identify astrocyte clusters according to canonical astrocyte markers such as *Gfap*, *S100β*, *Aqp4*, *Aldh1*, or *Vimentin* (Figure 4C). Gene expression analyses of WT and trisomic major cellular types revealed that the differentially expressed genes (DEG) segregated between oligodendroglia, astroglia and microglia (Figure 4D).

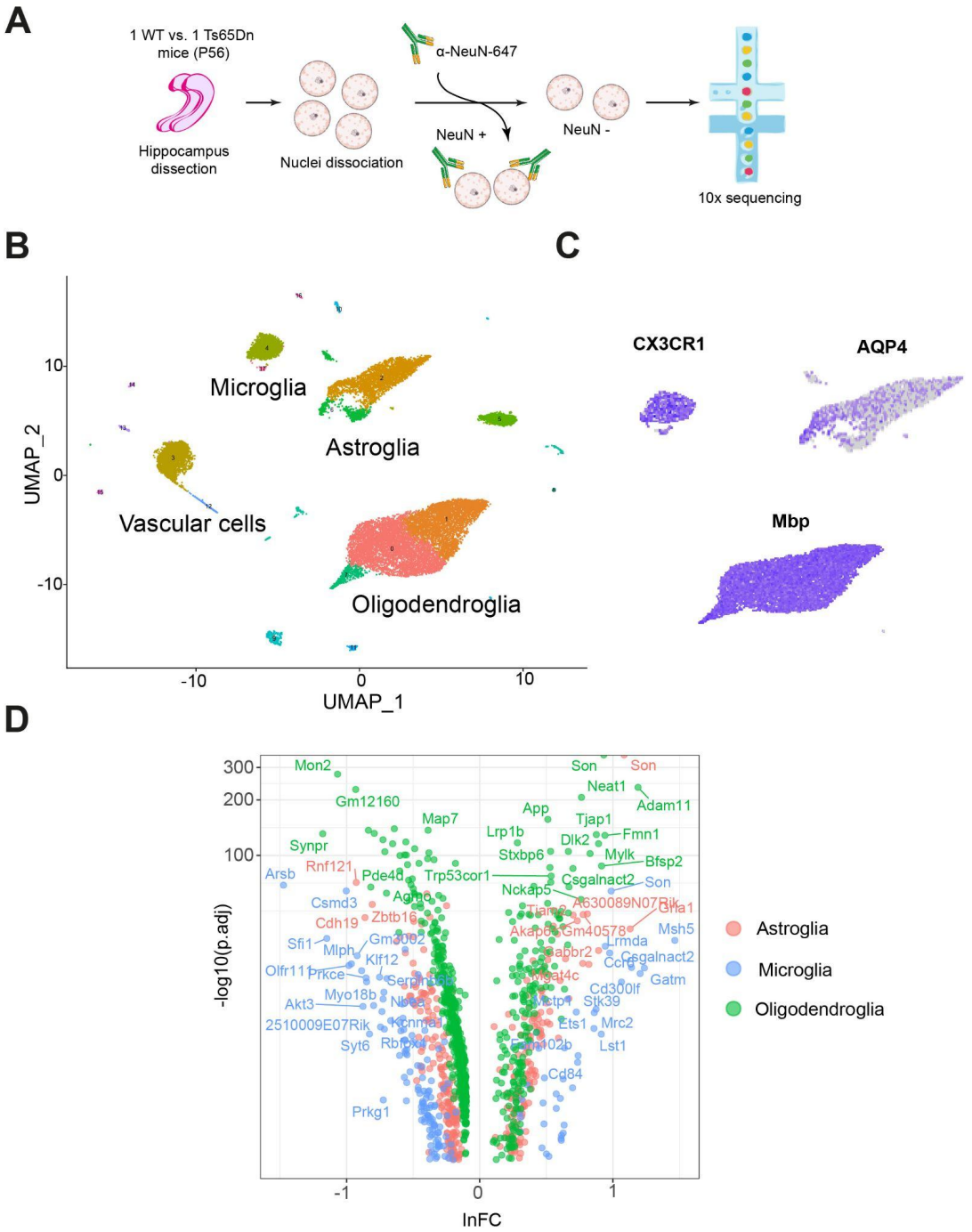

Figure 4. Single-nucleus sequencing and cell-type identification. (A) Overview of the experimental approach with a schematic showing the NeuN-negative cell sorting method. Hippocampus of WT and Ts65Dn were collected and nuclei suspension was prepared using enzymatic digestion and mechanical dissociation. Nuclei were incubated with anti-NeuN-Alexa647 and NeuN- nuclei were selected by FANS and subsequently sequenced using 10x sequencing. **(B)** All hippocampus single nuclei embedded in UMAP, displaying cell clusters in different colors. Each dot represents a single nucleus. **(C)** Mapping of known microglial (CX3CR1), astroglial (Aqp4) and oligodendroglia (Mbp) markers. **(D)** Volcano plot of DEGs colored by each major cell type.

The gene expression analysis revealed a total of 329 DEGs between trisomic and euploid astrocytes. Remarkably, the majority of DEGs predominantly upregulated, were found in the Mmu16 and Mmu17, portions of which are triplicated in Ts65Dn (Figure 5A). Triplicated genes involved in cell survival, proliferation and in the gliogenic shift [206] such as *Notch-3* and *Dyrk1A* were significantly upregulated in trisomic astrocytes approximately by 1.25 fold (Figure 5B). Other genes upregulated in trisomic astrocytes included the Brain lipid binding protein (*Blbp*) also called *Fabp7,* a marker of reactive astroglia [207] and biomarker of neurotrauma since it is released by injured astrocytes; the Interleukin 17 Receptor for inflammatory cytokines (*Il17rd)*, Angiotensin (*Agt*), that is related with angiogenesis and blood pressure regulation during neuroinflammation [208], or Aquaporin (*Aqp9*), usually found elevated in hypertrophied astrocytes in different pathological conditions [209,210]. Genes encoding for neurotransmitter receptor subunits, including *Gria1*, *Gabbr1*, *Gabbr2*, *Atp5o*, were also upregulated in Ts65Dn astrocytes. Conversely, phospholipase C beta 1, encoded by *Plcb1* and involved in calcium homeostasis was downregulated in trisomic astrocytes. *Akap6* is one of the top DEG genes, and encodes for A-kinase anchoring protein 6 and is involved in the positive regulation of sequestered calcium ions into the cytosol probably by interacting with Ryanodine receptor 2 [211]. Interestingly, we also found that *Gjb6*, encoding for connexin 30 was significantly downregulated in trisomic astrocytes (Figure 5C).

The Gene Ontology (GO) analysis of the overexpressed genes showed that the pathways affected were related to synaptic membrane, post- and presynaptic membrane, glutamatergic synapses, ion channel complex and to cognition and memory (Figure 5D). Because several studies, including ours, have reported that astrocytes are increased in number in DS, we decided to investigate whether astrocyte proliferation continues during adult stages. This can be addressed using the Cell-Cycle Scoring and Regression function [212] to classify the cell cycle phase and cell cycle score of euploid and trisomic astrocytes according to canonical markers. We found comparable numbers of astrocytes in the different cell cycle phases (G1, S and G2M) and expression of S and G2/M phase markers

in WT and Ts65Dn samples, which would suggest no changes in proliferation between WT and Ts65Dn astrocytes in adult stages.

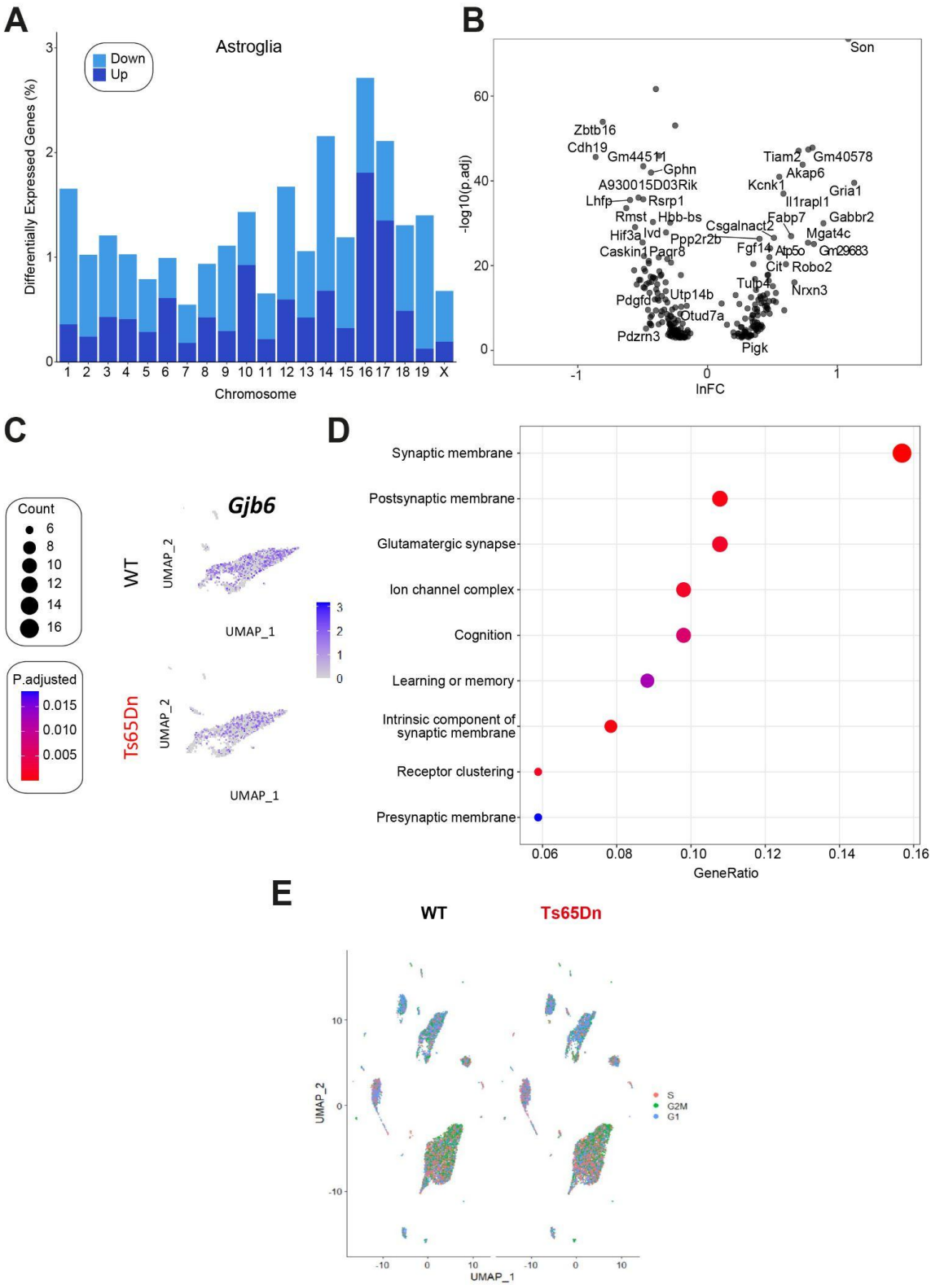

Figure 5. Differentially expressed genes in trisomic hippocampal astrocytes. (A) Distribution of the percentage of genes that are DEGs within every mouse chromosome. **(B)** Astrocyte-specific volcano plot of DEGs in Ts65Dn mice. **(C)** Mapping of *Gjb6* expression both in the astroglial cluster in WT (above) and Ts65Dn (below) mice. **(D)** Biological pathways enriched for DEGs in trisomic astrocytes. **(E)** Umap embedding all WT (left) and Ts65Dn (right) nuclei transcriptional profiles according to their specific phase of the cell cycle (S, G2M or G1).

5. Trisomic astroglia exhibit an abnormal calcium dynamics

Previous research on DS has found that astrocytes derived from patient iPSCs have more frequent spontaneous calcium oscillations [94], and calcium signaling in the astrocyte modulates neural circuit activity [79,213,214].

In the single-nuclei RNA sequencing analysis, we found that several genes involved in calcium signaling such as *Akap6* and *Plcb1* are significantly deregulated in Ts65Dn astrocytes. Thus, we decided to further investigate whether calcium oscillations were impaired in Ts65Dn astrocytes. To this aim, we expressed a genetically encoded calcium indicator (GCaMP6f) driven by the astrocyte-specific GfaABC1B promoter (a shortened 681 bp GFAP promoter) in CA1 astrocytes along with hM3D(Gq)-mCherry in WT and Ts65Dn mice (Figure 6A).

First, we evaluated spontaneous calcium oscillations in the presence of the $GABA_A$ receptor antagonist picrotoxin (50 μM) for 2 min. We found that the basal event frequency was very similar between WT and Ts65Dn astrocytes (Post hoc Tukey HSD; N.S.; Figure 6B-E). Nevertheless, the average basal amplitude of calcium events ($\Delta F/F_0$) was significantly higher in Ts65Dn astrocytes (Post hoc Tukey HSD; $p = 0.001$; Figure 6E). In order to further assess whether evoked intracellular calcium oscillations were altered in Ts65Dn astrocytes, we locally applied CNO (1 mM) with a puff (2 s; 1 bar) while examining the time course of calcium responses. CNO application led to a rise in the intracellular calcium signal of most of the astrocytes as shown in Figure 6F. Event frequency was reduced both in WT (Post hoc Tukey HSD; $p < 0.001$; Figure 6E) and in Ts65Dn astrocytes (Post hoc Tukey HSD; $p = 0.0059$; Figure 6E) after CNO application as depicted in Figure 6E. Remarkably, CNO application significantly reduced event amplitude

in Ts65Dn to levels comparable to WT mice (Post hoc Tukey HSD; p = 0.04; Figure 6E).

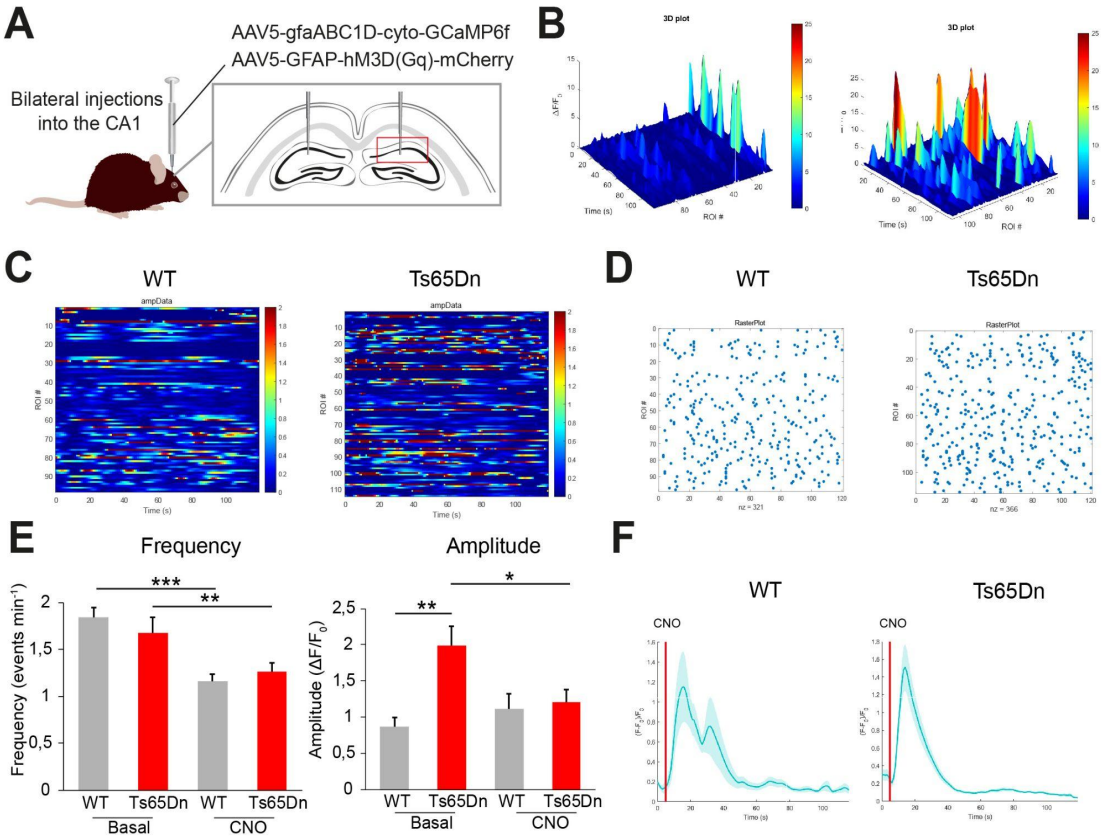

Figure 6: Ts65Dn astrocytes exhibit abnormal calcium dynamics. (A) Experimental design: AAV_5-GFAP-hM3D(Gq)-mCherry and AAV_5-gfaABC1D-cyto-GCaMP6f were targeted bilaterally to the dorsal CA1 region of WT and Ts65Dn mice. **(B)** Left: changes in ΔF/Fo over time for multiple WT astrocytes. Right: changes in ΔF/Fo over time for multiple Ts65Dn astrocytes (WT = 98 astrocytes from 3 mice, Ts65Dn = 114 astrocytes from 3 mice). **(C)** Changes in amplitude (ΔF/Fo) over time in WT (left) and Ts65Dn (right) astrocytes (WT = 98 astrocytes from 3 mice, Ts65Dn = 114 astrocytes from 3 mice). **(D)** Mapping of the different events for every astrocyte in WT (left) and Ts65Dn (right) mice. Each blue dot represents an event (WT = 321 events from 98 astrocytes, Ts65Dn = 366 events from 114 astrocytes). **(E)** Left: basal and post-CNO Ca^{2+} oscillation frequency both in WT (gray) and Ts65Dn (red) astrocytes. Right: basal and post-CNO Ca^{2+} oscillation amplitude in WT and Ts65Dn astrocytes (WT basal = 87 astrocytes from 3 mice, Ts65Dn basal = 109 astrocytes from 3 mice, WT post-CNO = 88 astrocytes from 3 mice, Ts65Dn post-CNO = 84 astrocytes from 3 mice). Two-way ANOVA, Tukey HSD as post hoc **(F)** Time course depicting the mean intracellular Ca^{2+} signal changes after the local application of CNO (1 mM). CNO application is indicated by a red line at second 5 (WT = 88 astrocytes from 3 mice, Ts65Dn = 84 astrocytes from 3 mice). Data are expressed as mean ± SEM. ****P* < 0.001, ***P* < 0.01, **P* < 0.05.

6. Chemogenetic activation of CA1 astrocytes in Ts65Dn mice

Previous studies provided evidence that astrocyte stimulation, either by chemogenetics or by optogenetics, induces Ca^{2+} oscillations in astrocytes and enhanced memory through NMDA-dependent *de novo* LTP in CA1 [82].

To test whether astrocyte activation may have an effect in the trisomic hippocampus, we expressed the Gq-coupled designer receptor into astrocytes by means of a adeno-associated virus serotype 5 (AAV_5) vector encoding hM3Dq fused to mCherry under the control of the GFAP promoter into CA1 (Figure 7A). Gq-coupled designer receptors allow the reversible and time-restricted Ca^{2+} oscillations in astrocytes by CNO [82,185,215]. We found that hM3Dq expression was restricted to the astroglial membranes of CA1 (Figure 7BC), with high specificity (+95% hM3Dq+ cells were also GFAP+) and penetrance (+95% of GFAP+ cells expressed hM3Dq), as shown by co-localization studies with the astroglial marker GFAP (Figure 7D). No differences in penetrance or specificity were observed between WT and Ts65Dn astrocytes (Two-tailed T test; N.S.; Figure 7DE). Co-staining with neuronal nuclei (NeuN) revealed no-colocalization with hM3Dq (Figure 7C). This result indicates that the microinjection of AAV_5 resulted in a robust and specific expression of hM3D(Gq)-mCherry in astrocytes in the hippocampal CA1 area of adult mice.

We first tested that hM3D(Gq) receptors were functional in hM3D(Gq)-mCherry expressing astrocytes by performing calcium imaging studies in brain slices. We locally applied CNO (1 mM) with a glass pipette in astrocytes expressing both hM3D(Gq)-mCherry and GCaMP6f and recorded astrocyte calcium oscillations. We verified that local application of CNO triggered intracellular Ca^{2+} increase both in WT and trisomic astrocytes (Figure 7F), while local application of aCSF did not evoke calcium responses in astrocytes (Figure 7F).

We next verified astrocyte activation *in vivo* by administering i.p. CNO (3 mg/kg) and collecting the brains after 90 min for c-Fos immunostaining (Figure 7G). CNO dramatically increased the number of c-Fos positive astrocytes both in WT and Ts65Dn astrocytes expressing hM3Dq-mCherry, compared to saline-injected controls (Post hoc Tukey HSD; $p < 0.001$; Figure 7GH), with no differences between genotypes (Post hoc Tukey HSD; N.S.; Figure 7H).

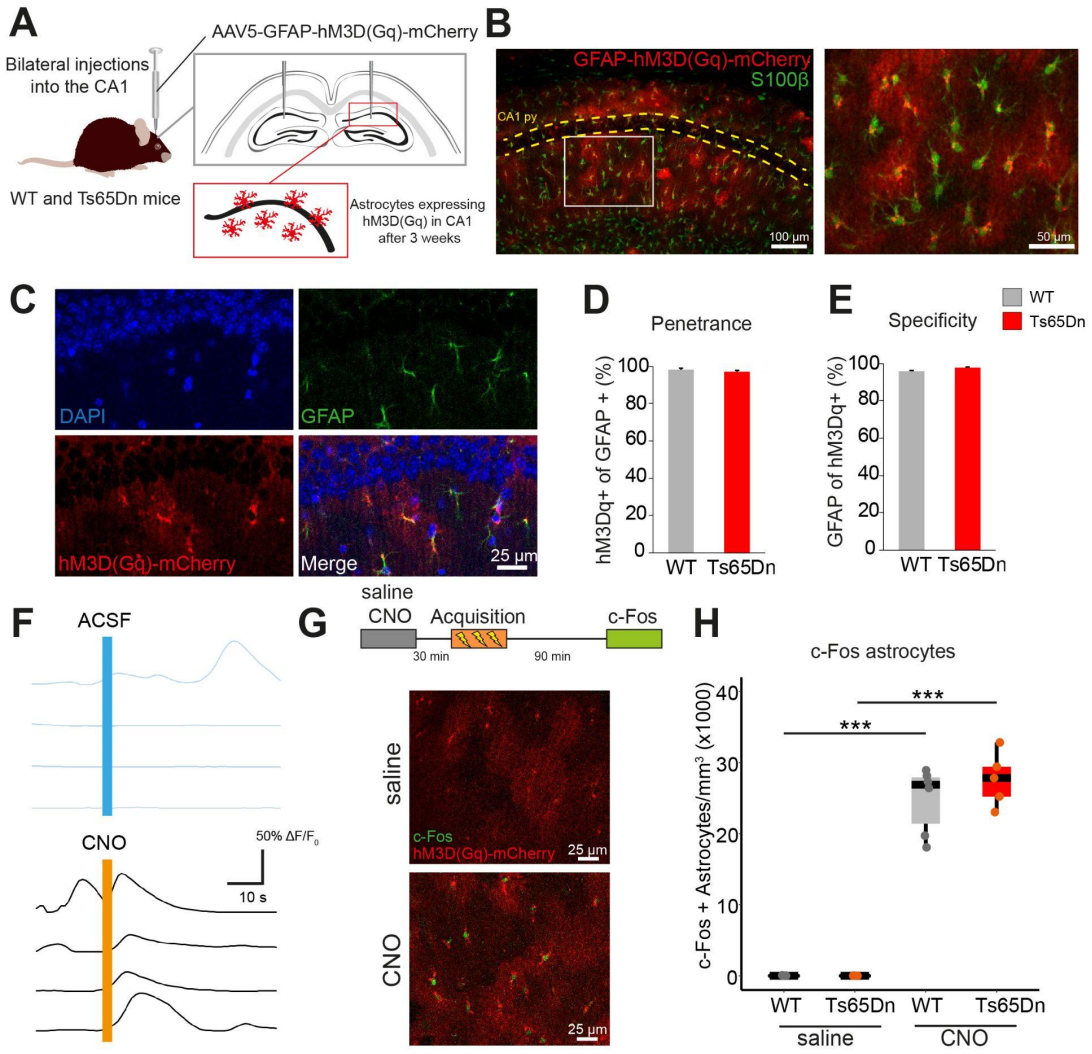

Figure 7: Chemogenetic activation of Ts65Dn astrocytes. (A) Experimental design: AAV5-GFAP-hM3D(Gq)-mCherry was targeted bilaterally to the dorsal CA1 region of WT and Ts65Dn mice. **(B)** Left**:** after 3 weeks, hM3D(Gq)-mCherry was expressed in the astroglial membrane and in the processes in the CA1 region as shown by the co-staining with S100β. Scale bar = 100 µm. Right: Magnification image. Scale bar = 50 µm. **(C)** Representative image showing the co-localization of hM3D(Gq)-mCherry (red) with GFAP (green) in CA1. Scale bar = 25 µm. **(D-E)** GFAP::hM3D(Gq)-mCherry was expressed in > 96% of astrocytes (WT = 337/344 cells from 3 mice, Ts65Dn = 511/528 cells from 4 mice) with > 95% specificity (WT = 337/353 cells from 3 mice, Ts65Dn = 528/540 cells from 4 mice). Two-tailed T test. Data are expressed as mean ± SEM. **(F)** Traces showing the fluorescence change (in $\Delta F/F_0$) over time from astrocytes expressing hM3D(Gq)-mCherry and GCaMP6f treated with ACSF (above) or CNO (below) for 2 s. Blue and orange rectangles indicate the moment of application of ACSF or CNO, respectively. **(G-H)** CNO administration (3 mg/kg) *in vivo* to WT and Ts65Dn mice expressing hM3D(Gq) in CA1 astrocytes (red) 30 min before the CFC training led to a significant increase of c-Fos expression (green), compared to saline-injected controls (WT saline = 8 mice, Ts65Dn saline = 7 mice, WT CNO = 6 mice, Ts65Dn CNO = 5 mice). Scale bar = 25 µm. Two-way ANOVA, Tukey HSD as post hoc. On the boxplots, the horizontal line indicates the median, the box indicates the first to third quartile of expression and whiskers indicate 1.5 × the interquartile range. ****P* < 0.001.

7. Astrocyte activation during memory acquisition promotes memory allocation and rescues contextual memory deficits in Ts65Dn mice

Several studies have shown that abolishing astrocyte function resulted in impaired performance in different behavioral tests [88–90]. Adamsky et al. also provided evidence that astrocyte stimulation before acquisition enhanced contextual memory by promoting synaptic plasticity [82].

We thus investigated whether manipulating astrocyte activity could overcome contextual fear memory deficits observed in Ts65Dn mice. Hence, we decided to activate the Gq pathway in trisomic astrocytes before the acquisition of a contextual memory using AAV_5-GFAP-hM3D(Gq)-mCherry to increase the number of activated neurons in Ts65Dn (see Chapter 1).

WT and Ts65Dn were injected in the dorsal CA1 hippocampal region with AAV_5-GFAP-hM3D(Gq)-mCherry (Figure 8A). After 3 weeks, mice were administered with either saline or CNO (3 mg/kg), 30 min before the acquisition of a contextual-fear memory (Figure 8A) and brains were collected 90 min later for c-Fos quantification. Saline-injected Ts65Dn mice showed a reduced number of c-Fos+ neurons in CA1 compared to WT mice during memory acquisition (Post hoc Tukey HSD; $p = 0.0012$; Figure 8B) confirming our previous results (Chapter 1). However, this sparser neuronal activation was completely rescued in Ts65Dn treated with CNO (Post hoc Tukey HSD; $p < 0.001$; Figure 8B). Instead, even though CNO increased c-Fos levels both in WT astrocytes expressing hM3Dq-mCherry (see above), no differences were detected in the number of c-Fos+ neurons comparing saline or CNO-injected WT mice after memory acquisition (Post hoc Tukey HSD; N.S.; Figure 8B) indicating that astrocyte activation had no impact on neuronal activation in WT mice.

Next, we sought to study whether the increase in the number of active neurons induced by astrocyte activation during memory acquisition was able to rescue memory deficits in Ts65Dn mice. Thus, in a different batch of WT and Ts65Dn mice injected with GFAP-hM3D(Gq)-mCherry, we tested memory performance 24 h after mice were treated with either CNO or saline during memory acquisition (Figure 8C). Brains were collected 90 min after memory recall. Along with our

hypothesis, we found that memory deficits in the recall test were completely rescued in Ts65Dn mice injected with CNO during training compared to saline-injected trisomic controls (Post hoc Tukey HSD; p = 0.0117; Figure 8D). Instead, CNO had no effect in WT mice (Post hoc Tukey HSD; N.S.; Figure 8D). This time, however, the reduced number of c-Fos+ neurons in Ts65Dn injected with saline was not detected (Post hoc Tukey HSD; N.S.; Figure 8E). We found a positive (R = 0.24), although not significant (p = 0.17) correlation comparing memory performance and c-Fos density (Spearman correlation method; Figure 8F).

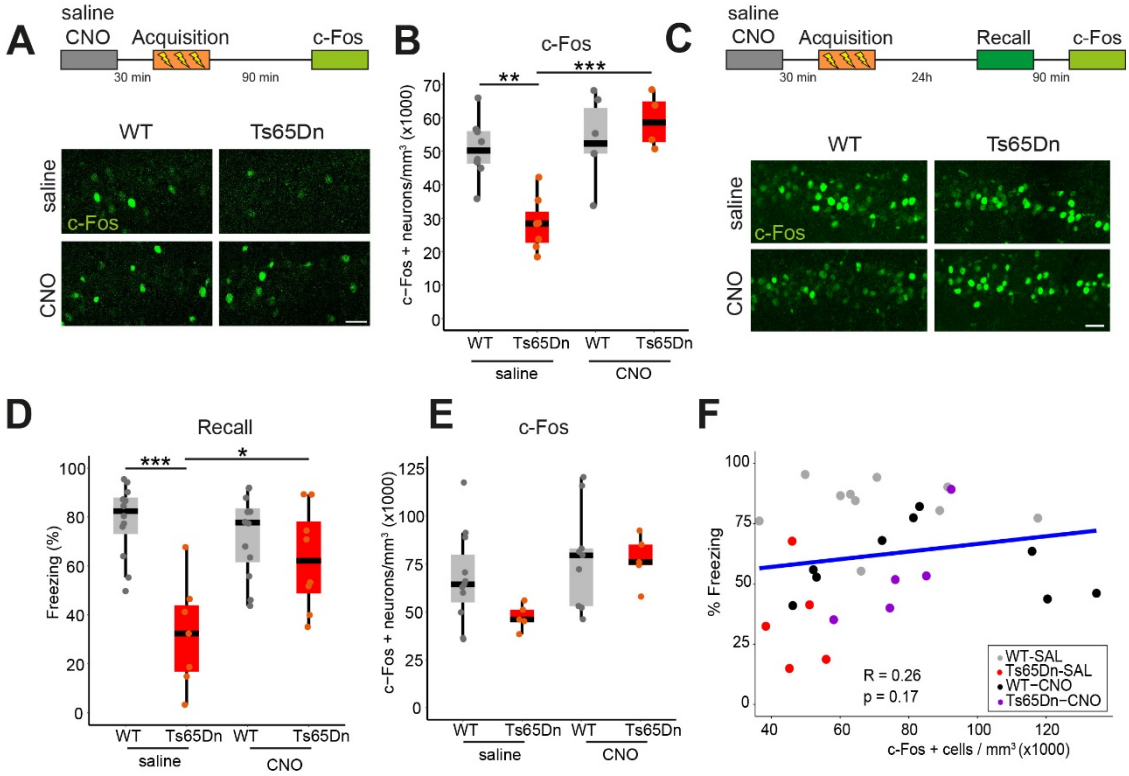

Figure 8: Chemogenetic activation of Ts65Dn astrocytes during memory acquisition promotes memory allocation and recovery of memory deficits during the recall. (A) Above: Behavioral schedule. Either CNO or saline was administered to WT and Ts65Dn mice expressing hM3D(Gq)-mCherry in astrocytes and after 30 min injected mice underwent CFC memory acquisition. Brains were extracted after 90 min and processed for c-Fos immunostaining. Below: Representative images showing c-Fos expression (in green) in the dorsal CA1 90 min after memory acquisition for WT and Ts65Dn mice that were injected with either saline or CNO 30 min before CFC training. Scale bar = 30 µm. **(B)** Density of neurons expressing c-Fos in CA1 after memory acquisition (WT saline = 8 mice, Ts65Dn saline = 7 mice, WT CNO = 6 mice, Ts65Dn CNO = 5 mice). Two-way ANOVA, TukeyHSD as post hoc. **(C)** Behavioral schedule (above): Either CNO or saline was administered to WT and Ts65Dn mice expressing hM3D(Gq)-mCherry in astrocytes after 30 min a CFC acquisition. 24h later, mice were reexposed to the conditioned context to evaluate memory recall. Brains were extracted after 90 min and processed for c-Fos immunostaining. Representative images of c-Fos expression (in green) in the dorsal CA1 after memory recall for WT and Ts65Dn that received either saline or CNO during memory acquisition. Scale bar = 20 µm. **(D)** Percentage of freezing of WT and Ts65Dn that received either saline or

CNO during training (WT saline = 12 mice, Ts65Dn saline = 7 mice, WT CNO = 12 mice, Ts65Dn CNO = 8 mice). Two-way ANOVA, TukeyHSD as post hoc. **(E)** c-Fos density of WT and Ts65Dn that received either saline or CNO during training (WT saline = 11 mice, Ts65Dn saline = 5 mice, WT CNO = 10 mice, Ts65Dn CNO = 5 mice). Two-way ANOVA, TukeyHSD as post hoc. **(F)** Correlation between freezing behavior during memory recall and c-Fos expression (WT saline = 11 mice, Ts65Dn saline = 5 mice, WT CNO = 10 mice, Ts65Dn CNO = 5 mice). R = 0.26; p = 0.17. Spearman correlation Method. On the boxplots, the horizontal line indicates the median, the box indicates the first to third quartile of expression and whiskers indicate 1.5 × the interquartile range. ****P* < 0.001, ***P* < 0.01, **P* < 0.05.

8. Stimulation of Ts65Dn astrocytes leads to synaptic depression

Ca^{2+} dynamics are essential for astrocyte-to-neuron communication. Several findings in this Thesis including impaired calcium dynamics and enhancement of memory performance in Ts65Dn after astrocyte activation indicate that probably astrocyte-neuron crosstalk is defective in Ts65Dn mice. To address this question, we first investigated whether the excitatory synaptic transmission in CA3-CA1 synapses was modified upon astrocyte activation. We expressed an excitatory DREADD fused to mCherry (AAV_5-GFAP-hM3D(Gq)-mCherry) in CA1 astrocytes. In collaboration with Gertrudis Perea laboratory, we performed a minimal axonal stimulation experiment, in which the CA3 Schaffer Collaterals were electrically stimulated to activate single CA1 hippocampal synapses (Figure 9AB). Evoked excitatory postsynaptic currents (EPSCs) were recorded in the presence of picrotoxin (50 μM) in basal conditions and after astrocyte stimulation by CNO (1mM) (Figure 9C) both in WT (Figure 9D) and in Ts65Dn mice (Figure 9I).

Potentiation was observed in 7 of 13 synapses (53.84%) as shown in Figure 9D. The local activation of WT astrocytes by CNO led to a synaptic potentiation as noted by the increase in the synaptic efficacy (Paired T test; N.S.; Figure 9E) and probability of neurotransmitter release (Pr), (Paired T test; p < 0.001 Figure 9EF) while no changes in the synaptic potency was observed (Paired T test; N.S.; Figure 9G). Paired-pulse ratio (PPR) was unaltered (Paired T test; N.S.; Figure 9H). Conversely, we found that trisomic astrocyte activation by CNO led to a synaptic depression in 43% of the synapses (6 of 14) during the 5 min after CNO local application (Figure 9I). Synaptic efficacy (Paired T test; p < 0.01; Figure 9J)

and Pr were significantly reduced in Ts65Dn (Paired T test; $p < 0.01$; Figure 9K). Synaptic potency and PPR remained unaltered (Paired T test; N.S.; Figure 9LM). Albeit non-significant, we found a trend to a higher Pr (Paired T test; $p = 0.136$; Figure 10A) and synaptic efficiency (Paired T test; $p = 0.09$; Figure 10B) in Ts65Dn mice several min after Gq-DREADD stimulation. No differences were observed in synaptic potency and PPR (Paired T test; N.S.; Figure 10CD).

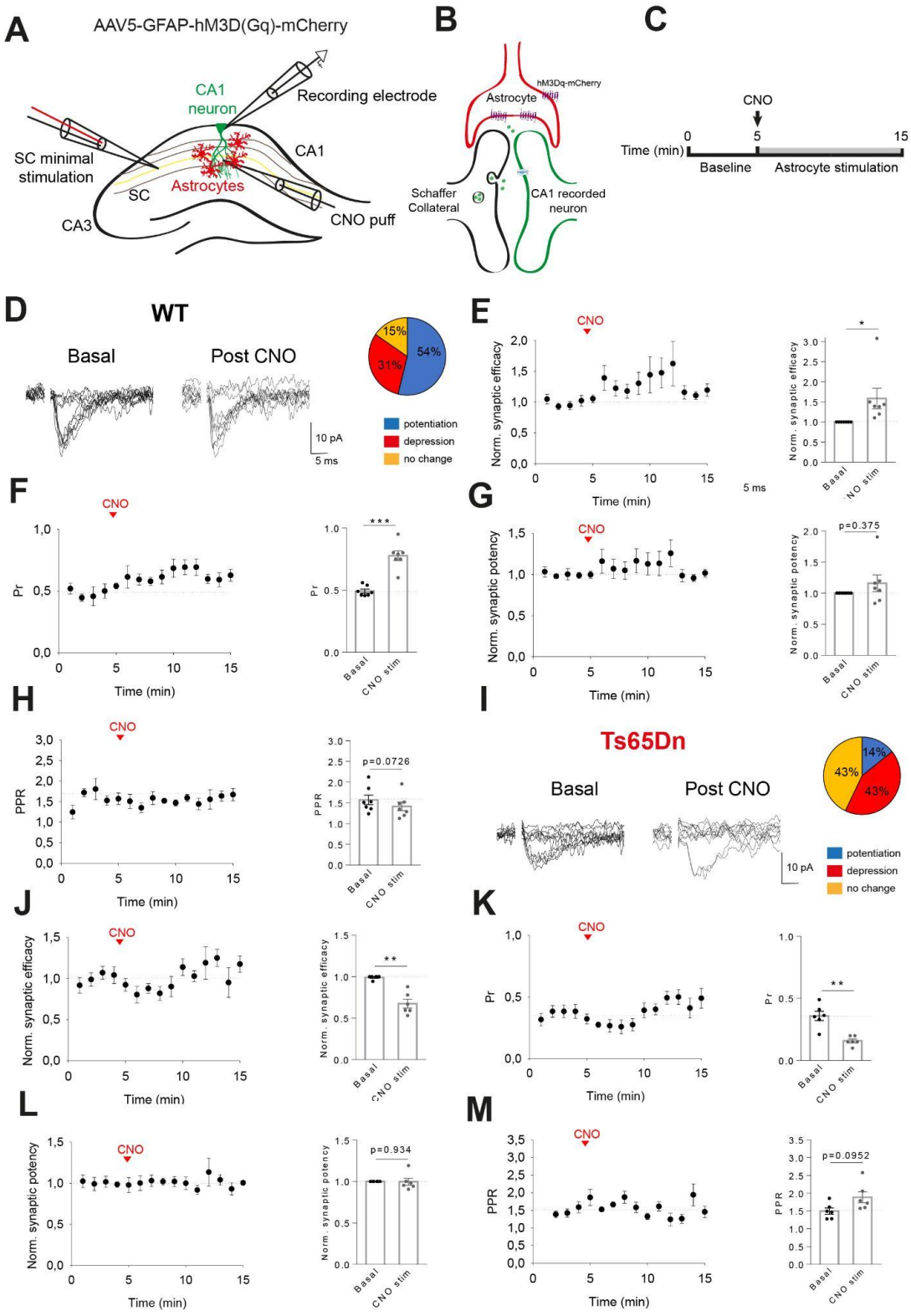

Figure 9: Trisomic astrocyte manipulation induced a short-term synaptic depression in single synapses. (A) Schematic drawing showing the minimal stimulation protocol. SCs are stimulated by a stimulating electrode while a CA1 pyramidal neuron is being recorded. Changes in synaptic transmission is evaluated upon hM3D(Gq)-expressing astrocytes by a CNO puff. **(B)** Schematic representation of the tripartite synapse in this system. hM3D(Gq)-mCherry surrounds

pre- and postsynaptic neurons. **(C)** Experimental timeline: evoked basal synaptic transmission is recorded during 5 min. At min 5, a CNO puff is applied and evoked synaptic responses are recorded for 10 min. **(D)** Responses evoked by minimal stimulation depicting EPSCs (failures and successes) both in basal conditions (left) and after CNO application (right). Proportion of synapses that were potentiated (blue), depressed (red) or without changes (orange) in WT mice. **(E)** Left: synaptic efficacy changes over 15 min in WT mice (n = 13 astrocyte-neuron pairs). Right: relative changes of synaptic efficacy in basal conditions and after astrocytes stimulation. **(F)** Left: probability of release (Pr) changes over 15 min in WT mice (n = 13 astrocyte-neuron pairs). Right: relative changes of Pr in basal conditions and after astrocytes stimulation. **(G)** Left: normalized synaptic potency changes over 15 min in WT mice (n =13 astrocyte-neuron pairs). Right: relative changes of the normalized synaptic potency in basal conditions and after astrocytes stimulation. **(H)** Left: paired-pulse ratio (PPR) changes over 15 min in WT mice (n = 13 astrocyte-neuron pairs). Right: relative changes of the PPRin basal conditions and after astrocytes stimulation. Data are expressed and mean ± SEM. **(I)** Responses evoked by minimal stimulation depicting EPSCs (failures and successes) both in basal conditions (left) and after CNO application (right). Proportion of synapses that were potentiated (blue), depressed (red) or without changes (orange) in Ts65Dn mice. **(J)** Left: synaptic efficacy changes over 15 min in Ts65Dn mice (n = 14 astrocyte-neuron pairs). Right: relative changes of synaptic efficacy in basal conditions and after astrocytes stimulation. **(K)** Left: Pr changes over 15 min in Ts65Dn mice (n =14 astrocyte-neuron pairs). Right: relative changes of Pr in basal conditions and after astrocytes stimulation. **(L)** Left: normalized synaptic potency changes over 15 min in Ts65Dn mice (n = 14 astrocyte-neuron pairs). Right: relative changes of the normalized synaptic potency in basal conditions and after astrocytes stimulation. **(M)** Left: normalized PPR changes over 15 min in Ts65Dn mice (n = 14 astrocyte-neuron pairs). Right: relative changes of the PPR in basal conditions and after astrocytes stimulation. Paired T test. Data are expressed as mean ± SEM. ***$P < 0.001$, **$P < 0.01$, *$P < 0.05$.

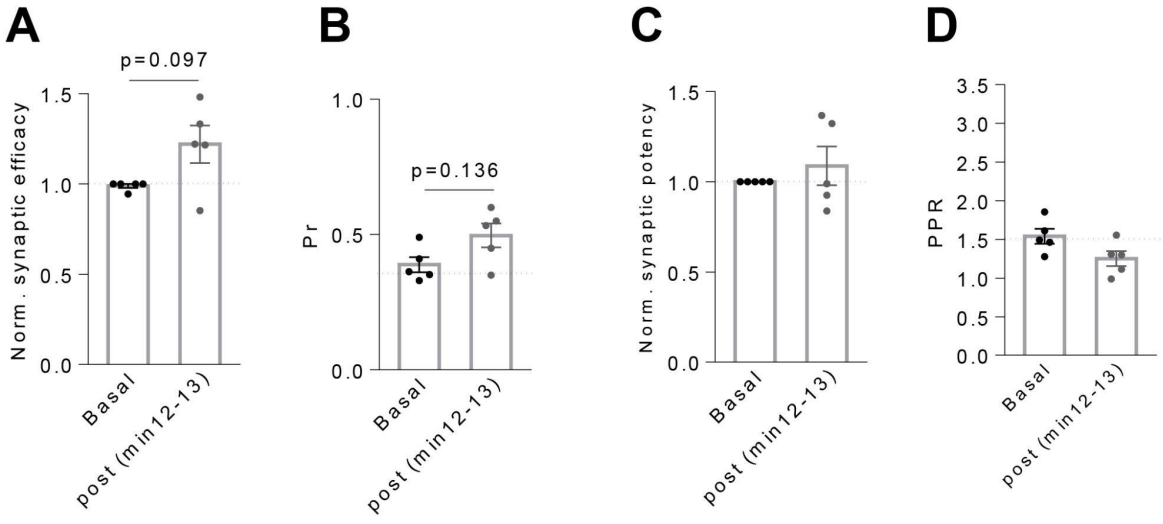

Figure 10: A trend towards a higher synaptic efficacy and Pr is observed after several min of Gq-DREADD stimulation of trisomic astrocytes. (A) Relative changes of synaptic efficacy in basal conditions and during min 12-13 in Ts65Dn mice. **(B)** Relative changes of Pr in basal conditions and during min 12-13 in Ts65Dn mice. **(C)** Relative changes of synaptic potency in basal conditions and during min 12-13 in Ts65Dn mice. **(D)** Relative changes of PPR in basal conditions and during min 12-13 in Ts65Dn mice. (n = 14 trisomic astrocyte-neuron pairs). Paired T test. Data are expressed as mean ± SEM.

9. Stimulation of Ts65Dn astrocytes during memory acquisition promotes neuronal allocation in the DG

As shown in this **Chapter**, we found that trisomic astrocyte Gq-activation in CA1, the region in which astrocytes were significantly more abundant in Ts65Dn mice, was able to promote memory allocation and rescue memory alterations in Ts65Dn mice. Given that in **Chapter 1** we found a sparser neuronal activation both during memory acquisition and recall in the DG, we decided to manipulate astrocyte activity in the DG to study whether we could restore the engram size. Although in this region we did not observe such marked differences in astrocyte number as compared to WT, we reasoned that there may be functional changes (such as increased S100β expression) that could also contribute to DG engram pathology.

For this reason, we expressed a Gq-DREADD under the GFAP promoter in the dorsal DG (Figure 11A). After 3 weeks of infection, hM3D(Gq)-mCherry expression was restricted to the dorsal DG region (Figure 11B) in the astroglial membrane and processes (Figure 11C) with a high penetrance (> 95%) and specificity (> 95%) both in WT and Ts65Dn mice (Figure 11EF). No differences in penetrance or specificity were observed between WT and Ts65Dn mice (Two-tailed T test; N.S.). CNO was administered i.p. (1 mg/kg) 30 min before memory acquisition. 90 min after training brains were collected and IF studies showed a robust increase of c-Fos expression in astrocytes upon CNO administration (Figure 11D). In **Chapter 1**, we found a significant reduction of 32% in the number of active cells during the acquisition of a contextual fear memory. Here, we show that trisomic astrocyte Gq pathway activation completely rescued sparser neuronal activation in the DG since no differences in the density of c-Fos+ neurons were observed comparing WT and Ts65Dn mice (Two-tailed T test; N.S.; Figure 11G). Astroglial c-Fos expression in the DG molecular layer was very similar between WT and Ts65Dn mice (Two-tailed T test; N.S.; Figure 11H). These results suggest that changes in astrocyte function, rather than in astrocyte number, is important to promote neuronal allocation to memory engrams in Ts65Dn mice.

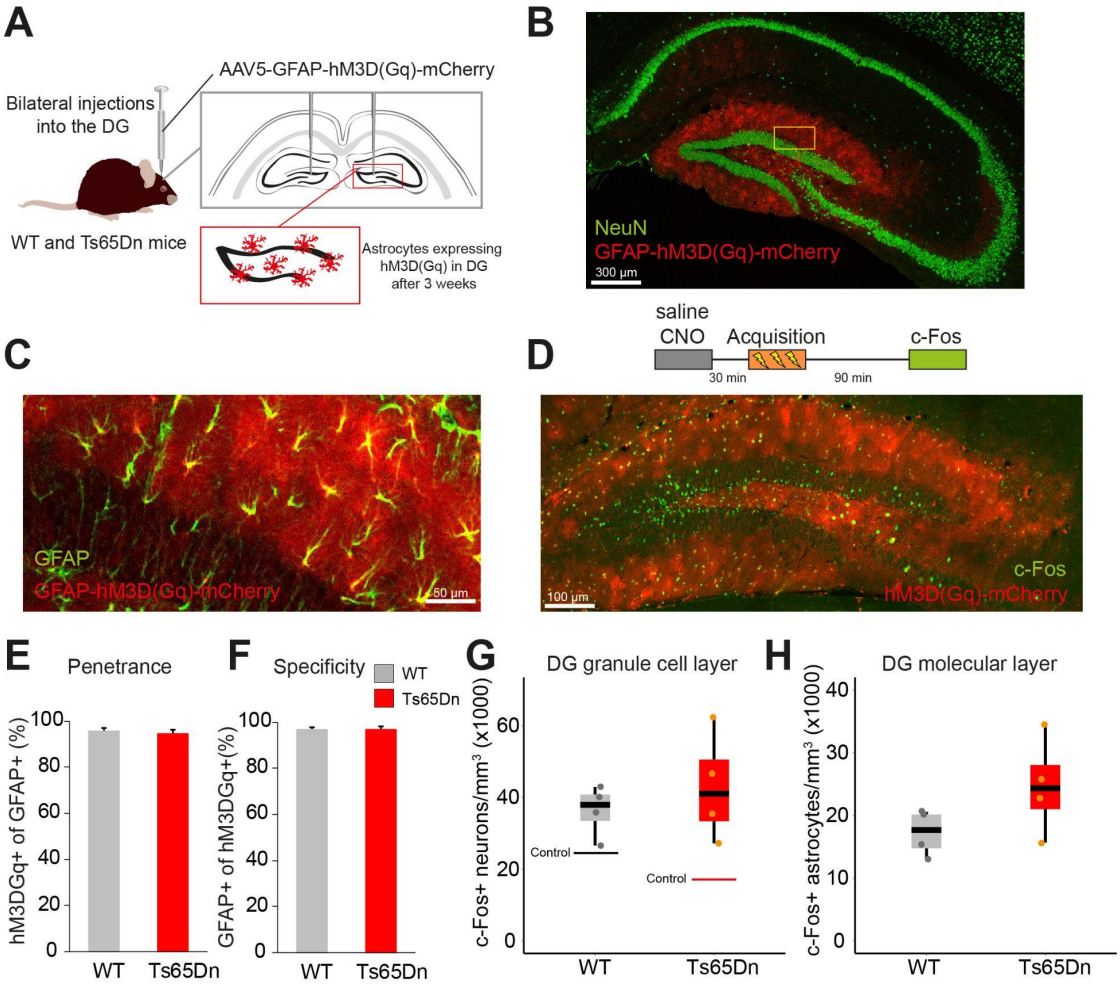

Figure 11: Chemogenetic activation of astrocytes in DG enhances granule cell activation in Ts65Dn mice. (A) Experimental design: AAV_5-GFAP-hM3D(Gq)-mCherry was targeted bilaterally to the dorsal DG region of WT and Ts65Dn mice. **(B)** After 3 weeks, hM3D(Gq)-mCherry was exclusively expressed in the astroglial membrane and in the processes in the DG region. Scale bar = 300 µm. **(C)** Representative image showing the co-localization of hM3D(Gq)-mCherry (red) with GFAP (green) in the dorsal DG. Scale bar = 50 µm. **(D)** CNO administration (1 mg/kg) *in vivo* to WT and Ts65Dn mice expressing hM3D(Gq) in DG astrocytes (red) 30 min before the CFC training led to a significant increased to c-Fos expression (green) in neurons and astrocytes. Scale bar = 50 µm. **(E-F)** GFAP-hM3D(Gq)-mCherry was expressed in > 95% of astrocytes (WT = 276/288 cells from 3 mice, Ts65Dn = 273/287 cells from 3 mice) with > 96% specificity (WT = 288/298 cells from 3 mice, Ts65Dn = 287/296 cells from 3 mice). Two-tailed T test. Data are expressed as mean ± SEM. **(G)** c-Fos neuronal density 90 min after memory acquisition in the granule cell layer (WT CNO = 4 mice, Ts65Dn CNO = 4 mice). Two-tailed T test. The horizontal lines indicate the average c-Fos density during a contextual fear memory acquisition in non-injected animals. **(H)** c-Fos astrocyte density 90 min after memory acquisition in the DG molecular layer (WT CNO = 4 mice, Ts65Dn CNO = 4 mice). Two-tailed T test. On the boxplots, the horizontal line indicates the median, the box indicates the first to third quartile of expression and whiskers indicate 1.5 × the interquartile range.

Discussion

In this Chapter, we have explored astrocyte distribution, structure, transcriptomic profile and neuron-astrocyte interaction at the synaptic and circuit level in the Ts65Dn hippocampus. We have also studied whether alterations in astroglial function might contribute to hippocampal circuit alterations and memory deficits in Ts65Dn.

In the first place, we systematically quantified and analyzed astrocytes within the Ts65Dn hippocampus, as this has not yet been reported. We observed a subregion-specific astrocytosis as noted by the increased number, volume and expression of astroglial proteins such as S100β. CA1 was the region where the astrocyte number was more notably increased, and thus we performed the rest of the experiments in this subregion. Our results confirm previous studies in postmortem brains of individuals with DS [114,115]. An increase in the number and size of astrocytes has been described in the frontal lobe of 18–20 weeks fetuses with DS [216]. Another study reported lower expression of GFAP in the hippocampus fetuses with DS during the middle pregnancy [217] and fetuses with DS at 17–21 gestational weeks showed a higher percentage of GFAP-positive astrocytes in the fusiform and inferior temporal gyrus [39]. Astrogliosis is also reported linked to AD in DS [119]. Astrogliosis is a reversible mechanism whose main aim is to combat brain insult such as infection, oxidative stress or inflammation [111]. However, in DS, astrocytes are in a chronic reactive state that might contribute to its pathophysiology [114,115]. Therefore, astrogliosis in DS should be considered as a life-long condition that starts early during neurodevelopment [218,219] and persists during adulthood. Although compatible with life, astrogliosis can have profound consequences on brain function including impaired synapse maturation and synaptogenesis.

Previous studies found that the trisomy produces a gene deregulation in trisomic astrocytes [104] that is responsible for some of the structural and functional alterations of trisomic astroglia. Thus, we next sought to identify differentially expressed genes in trisomic astroglia that would help us to better understand how astrocyte dysfunction in DS might contribute to synaptic alterations. Thus, we

generated a single nuclei atlas of the different glial subtypes in the hippocampus including oligodendroglia, astroglia and microglia. Focusing on the astrocyte-specific transcriptomic perturbations, we detected that most DEG were encoded by Mmu16 genes, and were mainly upregulated. We found several markers of reactive astroglia such as *Fapb7*, *Il17r, Agt* and *Aqp9* that have been associated with neurotrauma and neuroinflammation [207–210,220,221] and *Aqp9* which is overexpressed in hypertrophied astrocytes [209,210]. Contrary to what we expected, we observed a similar number of astrocytes in Ts65Dn compared to WT. Moreover, we found a similar number of astrocytes in the different phases of the cell cycle (including G2/M) comparing WT and Ts65Dn mice. As most of the astrocytes in the adult healthy brain are post-mitotic and long-lived, whereas the newly generated astrocytes are very limited [222,223], one possible interpretation of the similar number of astrocytes in the G2/M phase might be that the proliferation of trisomic astrocytes occurs during the neurodevelopment rather during adult stages. In fact, this notion would be in line with several studies that found that the neurogenic-to-astrogliogenic is shifted towards promoting a gliogenic cell fate during neurodevelopment [218,219]. Even so, since the increased astrocyte number was only found in certain Ts65Dn hippocampal regions, while in the snRNAseq experiments we have a mixture of all the hippocampal astrocytes, thus diluting the results.

Interestingly, we found that *Gjb6*, encoding for Cx30 was significantly downregulated in trisomic astrocytes, that may negatively impact neuronal communication and, consequently, memory function in Ts65Dn mice. Contrary to the discrete neuronal circuits, astrocytes share their cytoplasm through gap junctional coupling into a syncytium, and these glial networks are intimately interwoven with the neuronal circuits. Astrocytes are interconnected by different connexins (mainly Cx30 and 43) that enable them to act as a neuronal safeguarding system by buffering extracellular potassium and glutamate resulting from synaptic transmission [224]. Moreover, Ca^{2+} elevations as a response of synaptic activity in a single astrocyte spread to distant astrocytes by means of connexins [225]. Cx30 is upregulated in mice raised in enriched environments, which are known to improve memory [226], while Cx30-deficient mice showed

alterations in different behavioral tests [227], decreased AMPAR-mediated excitatory synaptic transmission [228], impaired synaptic plasticity and present a significant reduction in contextual fear memory.

In fact, most of the trisomic DEG were related with synaptic transmission thus suggesting that astrocyte to neuron crosstalk is probably impaired. For instance, genes encoding for subunits of both AMPA and GABAB receptors such as *Gria5* and *Gabbr2* were dramatically upregulated in Ts65Dn astrocytes. Contrarily, *Grin2c* and *Grm5*, encoding for NMDA subunit 1 and $mGluR_5$, respectively, were downregulated in Ts65Dn. $mGluR_5$ is one of the main astroglial glutamate sensors and is responsible for detecting and responding to glutamatergic transmission as its activation induces the regulation of synaptic transmission [78]. $mGluR_5$ activation in astrocytes controls neuronal excitability and synchrony [229,230], and thus, its downregulation would made trisomic astrocytes less likely to detect glutamate, therefore preventing the astroglial modulation of glutamatergic transmission. This would hinder neuronal excitability and synchrony, fundamental processes for engram formation [9] and reactivation [13]. One interesting finding is that *Unc13*, which is involved in the vesicular release of glutamate [231], is highly downregulated in Ts65Dn hippocampal astrocytes, possibly indicating deficits in astroglial glutamate release.

In our experiments, we also found significantly increased expression of S100β in trisomic astrocytes. This was expected as S100β is encoded by a HSA21 gene. S100β is a Ca^{2+}-binding peptide that is often used as a marker of astroglial activation and is informative about the pathology in different neurological disorders [111]. As a matter of fact, there is a significant increase of S100β levels in patients of AD and frontotemporal lobe dementia [232,233]. Similarly, in the brains of individuals with DS, there is a significant correlation between S100β expression and cerebral cortical β-amyloid deposition [234]. However, the impact of S100β overexpression in the adult brain is not clear. The upregulation of S100β in astroglia from DS patient-derived iPSCs has been directly associated with a reduction of neuronal excitability and aberrant Ca^{2+} oscillations in astrocytes [94]. Remarkably, astrocyte-specific overexpression of S100β in mice prevented those

animals from forming spatial memories but also impaired hippocampal neuronal plasticity [91], suggesting that S100β is important for learning and memory.

Considering that S100β was directly associated with more frequent Ca^{2+} oscillations in DS astrocytes [94] its overexpression of S100β in Ts65Dn astrocytes, would lead to altered Ca^{2+} oscillations. Thus, we next studied both spontaneous and evoked Ca^{2+} events in astrocytes by co-expressing the genetically encoded calcium indicator (GECI) GCaMP6f and an excitatory DREADD under astrocyte-specific promoters. Contrary to what we anticipated, we found that spontaneous Ca^{2+} events had a similar event frequency comparing WT and Ts65Dn astrocytes. However, the amplitude of the transients was significantly higher in trisomic astrocytes. Although the use of different models to study Ca^{2+} signals in trisomic astrocytes (patient-derived iPSCs vs. *in vitro* slices from a mice model of DS) might account for these differences, we cannot exclude that alternative mechanisms can contribute to a differential Ca^{2+} oscillation pattern. For instance, it has been recently reported that basal Ca^{2+} levels can predict the amplitude of Ca^{2+} signals in astrocytes [235]. Of interest for DS, it was described that the resting cytosolic Ca^{2+} concentration was increased in Ts65Dn mice [192] and in Ts16 mice [191], which might explain the specific increase in Ca^{2+} amplitude, but not in frequency in Ts65Dn astrocytes. Another study reported that secreted S100β increased intracellular Ca^{2+} concentrations in neurons and in glia [236], which could also be a contributing factor in trisomic astrocytes.

Even so, the implications of higher Ca^{2+} oscillations transients amplitude for CA1 hippocampal circuits in the Ts65Dn mice are not completely understood. Recent advancements in Ca^{2+} imaging have underscored that the amplitude, location and spatiotemporal dynamics of Ca^{2+} oscillations could represent how astrocytes could encode synaptic information [237], but those vary widely across astrocytes [238,239]. Thus, the decoding of astrocyte signals is thought to disclose functional elements, such as the short- and long-term modulation of synaptic activity [240]. It has been proposed that changes in the spatiotemporal Ca^{2+} dynamics in astrocytes may influence the release of gliotransmitters into the synaptic cleft in distinct manners, hence modulating nearby synapses in multiple

forms. Herein, we show a higher Ca^{2+} oscillation amplitude in trisomic astrocytes that might suggest that aberrant Ca^{2+} activity in Ts65Dn astrocytes might exert a negative impact in neuronal communication. Interestingly, activation of the Gq pathway in astrocytes by CNO, normalized the higher peak amplitude of the astroglial transients in trisomic astrocytes. Our work by now showed alterations in the number, size and function of trisomic astrocytes. Even so, the specific mechanisms by which such alterations in trisomic astrocytes might impair synaptic transmission are difficult to anticipate.

Despite the role of astrocytes in synaptic and cognitive functions is highly controversial, many studies have demonstrated that astrocytes are able to induce neuronal activation, promote memory allocation and even enhance or impair memory performance [82,89]. Given the structural and functional alterations of trisomic astroglia it was plausible that astrocyte dysfunction could contribute to memory deficits in Ts65Dn mice. For this reason, we decided to manipulate the activity of CA1 astrocytes by expressing hM3D(Gq) while mice acquired a contextual fear memory. hM3D(Gq) inserted receptors were astrocyte-specific and functional both *ex vivo* and *in vivo* as evidenced by elevations in Ca^{2+} transients and the expression of c-Fos in astrocytes, respectively, after the administration of CNO.

In trisomic mice, astrocyte activation by CNO during the acquisition of a contextual fear memory recovered the CA1 sparser neuronal activation increasing the number of active neurons to WT levels, as shown by increased c-Fos+ cells. Conversely, no effects of CNO were detected in WT on the number of activated neurons after training. Our findings indicate that astrocyte activation in Ts65Dn mice would promote a higher neuronal activation leading to more favorable conditions for neuronal ensembles to be allocated into memory engrams.

To gain more insights into the effects of astrocyte Gq activation into memory recall, we next injected a different batch of GFAP::hM3D(Gq) WT and Ts65Dn mice but this time we sacrificed the animals after the recall session. Again, in our hands, CNO administration to WT GFAP::hM3Dq mice did not significantly increase c-Fos levels compared to saline-injected controls nor enhanced memory

performance, contrary to previous findings [82]. These differences might be explained by the different infection coverage of hM3D(Gq)-mCherry, since Adamsky et al. performed four different microinjections in order to cover a higher area of the CA1 dorsal region [82]. Another difference is that they used the AAV_8 serotype that might produce a higher expression of Gq-DREADD in astrocytes and result in higher neuronal activation. Last, our CFC protocol uses a higher shock intensity (0.6 mA; instead of 0.3 mA) along with three shocks (instead of one shock) which might explain part of these differences.

Importantly, memory performance of Ts65Dn was completely rescued in the CFC context test when astrocytes were activated with CNO during memory acquisition compared to saline-injected Ts65Dn mice. However, and opposite to what we found after training, after the CFC test, we found no differences in the number of c-Fos+ neurons comparing saline-injected and CNO-injected groups. Thus, Gq astrocyte activation improved memory in Ts65Dn mice possibly by restoring the number of active neurons during memory acquisition but not during memory recall. A possible mechanistic explanation for the rescuing effect is that astrocytes regulate synaptic transmission and plasticity so that astroglial regulation may help to modify synaptic efficacy during memory acquisition.

In order to specifically investigate how trisomic astrocytes might be involved at the synaptic level, we employed a minimal stimulation protocol to monitor the activity of a small number of synapses and evaluate whether astrocyte manipulation influenced their activity. Our results showed that activation of WT astrocytes expressing hM3D(Gq) by CNO increased the probability of neurotransmitter release and enhanced synaptic efficacy of CA1 pyramidal neurons, while synaptic potency remained unaltered, as previously described [79]. Given the ability of astrocytes to potentiate synaptic efficacy in the short-term, we would have expected a subsequent increase of number of active neurons and probably enhanced memory in WT mice, but, as described above, this was not the case. These controversial findings might be explained by the different experimental conditions: while in the *ex vivo* experiments we were monitoring single synapses in a very controlled environment (holding the membrane voltage and in the presence of picrotoxin), in the *in vivo* experiment,

we activated all the astrocytes in CA1 while mice were subjected to the acquisition of a fear memory. Moreover, whether the increased synaptic efficacy in single synapses translates to a firing rate is difficult to anticipate as it depends on the local integration of all the incoming synaptic inputs in the neuronal soma. Surprisingly, even though a rescuing effect was detected in CFC memory when trisomic astrocytes were activated during memory acquisition, trisomic astrocyte stimulation *ex vivo* resulted in decreased probability of neurotransmitter release and depressed synaptic efficacy, with no changes in synaptic potency. Interestingly, several minutes after astrocyte Gq-DREADD stimulation, synaptic efficacy started to increase. We could speculate that Ca^{2+} elevations in response to CNO activation would spread to neighboring astrocytes at a slower pace in trisomic hippocampi, due to the downregulation of Cx30 detected in the snRNA-seq experiment, thus potentiating trisomic CA1 neurons with some minutes of delay. Downregulation of Cx30 in Ts65Dn astrocytes would indicate a reduced connectivity within the astroglial syncytium that might explain this delay.

In summary, our results indicate that WT astrocytes would produce short-term potentiation of CA1 synapses by the release of glutamate whereas trisomic astrocytes would evoke a short-term depression of neurotransmitter release. However, to what extent these short-term changes in synaptic transmission might translate to hippocampal network alterations in Ts65Dn is difficult to anticipate. It has been proved that long-term changes in synaptic efficacy can be elicited by the temporal coincidence of astrocyte and post-synaptic activity [79,82]. Although we did not explore this in our experiment, it can be informative to understand how astrocytes might hinder short- and long-term changes in synaptic plasticity in the Ts65Dn hippocampus. Though minimal stimulation is a particularly helpful technique to determine how astrocyte activity influences neural communication at the single synapse level, it might not provide information about how astrocytes modulate neuronal activity at the circuit level. We are now exploring whether trisomic astrocyte Gq-activation is able to restore LTP deficits that have been extensively described in Ts65Dn mice [73,74]. Unfortunately, these results could not be included in the Thesis before the submission.

In this study, we have provided evidence at different levels of analysis that astroglia is altered in the Ts65Dn hippocampus. We have also identified several candidate mechanisms that can help to understand how dysfunctional astrocytes contribute to circuit and memory alterations in DS. The addition of the astrocyte as an additional player contributing to DS pathophysiology will hopefully help to better understand the enormous complexity of DS.

GENERAL DISCUSSION

GENERAL DISCUSSION

The purpose of the research presented in this Thesis was (i) to dissect the mechanisms underlying memory deficits resulting the trisomy of HSA21 focusing on memory engrams and (ii) to investigate the contribution of the astroglia to memory impairment and the underlying synaptic alterations found in Ts65Dn mice.

We hypothesized that memory deficits in DS are contributed by defective memory engrams and, to some extent, by dysfunctional astrocytes, due to the HSA21 triplication.

This Thesis has centered on a particular brain region: the hippocampus. The hippocampus is a widely studied area owing to its well-established trisynaptic circuit and its crucial involvement in the acquisition of episodic memories [241,242]. Besides, the hippocampus is one of the most affected areas in individuals with DS [243,244]. In this Thesis, the hippocampal-dependent episodic memories were studied in Ts65Dn mice, whose performance in contextual fear paradigms is impaired [73] and the DG might be involved in this impairment. This Thesis also studied the astrocyte abnormalities that may affect key systems essential for memory function, such as neuronal communication and synaptic function in the Ts65Dn hippocampus. These studies were focused in CA1 because it is the region where we detected a most severe astrogliosis within the Ts65Dn hippocampus. In addition, relevant studies studying astrocyte role in synaptic physiology and memory function were focused on the CA3-CA1 circuit.

Identifying engram alteration in the trisomic hippocampus

The application of engram tagging technology to study engrams has suggested that engram function might be impaired in different neurological disorders [6,14,15]. Several lines of evidence made us propose DS to be a model to study defective engrams. To determine whether this hypothesis was true, we studied how engrams form and reactivate in the Ts65Dn DG region of the dorsal hippocampus using different techniques such as activity-dependent tagging,

chemogenetics and electrophysiology, among others, in order to delineate the specific alterations of trisomic engram ensembles.

We showed that the number of activated neurons during the memory acquisition of a contextual fear memory was decreased in the Ts65Dn DG. Using activity-dependent tagging, we also found that the number of engram cells was also reduced. To date, this is the first study showing a reduced number of engram cells in DS research. However, there were several pieces of evidence showing increased sparsity of active neurons during the exposure to novel environments in Ts65Dn [68] as well as reduced levels of IEGs immediately after learning also in Ts65Dn [63]. Consistent with our findings, a recent study on engrams found that the number of active cells during memory acquisition and also during recall were decreased in a mouse model of AD [6]. We next decided to activate by chemogenetics the trisomic engram cells in order to test whether engram reactivation was defective in Ts65Dn. The chemogenetic reactivation of engram cells in the trained context was not sufficient to rescue memory deficits, suggesting that engram reactivation would be preserved in Ts65Dn mice. In previous works, memory deficits were completely rescued in a mouse model of AD when engram cells were artificially reactivated during memory recall [6]. Taking all this evidence into consideration, we reasoned that defective engram allocation during memory acquisition, and not engram reactivation, would contribute to memory alterations in Ts65Dn mice.

For this reason, we decided to increase neuronal excitability prior to learning by upregulating CREB levels in the DG of Ts65Dn mice, as increased excitability would increase the probability of engram allocation, using AAV_2-hSyn-CREB-EGFP. We found that although CREB expression was upregulated in granule cells expressing CREB-EGFP both in WT and in Ts65Dn mice, memory deficits were not rescued in Ts65Dn mice nor in WT. Reduced neuronal ensemble reactivation after memory retrieval was not recovered either. Our findings in Ts65Dn are not in accordance with the findings of Yiu et al. that recovered reduced neuronal activation, enhanced dendritic complexity and rescued memory alterations by upregulating CREB in a transgenic mouse model of AD [14]. One possible explanation of these discrepancies is that, in our study, direct

reactivation of the engram was also not able to rescue the memory alterations. Also, in our experiments we increased excitability not only in granule neurons, but also in inhibitory interneurons of the DG granule cell layer since we used a general neuronal promoter (hSyn) to overexpress CREB. Multiple studies have demonstrated that an imbalance between excitatory and inhibitory transmission in the trisomic brain contributes to synaptic alterations in mouse models of DS [245–247]. Indeed, some studies that reported hyperinnervation of basket cells into the granule cells in the DG of Ts65Dn [165] make us consider that enhancing excitability in interneurons might either promote or maintain the over inhibition that has already been reported in Ts65Dn and that is thought to hinder LTP induction [75], impair synaptic plasticity [76] and contribute to memory deficits [66]. Thus, enhancing CREB expression only in excitatory granule cells by utilizing an excitatory promoter such as CaMKIIa might promote a higher neuronal ensemble allocation to memory engrams in Ts65Dn mice. Future analysis will help to elucidate if this is the case.

In recent years, engram research has underscored several changes in engram cell structure and function that are of paramount importance to enable them to reactivate upon specific recall cues. In agreement with these studies [3,4,6,13], we found an increased spine density, reduced rheobase in WT engram cells compared to non-engram cells, showing that WT engram cells have not only undergone synaptic potentiation, but are also more excitable than non-engram counterparts. Whereas in Ts65Dn engram cells we found a higher number of spines than non-engram cells, the number of mature spines was significantly reduced compared to WT engram cells, supporting the notion that although synaptic potentiation occur in trisomic engram cells, it might not be enough to faithfully store learning cues during memory acquisition and consolidation. Remarkably, no differences were detected in trisomic engram cells after memory recall regarding rheobase indicating a lack of enhanced excitability at the time of memory retrieval.

It was shown that enhanced excitability immediately after memory recall [13] could be explained by a downregulation of Kir2.1 channels in engram cells. Of interest for DS, triplication of the *Kcnj6* gene, encoding for Kir3.2, occurs both in

humans and in Ts65Dn mice. Kir3.2 normalization resulted in a complete rescue of short- and long term potentiation and memory deficits in Ts65Dn mice [65]. We found that Kir3.2 was overexpressed not only in the DG of Ts65Dn but also in engram and non-engram cells compared to WT mice. In WT mice, engram cells showed reduced levels of Kir3.2 compared to non-engram cells whereas in Ts65Dn mice this effect was not observed. These findings suggest that Kir3.2 downregulation might serve as an additional mechanism to regulate engram cell excitability in control conditions. Nonetheless, this was not the case in the trisomic scenario. Reduced excitability due to basal higher expression of Kir3.2 might not only impede trisomic neuronal ensembles activate, and therefore allocate to an engram during memory acquisition, but also would hinder their reactivation when recall cues are presented. Further insights on whether the lack of excitability contributes to engram alterations in Ts65Dn will be revealed if the normalization of Kir3.2 expression on excitatory granule cells is sufficient to promote neuronal allocation to an engram and we observe an enhancement of memory performance on Ts65Dn mice. We would also expect a higher excitability at the time of memory recall. This short-term window of higher excitability has been associated not only with enhanced pattern separation as evidenced by a higher context recognition but also to a greater ability for pattern completion-mediated retrieval of encoded memory content [13]. Hence, normalization Kir3.2 in Ts65Dn mice would facilitate the transient rise in engram cell excitability in response to relevant contextual cues enhancing memory retrieval capacity.

In the last decade, the discovery of engram cells has completely changed the understanding of how memory works, providing unimaginable possibilities for rethinking intellectual disability and investigating memory alterations from a different perspective. Altogether, our findings reveal that memory deficits in Ts65Dn mice would not be completely explained by a failure of trisomic engram cells to reawaken during memory recall since activation of training activated cells do not recover memory deficits in Ts65Dn mice. Instead, sparser neural ensemble activation during memory acquisition in Ts65Dn mice would hinder an adequate memory encoding and/or consolidation that is indispensable for subsequent faithful and trustworthy expression of acquired memories.

Examining astrocyte alterations in the trisomic hippocampus

Lately, the development of new techniques have made it possible the manipulation and visualization of astrocyte activity providing unprecedented opportunities to uncover how dysfunctional astrocytes can be responsible for part of the neuronal alterations found in different neurodevelopmental disorders. In this Thesis, I have examined how astrocyte abnormalities can impair important memory-related functions including synaptic transmission and mnemonic processes such as memory acquisition and recall in the Ts65Dn hippocampus.

I generated, to the best of our knowledge, the first systematic quantification of astrocyte distribution in the dorsal hippocampus of Ts65Dn mice using unbiased stereological techniques. We detected an increased astrocyte number in different dendritic regions of CA1 and in the granule cell layer of the DG of Ts65Dn mice. In contrast, neuronal numbers did not vary in the main neuronal layers. Astrocytes coordinate in non-overlapping territories the synchronization of different neurons [248]. Thus, these region-specific changes in astroglia/neuron number may cause subtle but relevant alterations in the computation capacity of different hippocampal regions whose function is established in different mnemonic processes. For instance, the separation of similar patterns during learning takes place in the DG while the retrieval of memories is dependent on CA1. Although we cannot exclude that higher astrocyte number in CA1 or DG might contribute to some extent to the deficits in hippocampal-dependent tasks that are found in Ts65Dn mice, what we can certainly argue is that alterations in trisomic astrocyte function is instrumental for circuit in memory alterations in DS.

Using a chemogenetic approach, we were able to enhance neuronal recruitment in CA1 by activating the Gq pathway in trisomic astrocytes during memory acquisition. Moreover, Gq-DREADD activation in CA1 during memory acquisition was able to completely recover contextual fear memory deficits in Ts65Dn. Given the paramount importance of an adequate number of neurons allocated to a memory engram for memory consolidation and recall [6,9,14,15], our results suggest that astrocyte Gq-pathway activation would promote a higher recruitment of trisomic neurons into memory engrams. Astrocyte release of gliotransmitters has been shown to potentiate synapses in short [79] and in the long-term [82].

Perea et al. reported that astrocytes were able to potentiate single hippocampal synapses in the short-term by activating neuronal mGluRs through the glutamate release from astrocytes [79]. This potentiation became persistent when astrocyte stimulation coincided with neuronal depolarization and was independent of NMDA receptors [79]. Contrarily, Adamsky et al. showed that astrocyte-dependent potentiation by Gq-DREADD activation was mediated by NMDAR but not by presynaptic mGluRs [82]. Additionally, blocking D-serine, which is another astrocyte-dependent critical factor needed for LTP [249], prevented astrocyte-mediated potentiation [82]. Altogether, these studies suggest that multiple factors such as glutamate and D-serine can contribute to the astrocyte-dependent induction of LTP. However, both studies found that astrocyte-mediated persistent potentiation required the coincident activity of astrocytes and neurons. In our single nucleus RNA-seq dataset, we found that main astroglial sensors of glutamatergic activity, NMDA and $mGluR_5$ were dramatically downregulated in trisomic astrocytes. These findings would indicate that trisomic astrocytes would be less likely to sense and, consequently, to respond with Ca^{2+} elevations to excitatory neurotransmission. Hence, trisomic astrocytes would fail to enhance excitatory transmission during learning events. However, Gq-DREADDs allow to bypass deficient glutamate sensors by activating intracellular signaling responsible leading to gliotransmitter release [100,215]. Our results showing a complete memory recovery in Ts65Dn would indicate that eliciting gliotransmitter release by activating Gq pathway through an excitatory DREADD would be sufficient to compensate for downregulation of NMDA and $mGluR_5$ in trisomic astrocytes. Future analyses are needed to further understand the full complexity of astrocyte deregulation in DS.

While in **Chapter II** we focused our studies of astrocyte-neuron crosstalk in the CA1 region of the hippocampus, the characterization of engram alterations in **Chapter I** were done in the dorsal DG. Although we would expect that part of the findings that we observed manipulating astrocyte activity in CA1 would be replicated in the DG, further studies are needed to corroborate that this is the case. As a proof of concept for this Thesis, we activated trisomic astrocytes in the dorsal DG with a Gq-DREADD before the acquisition of a contextual fear

memory. We found that trisomic astrocyte activation completely recovered the decreased neuronal activation in the DG that was described in **Chapter I** in the DG during memory acquisition. These results would suggest that in the DG, astrocytes are also able to enhance the recruitment of a higher number of neurons into memory engrams. Actually, it was found that astrocyte repeated depolarization in the DG molecular layer led to a potentiation of granular neurons as evidenced by their higher amplitude of elicited EPSCs [250]. Similarly, it was shown that astrocyte-mediated potentiation occurs in the granule neurons when astroglial P2Y1R receptors are activated in the presence of TNF-α [251]. Further analysis will help to elucidate whether astrocyte dysfunction in DS is directly responsible for synaptic dysfunction or, in opposition, astrocytes can be used as a mechanistic tool to enhance synaptic plasticity that is required for memory formation.

Besides the information we gathered from structural and functional techniques, we also found that the transcriptomic profile of trisomic astroglia was dramatically deregulated as a result of the trisomy. In our analysis we were able to identify relevant DEG in trisomic astroglia that were not previously described thus providing new avenues to investigate how gene deregulation in trisomic astroglia can impact the pathophysiology of DS. This is particularly relevant since most of the transcriptomic studies in DS have focused on the neuronal population [63,252,253].

An especially compelling example is the upregulation of several markers of reactive astroglia associated with neuronal injury and inflammation that would confirm the astrogliosis that we and others have reported in Ts65Dn [117]. Supporting these findings, it has been found in post mortem studies that in the hippocampus of fetuses with DS there is a higher fraction of cells with astroglial phenotype [30]. Similarly, gene analysis from iPSCs from monozygotic twins discordant for trisomy 21, revealed a shift towards the astroglial phenotype [116].

Establishment of long-range communication and transport of astrocytic networks is enabled by extensive gap junctional coupling [254,255]. As a matter of fact, hippocampal slices from Cx30/43 double-knockout showed a reduction of the diffusion of glucose and its metabolites such as lactate within the network that led

to a synaptic depression compared to control conditions [256]. Our findings suggest that astroglial syncytium in Ts65Dn would be less interconnected as evidenced by the downregulation of Cx30. Although the consequences of downregulation of Cx30 are difficult to anticipate, several studies have reported that Cx30-deficient mice showed impaired synaptic plasticity and memory impairments in contextual fear conditioning tests [228]. These alterations in hippocampal glutamatergic signaling were due to an increase in the extracellular glutamate uptake from astrocytes, resulting in decreased glutamate levels in the synaptic cleft.

Until very recently, both cognitive and behavioral impairments found in people with DS were ascribed to neuronal abnormalities. However, in the last two decades, astrocytes have emerged as important players in neurotransmission, allowing researchers to look at long-standing concerns in the field of intellectual disability from a different perspective. Astrocytes are also promising in terms of cognitive and behavioral recovery since their ability to influence energy metabolism, control synaptic transmission, modify blood supply and respond to inflammatory signals. Although further studies are needed to understand the full complexity of astrocyte dysfunction in DS, our results suggest that strategies with focus on ameliorating astrocyte alterations might provide new therapeutic avenues to treat cognitive dysfunction in DS.

CONCLUSIONS

CONCLUSIONS

1. Neuronal allocation to an engram is impaired in Ts65Dn mice as shown by the reduced granule cell activation during memory acquisition.

2. Chemogenetic reactivation of the engram did not recover worse memory performance in Ts65Dn mice, suggesting that memory deficits depend on the reduced number of engram cells that could not be bypassed by engram reactivation during recall.

3. Trisomic engram cells undergo plastic changes during learning but exhibit a lowered number of mature spines compared to WT engram cells, suggesting that plasticity would be limited in trisomic engram cells.

4. Trisomic engram cells did not undergo transient excitability enhancement after memory retrieval, which would hinder context discrimination capacity during context test. These observations could be explained by the upregulation of Kir3.2 in the DG along with lack of internalization of Kir3.2 in Ts65Dn engram cells.

5. Enhancing CREB expression of granule cells prior to learning does not recover memory deficits nor the reduced neuronal ensemble reactivation during memory recall neither in WT nor in Ts65Dn.

6. In the Ts65Dn hippocampus there is a sub-region specific astrocytosis being CA1 and DG the regions where astrocytes are more abundant.

7. The analysis of the single nuclei transcriptomics data highlighted unique potential genes that might be responsible for astrocyte dysfunction in DS.

8. Activation of Gq-DREADD in trisomic astrocytes during memory acquisition recovers the reduced neuronal activation in Ts65Dn and completely rescues deficits in contextual fear memory in Ts65Dn mice.

BIBLIOGRAPHY

BIBLIOGRAPHY

This section contains the bibliography of the General Introduction, Chapter I, Chapter II and General Discussion.

1. Attneave F, B. M, Hebb DO. The Organization of Behavior; A Neuropsychological Theory. Am J Psychol. 1950;63(4):633.
2. Semon R. Die Mneme. VERLAG VON WILHELM ENGELMANN. 1904.
3. Liu X, Ramirez S, Pang PT, Puryear CB, Govindarajan A, Deisseroth K, et al. Optogenetic stimulation of a hippocampal engram activates fear memory recall. Nature. 2012;
4. Ryan TJ, Roy DS, Pignatelli M, Arons A, Tonegawa S. Engram cells retain memory under retrograde amnesia. Science (80). 2015;
5. Reijmers LG, Perkins BL, Matsuo N, Mayford M. Localization of a stable neural correlate of associative memory. Science (80-). 2007;
6. Roy DS, Arons A, Mitchell TI, Pignatelli M, Ryan TJ, Tonegawa S. Memory retrieval by activating engram cells in mouse models of early Alzheimer's disease. Nature. 2016 Mar 24;531(7595):508–12.
7. Sekeres MJ, Neve RL, Frankland PW, Josselyn SA. Dorsal hippocampal CREB is both necessary and sufficient for spatial memory. Learn Mem. 2010 Jun;17(6):280–3.
8. Han JH, Kushner SA, Yiu AP, Hsiang HL, Buch T, Waisman A, et al. Selective erasure of a fear memory. Science. 2009 Mar 13;323(5920):1492–6.
9. Han JH, Kushner SA, Yiu AP, Cole CJ, Matynia A, Brown RA, et al. Neuronal competition and selection during memory formation. Science (80-). 2007;
10. Kim J, Kwon JT, Kim HS, Josselyn SA, Han JH. Memory recall and modifications by activating neurons with elevated CREB. Nat Neurosci. 2014;
11. Leake J, Zinn R, Corbit LH, Fanselow MS, Vissel B. Engram Size Varies with Learning and Reflects Memory Content and Precision. J Neurosci. 2021 May 5;41(18):4120–30.

12. Choi JH, Sim SE, Kim J il, Choi DII, Oh J, Ye S, et al. Interregional synaptic maps among engram cells underlie memory formation. Science. 2018 Apr 27;360(6387):430–5.
13. Pignatelli M, Ryan TJ, Roy DS, Lovett C, Smith LM, Muralidhar S, et al. Engram Cell Excitability State Determines the Efficacy of Memory Retrieval. Neuron. 2019;
14. Yiu AP, Rashid AJ, Josselyn SA. Increasing CREB function in the CA1 region of dorsal hippocampus rescues the spatial memory deficits in a mouse model of Alzheimer's disease. Neuropsychopharmacology. 2011 Oct;36(11):2169–86.
15. Li J, Jiang RY, Arendt KL, Hsu YT, Zhai SR, Chen L. Defective memory engram reactivation underlies impaired fear memory recall in Fragile X syndrome. Elife. 2020 Oct 1;9:1–20.
16. Shin M, Besser LM, Kucik JE, Lu C, Siffel C, Correa A. Prevalence of Down syndrome among children and adolescents in 10 regions of the United States. Pediatrics. 2009 Dec;124(6):1565–71.
17. de Graaf G, Buckley F, Skotko BG. Estimation of the number of people with Down syndrome in Europe. Eur J Hum Genet. 2021 Mar 1;29(3):402–10.
18. Lott IT, Head E. Alzheimer disease and Down syndrome: factors in pathogenesis. Neurobiol Aging. 2005 Mar;26(3):383–9.
19. Lott IT, Head E. Dementia in Down syndrome: unique insights for Alzheimer disease research. Nat Rev Neurol. 2019 Mar 1;15(3):135–47.
20. Down JL. Observations on an ethnic classification of idiots. 1866. Ment Retard. 1995 Feb;33(1):54–6.
21. LEJEUNE J, TURPIN R, GAUTIER M. [Mongolism; a chromosomal disease (trisomy)]. Bull Acad Natl Med. 143(11–12):256–65.
22. Pinter JD, Eliez S, Schmitt JE, Capone GT, Reiss AL. Neuroanatomy of Down's syndrome: A high-resolution MRI study. Am J Psychiatry. 2001;158(10):1659–65.
23. Raz N, Torres IJ, Briggs SD, Spencer WD, Thornton AE, Loken WJ, et al. Selective neuroanatomic abnormalities in down's syndrome and their cognitive correlates: Evidence from mri morphometry. Neurology.

1995;45(2):356–66.

24. Menghini D, Costanzo F, Vicari S. Relationship between brain and cognitive processes in Down syndrome. Behav Genet. 2011 May;41(3):381–93.
25. Rodrigues M, Nunes J, Figueiredo S, Martins de Campos A, Geraldo AF. Neuroimaging assessment in Down syndrome: a pictorial review. Insights Imaging. 2019 Dec 1;10(1):1–13.
26. Pujol J, del Hoyo L, Blanco-Hinojo L, de Sola S, Macià D, Martínez-Vilavella G, et al. Anomalous brain functional connectivity contributing to poor adaptive behavior in Down syndrome. Cortex. 2015 Mar 1;64:148–56.
27. Imai M, Watanabe H, Yasui K, Kimura Y, Shitara Y, Tsuchida S, et al. Functional connectivity of the cortex of term and preterm infants and infants with Down's syndrome. Neuroimage. 2014 Jan 15;85:272–8.
28. Wilson LR, Vatansever D, Annus T, Williams GB, Hong YT, Fryer TD, et al. Differential effects of Down's syndrome and Alzheimer's neuropathology on default mode connectivity. Hum Brain Mapp. 2019 Oct 15;40(15):4551–63.
29. Stagni F, Giacomini A, Emili M, Guidi S, Bartesaghi R. Neurogenesis impairment: An early developmental defect in Down syndrome. Free Radic Biol Med. 2018 Jan 1;114:15–32.
30. Guidi S, Bonasoni P, Ceccarelli C, Santini D, Gualtieri F, Ciani E, et al. Neurogenesis impairment and increased cell death reduce total neuron number in the hippocampal region of fetuses with Down syndrome. Brain Pathol. 2008;
31. Guidi S, Ciani E, Bonasoni P, Santini D, Bartesaghi R. Widespread proliferation impairment and hypocellularity in the cerebellum of fetuses with down syndrome. Brain Pathol. 2011 Jul;21(4):361–73.
32. Contestabile A, Fila T, Ceccarelli C, Bonasoni P, Bonapace L, Santini D, et al. Cell cycle alteration and decreased cell proliferation in the hippocampal dentate gyrus and in the neocortical germinal matrix of fetuses with Down syndrome and in Ts65Dn mice. Hippocampus. 2007;17(8):665–78.
33. Winter TC, Ostrovsky AA, Komamiski CA, Uhrich SB. Cerebellar and frontal

lobe hypoplasia in fetuses with trisomy 21: usefulness as combined US markers. Radiology. 2000;214(2):533–8.

34. Guihard-Costa AM, Khung S, Delbecque K, Ménez F, Delezoide AL. Biometry of face and brain in fetuses with trisomy 21. Pediatr Res. 2006 Jan;59(1):33–8.
35. Golden JA, Hyman BT. Development of the superior temporal neocortex is anomalous in trisomy 21. J Neuropathol Exp Neurol. 1994;53(5):513–20.
36. Jernigan TL, Hesselink JR, Bellugi U, Doherty S, Sowell E, Jernigan TL, et al. Cerebral morphologic distinctions between Williams and Down syndromes. Arch Neurol. 1993;50(2):186–91.
37. KE W, M LK, HM W. Evidence of arrest of neurogenesis and synaptogenesis in brains of patients with Down's syndrome. N Engl J Med. 1984 Nov;311(18):1187–1187.
38. Pine SS, Landing BH, Shankle WR. Reduced inferior olivary neuron number in early Down syndrome. Pediatr Pathol Lab Med. 1997;17(4):537–45.
39. Guidi S, Giacomini A, Stagni F, Emili M, Uguagliati B, Bonasoni MP, et al. Abnormal development of the inferior temporal region in fetuses with Down syndrome. Brain Pathol. 2018 Nov 1;28(6):986–98.
40. Alemany-González M, Gener T, Nebot P, Vilademunt M, Dierssen M, Puig MV. Prefrontal-hippocampal functional connectivity encodes recognition memory and is impaired in intellectual disability. Proc Natl Acad Sci U S A. 2020 May 26;117(21).
41. Lorenzi HA, Reeves RH. Hippocampal hypocellularity in the Ts65Dn mouse originates early in development. Brain Res. 2006;
42. Belichenko P V., Kleschevnikov AM, Salehi A, Epstein CJ, Mobley WC. Synaptic and cognitive abnormalities in mouse models of Down syndrome: exploring genotype-phenotype relationships. J Comp Neurol. 2007 Oct 1;504(4):329–45.
43. Belichenko NP, Belichenko P V., Kleschevnikov AM, Salehi A, Reeves RH, Mobley WC. The "Down syndrome critical region" is sufficient in the mouse model to confer behavioral, neurophysiological, and synaptic phenotypes

characteristic of Down syndrome. J Neurosci. 2009 May 6;29(18):5938–48.
44. Insausti AM, Megías M, Crespo D, Cruz-Orive LM, Dierssen M, Vallina TF, et al. Hippocampal volume and neuronal number in Ts65Dn mice: A murine model of Down syndrome. Neurosci Lett. 1998 Sep 3;253(3):175–8.
45. Chakrabarti L, Galdzicki Z, Haydar TF. Defects in embryonic neurogenesis and initial synapse formation in the forebrain of the Ts65Dn mouse model of Down syndrome. J Neurosci. 2007 Oct 24;27(43):11483–95.
46. Baxter LL, Moran TH, Richtsmeier JT, Troncoso J, Reeves RH. Discovery and genetic localization of Down syndrome cerebellar phenotypes using the Ts65Dn mouse. Hum Mol Genet. 2000;9(2):195–202.
47. Olson LE, Roper RJ, Baxter LL, Carlson EJ, Epstein CJ, Reeves RH. Down syndrome mouse models Ts65Dn, Ts1Cje, and Ms1Cje/Ts65Dn exhibit variable severity of cerebellar phenotypes. Dev Dyn. 2004 Jul;230(3):581–9.
48. Bianchi P, Ciani E, Contestabile A, Guidi S, Bartesaghi R. Lithium restores neurogenesis in the subventricular zone of the Ts65Dn mouse, a model for Down syndrome. Brain Pathol. 2010 Jan;20(1):106–18.
49. Clark S, Schwalbe J, Stasko MR, Yarowsky PJ, Costa ACS. Fluoxetine rescues deficient neurogenesis in hippocampus of the Ts65Dn mouse model for Down syndrome. Exp Neurol. 2006 Jul;200(1):256–61.
50. Pons-Espinal M, Martinez de Lagran M, Dierssen M. Environmental enrichment rescues DYRK1A activity and hippocampal adult neurogenesis in TgDyrk1A. Neurobiol Dis. 2013 Dec;60:18–31.
51. Dierssen M, Benavides-Piccione R, Martínez-Cué C, Estivill X, Flórez J, Elston GN, et al. Alterations of neocortical pyramidal cell phenotype in the Ts65Dn mouse model of Down syndrome: Effects of environmental enrichment. Cereb Cortex. 2003;
52. Uguagliati B, Al-Absi AR, Stagni F, Emili M, Giacomini A, Guidi S, et al. Early appearance of developmental alterations in the dendritic tree of the hippocampal granule cells in the Ts65Dn model of Down syndrome. Hippocampus. 2021 Apr 1;31(4):435–47.
53. Emili M, Stagni F, Salvalai ME, Uguagliati B, Giacomini A, Albach C, et al.

Neonatal therapy with clenbuterol and salmeterol restores spinogenesis and dendritic complexity in the dentate gyrus of the Ts65Dn model of Down syndrome. Neurobiol Dis. 2020 Jul 1;140.

54. Becker W, Soppa U, Tejedor F. DYRK1A: a potential drug target for multiple Down syndrome neuropathologies. CNS Neurol Disord Drug Targets. 2014 Feb 11;13(1):26–33.
55. Ruiz-Mejias M, de Lagran MM, Mattia M, Castano-Prat P, Perez-Mendez L, Ciria-Suarez L, et al. Overexpression of Dyrk1A, a Down Syndrome Candidate, Decreases Excitability and Impairs Gamma Oscillations in the Prefrontal Cortex. J Neurosci. 2016 Mar 30;36(13):3648–59.
56. Ferrer I, Barrachina M, Puig B, Martínez De Lagrán M, Martí E, Avila J, et al. Constitutive Dyrk1A is abnormally expressed in Alzheimer disease, Down syndrome, Pick disease, and related transgenic models. Neurobiol Dis. 2005 Nov;20(2):392–400.
57. Sago H, Carlson EJ, Smith DJ, Rubin EM, Crnic LS, Huang TT, et al. Genetic dissection of region associated with behavioral abnormalities in mouse models for Down syndrome. Pediatr Res. 2000;48(5):606–13.
58. Kida E, Rabe A, Walus M, Albertini G, Golabek AA. Long-term running alleviates some behavioral and molecular abnormalities in Down syndrome mouse model Ts65Dn. Exp Neurol. 2013 Feb;240(1):178–89.
59. Doran E, Keator D, Head E, Phelan MJ, Kim R, Totoiu M, et al. Down Syndrome, Partial Trisomy 21, and Absence of Alzheimer's Disease: The Role of APP. J Alzheimers Dis. 2017;56(2):459–70.
60. Lu J, Esposito G, Scuderi C, Steardo L, Delli-Bovi LC, Hecht JL, et al. S100B and APP promote a gliocentric shift and impaired neurogenesis in Down syndrome neural progenitors. PLoS One. 2011;6(7).
61. Jiang Y, Mullaney KA, Peterhoff CM, Che S, Schmidt SD, Boyer-Boiteau A, et al. Alzheimer's-related endosome dysfunction in Down syndrome is Abeta-independent but requires APP and is reversed by BACE-1 inhibition. Proc Natl Acad Sci U S A. 2010 Jan 26;107(4):1630–5.
62. Altafaj X, Martín ED, Ortiz-Abalia J, Valderrama A, Lao-Peregrín C, Dierssen M, et al. Normalization of Dyrk1A expression by AAV2/1-

shDyrk1A attenuates hippocampal-dependent defects in the Ts65Dn mouse model of Down syndrome. Neurobiol Dis. 2013 Apr;52:117–27.

63. Sierra C. SM. FBA. & DM. The lncRNA Snhg11 is required for synaptic function, neurogenesis and memory and is downregulated in the dentate gyrus of Down syndrome mouse models. Res Sq. 2022;
64. Park S, Kramer EE, Mercaldo V, Rashid AJ, Insel N, Frankland PW, et al. Neuronal Allocation to a Hippocampal Engram. Neuropsychopharmacology. 2016;
65. Kleschevnikov AM, Yu J, Kim J, Lysenko L V., Zeng Z, Yu YE, et al. Evidence that increased Kcnj6 gene dose is necessary for deficits in behavior and dentate gyrus synaptic plasticity in the Ts65Dn mouse model of Down syndrome. Neurobiol Dis. 2017;
66. Kleschevnikov AM, Belichenko P V., Gall J, George L, Nosheny R, Maloney MT, et al. Increased efficiency of the GABAA and GABAB receptor-mediated neurotransmission in the Ts65Dn mouse model of Down syndrome. Neurobiol Dis. 2012 Feb;45(2):683–91.
67. Stagni F, Magistretti J, Guidi S, Ciani E, Mangano C, Calzà L, et al. Pharmacotherapy with Fluoxetine Restores Functional Connectivity from the Dentate Gyrus to Field CA3 in the Ts65Dn Mouse Model of Down Syndrome. PLoS One. 2013;
68. Smith-Hicks CL, Cai P, Savonenko A V., Reeves RH, Worley PF. Increased sparsity of hippocampal CA1 neuronal ensembles in a mouse model of down syndrome assayed by Arc expression. Front Neural Circuits. 2017;
69. Popov VI, Kleschevnikov AM, Klimenko OA, Stewart MG, Belichenko P V. Three-dimensional synaptic ultrastructure in the dentate gyrus and hippocampal area CA3 in the Ts65Dn mouse model of Down syndrome. J Comp Neurol. 2011 May 1;519(7):1338–54.
70. Marin-Padilla M. Pyramidal cell abnormalities in the motor cortex of a child with Down's syndrome. A Golgi study. J Comp Neurol. 1976;
71. Becker LE, Armstrong DL, Chan F. Dendritic atrophy in children with Down's syndrome. Ann Neurol. 1986;20(4):520–6.
72. Takashima S, Becker LE, Armstrong DL, Chan F. Abnormal neuronal

development in the visual cortex of the human fetus and infant with down's syndrome. A quantitative and qualitative golgi study. Brain Res. 1981 Nov 23;225(1):1–21.

73. Costa ACS, Scott-McKean JJ, Stasko MR. Acute injections of the NMDA receptor antagonist memantine rescue performance deficits of the Ts65Dn mouse model of Down syndrome on a fear conditioning test. Neuropsychopharmacology. 2008 Jun;33(7):1624–32.
74. Navarro-Romero A, Vázquez-Oliver A, Gomis-González M, Garzón-Montesinos C, Falcón-Moya R, Pastor A, et al. Cannabinoid type-1 receptor blockade restores neurological phenotypes in two models for Down syndrome. Neurobiol Dis. 2019 May 1;125:92–106.
75. Kleschevnicov AM, Belichenko P V., Villar AJ, Epstein CJ, Malenka RC, Mobley WC. Hippocampal long-term potentiation suppressed by increased inhibition in the Ts65Dn mouse, a genetic model of Down syndrome. J Neurosci. 2004 Sep 15;24(37):8153–60.
76. Siarey RJ, Carlson EJ, Epstein CJ, Balbo A, Rapoport SI, Galdzicki Z. Increased synaptic depression in the Ts65Dn mouse, a model for mental retardation in Down syndrome. Neuropharmacology. 1999;38(12):1917–20.
77. Durkee CA, Araque A. Diversity and Specificity of Astrocyte–neuron Communication. Neuroscience. 2019.
78. Panatier A, Robitaille R. Astrocytic mGluR5 and the tripartite synapse. Neuroscience. 2016.
79. Perea G, Araque A. Astrocytes potentiate transmitter release at single hippocampal synapses. Science (80-). 2007;
80. Achour S Ben, Pont-Lezica L, Béchade C, Pascual O. Is astrocyte calcium signaling relevant for synaptic plasticity? Neuron Glia Biology. 2010.
81. Mederos S, Perea G. GABAergic-astrocyte signaling: A refinement of inhibitory brain networks. Glia. 2019;67(10):1842–51.
82. Adamsky A, Kol A, Kreisel T, Doron A, Ozeri-Engelhard N, Melcer T, et al. Astrocytic Activation Generates De Novo Neuronal Potentiation and Memory Enhancement. Cell. 2018;

83. Cavaccini A, Durkee C, Kofuji P, Tonini R, Araque A. Astrocyte signaling gates long-term depression at corticostriatal synapses of the direct pathway. J Neurosci. 2020;40(30):5757–68.
84. Araque A, Parpura V, Sanzgiri RP, Haydon PG. Tripartite synapses: Glia, the unacknowledged partner. Trends in Neurosciences. 1999.
85. Araque A, Carmignoto G, Haydon PG, Oliet SHR, Robitaille R, Volterra A. Gliotransmitters travel in time and space. Neuron. 2014.
86. Volterra A, Liaudet N, Savtchouk I. Astrocyte Ca2+ signalling: An unexpected complexity. Nature Reviews Neuroscience. 2014.
87. Savtchouk I, Volterra A. Gliotransmission: Beyond black-and-white. J Neurosci. 2018;
88. Suzuki A, Stern SA, Bozdagi O, Huntley GW, Walker RH, Magistretti PJ, et al. Astrocyte-neuron lactate transport is required for long-term memory formation. Cell. 2011;
89. Kol A, Adamsky A, Groysman M, Kreisel T, London M, Goshen I. Astrocytes contribute to remote memory formation by modulating hippocampal–cortical communication during learning. Nat Neurosci. 2020;
90. Lee HS, Ghetti A, Pinto-Duarte A, Wang X, Dziewczapolski G, Galimi F, et al. Astrocytes contribute to gamma oscillations and recognition memory. Proc Natl Acad Sci U S A. 2014;
91. Gerlai R, Wojtowicz JM, Marks A, Roder J. Overexpression of a calcium-binding protein, S100 beta, in astrocytes alters synaptic plasticity and impairs spatial learning in transgenic mice. Learn Mem. 1995;
92. Nishiyama H, Knöpfel T, Endo S, Itohara S. Glial protein S100B modulates long-term neuronal synaptic plasticity. Proc Natl Acad Sci U S A. 2002;
93. Morquette P, Verdier D, Kadala A, Féthière J, Philippe AG, Robitaille R, et al. An astrocyte-dependent mechanism for neuronal rhythmogenesis. Nat Neurosci. 2015;
94. Mizuno GO, Wang Y, Shi G, Wang Y, Sun J, Papadopoulos S, et al. Aberrant Calcium Signaling in Astrocytes Inhibits Neuronal Excitability in a Human Down Syndrome Stem Cell Model. Cell Rep. 2018;
95. Ahlemeyer B, Beier H, Semkova I, Schaper C, Krieglstein J. S-100β

protects cultured neurons against glutamate- and staurosporine-induced damage and is involved in the antiapoptotic action of the 5 HT(1A)-receptor agonist, Bay x 3702. Brain Res. 2000;

96. Mori T, Tan J, Arendash GW, Koyama N, Nojima Y, Town T. Overexpression of human S100B exacerbates brain damage and periinfarct gliosis after permanent focal ischemia. Stroke. 2008;
97. Villarreal A, Aviles Reyes RX, Angelo MF, Reinesf AG, Ramos AJ. S100B alters neuronal survival and dendrite extension via RAGE-mediated NF-κB signaling. J Neurochem. 2011;
98. Benchenane K, Tiesinga PH, Battaglia FP. Oscillations in the prefrontal cortex: A gateway to memory and attention. Current Opinion in Neurobiology. 2011.
99. Borroto-Escuela DO, Carlsson J, Ambrogini P, Narváez M, Wydra K, Tarakanov AO, et al. Understanding the Role of GPCR Heteroreceptor Complexes in Modulating the Brain Networks in Health and Disease. Front Cell Neurosci. 2017 Feb 21;11.
100. Durkee CA, Covelo A, Lines J, Kofuji P, Aguilar J, Araque A. G i/o protein-coupled receptors inhibit neurons but activate astrocytes and stimulate gliotransmission. Glia. 2019;
101. Doron A, Goshen I. Investigating the transition from recent to remote memory using advanced tools. Brain Research Bulletin. 2018.
102. Frankland PW, Bontempi B. The organization of recent and remote memories. Nature Reviews Neuroscience. 2005.
103. Moscovitch M, Cabeza R, Winocur G, Nadel L. Episodic memory and beyond: The hippocampus and neocortex in transformation. Annu Rev Psychol. 2016;
104. Ponroy Bally B, Farmer WT, Jones E V., Jessa S, Kacerovsky JB, Mayran A, et al. Human iPSC-derived Down syndrome astrocytes display genome-wide perturbations in gene expression, an altered adhesion profile, and increased cellular dynamics. Hum Mol Genet. 2020;29(5):785–802.
105. Araujo BHS, Kaid C, De Souza JS, Gomes da Silva S, Goulart E, Caires LCJ, et al. Down Syndrome iPSC-Derived Astrocytes Impair Neuronal

Synaptogenesis and the mTOR Pathway In Vitro. Mol Neurobiol. 2018;55(7):5962–75.

106. Simpson JE, Ince PG, Lace G, Forster G, Shaw PJ, Matthews F, et al. Astrocyte phenotype in relation to Alzheimer-type pathology in the ageing brain. Neurobiol Aging. 2010;
107. Mito T, Becker LE. Developmental changes of S-100 protein and glial fibrillary acidic protein in the brain in Down syndrome. Exp Neurol. 1993;
108. Murphy GM, Ellis WG, Lee YL, Stultz KE, Shrivastava R, Tinklenberg JR, et al. Astrocytic gliosis in the amygdala in Down's syndrome and Alzheimer's disease. Prog Brain Res. 1992;
109. Guttenplan KA, Stafford BK, El-Danaf RN, Adler DI, Münch AE, Weigel MK, et al. Neurotoxic Reactive Astrocytes Drive Neuronal Death after Retinal Injury. Cell Rep. 2020;31(12).
110. Kia A, McAvoy K, Krishnamurthy K, Trotti D, Pasinelli P. Astrocytes expressing ALS-linked mutant FUS induce motor neuron death through release of tumor necrosis factor-alpha. Glia. 2018;66(5):1016–33.
111. Sofroniew M V. Astrogliosis. Cold Spring Harb Perspect Biol. 2015;
112. Pekny M, Pekna M. Astrocyte reactivity and reactive astrogliosis: Costs and benefits. Physiol Rev. 2014;94(4):1077–98.
113. Sofroniew M V. Molecular dissection of reactive astrogliosis and glial scar formation. Vol. 32, Trends in Neurosciences. 2009. p. 638–47.
114. Griffin WST, Sheng JG, Mckenzie JE, Royston MC, Gentleman SM, Brumback RA, et al. Life-long overexpression of S100β in Down's syndrome: Implications for Alzheimer pathogenesis. Neurobiol Aging. 1998;19(5):401–5.
115. Griffin WST, Stanley LC, Ling C, White L, MacLeod V, Perrot LJ, et al. Brain interleukin 1 and S-100 immunoreactivity are elevated in Down syndrome and Alzheimer disease. Proc Natl Acad Sci U S A. 1989;86(19):7611–5.
116. Letourneau A, Santoni FA, Bonilla X, Sailani MR, Gonzalez D, Kind J, et al. Domains of genome-wide gene expression dysregulation in Down's syndrome. Nat 2014 5087496. 2014 Apr 16;508(7496):345–50.
117. Lockrow JP, Fortress AM, Granholm ACE. Age-related neurodegeneration

and memory loss in down syndrome. Current Gerontology and Geriatrics Research. 2012.

118. Kurabayashi N, Nguyen MD, Sanada K. DYRK 1A overexpression enhances STAT activity and astrogliogenesis in a Down syndrome mouse model . EMBO Rep. 2015;
119. Colombo JA, Reisin HD, Jones M, Bentham C. Development of interlaminar astroglial processes in the cerebral cortex of control and Down's syndrome human cases. Exp Neurol. 2005;
120. Torres MD, Garcia O, Tang C, Busciglio J. Dendritic spine pathology and thrombospondin-1 deficits in Down syndrome. Free Radical Biology and Medicine. 2018.
121. Garcia O, Torres M, Helguera P, Coskun P, Busciglio J. A role for thrombospondin-1 deficits in astrocyte-mediated spine and synaptic pathology in down's syndrome. PLoS One. 2010;
122. Fernández-blanco Á, Dierssen M. Rethinking Intellectual Disability from Neuro- to Astro-Pathology. Int J Mol Sci. 2020 Dec 1;21(23):1–20.
123. Sturgeon X, Gardiner KJ. Transcript catalogs of human chromosome 21 and orthologous chimpanzee and mouse regions. Mamm Genome. 2011 Jun;22(5–6):261–71.
124. Antonarakis SE, Skotko BG, Rafii MS, Strydom A, Pape SE, Bianchi DW, et al. Down syndrome. Nat Rev Dis Prim. 2020 Jan 1;6(1).
125. Davisson MT, Schmidt C, Reeves RH, Irving NG, Akeson EC, Harris BS, et al. Segmental trisomy as a mouse model for Down syndrome. Prog Clin Biol Res. 1993;384:117–33.
126. Duchon A, Raveau M, Chevalier C, Nalesso V, Sharp AJ, Herault Y. Identification of the translocation breakpoints in the Ts65Dn and Ts1Cje mouse lines: relevance for modeling Down syndrome. Mamm Genome. 2011 Dec;22(11–12):674–84.
127. Duchon A, Del Mar Mun˜ Iz Moreno M, Chevalier C, Nalesso VV, Andre P, Fructuoso-Castellar M, et al. Ts66Yah, a mouse model of Down syndrome with improved construct and face validity. Dis Model Mech. 2022 Dec 1;15(12).

128. Richtsmeier JT, Zumwalt A, Carlson EJ, Epstein CJ, Reeves RH. Craniofacial phenotypes in segmentally trisomic mouse models for Down syndrome. Am J Med Genet. 2002 Feb 1;107(4):317–24.
129. Escorihuela RM, Fernández-Teruel A, Vallina IF, Baamonde C, Lumbreras MA, Dierssen M, et al. A behavioral assessment of Ts65Dn mice: a putative Down syndrome model. Neurosci Lett. 1995 Oct 20;199(2):143–6.
130. Ruparelia A, Pearn ML, Mobley WC. Cognitive and pharmacological insights from the Ts65Dn mouse model of Down syndrome. Curr Opin Neurobiol. 2012 Oct;22(5):880–6.
131. Demas GE, Nelson RJ, Krueger BK, Yarowsky PJ. Impaired spatial working and reference memory in segmental trisomy (Ts65Dn) mice. Behav Brain Res. 1998;90:199–201.
132. Hanson JE, Weber M, Meilandt WJ, Wu T, Luu T, Deng L, et al. GluN2B Antagonism Affects Interneurons and Leads to Immediate and Persistent Changes in Synaptic Plasticity, Oscillations, and Behavior. Neuropsychopharmacol 2013 387. 2013 Jan 22;38(7):1221–33.
133. Chang Q, Gold PE. Age-related changes in memory and in acetylcholine functions in the hippocampus in the Ts65Dn mouse, a model of Down syndrome. Neurobiol Learn Mem. 2008 Feb;89(2):167–77.
134. De la Torre R, De Sola S, Pons M, Duchon A, de Lagran MM, Farré M, et al. Epigallocatechin-3-gallate, a DYRK1A inhibitor, rescues cognitive deficits in Down syndrome mouse models and in humans. Mol Nutr Food Res. 2014;
135. de la Torre R, de Sola S, Hernandez G, Farré M, Pujol J, Rodriguez J, et al. Safety and efficacy of cognitive training plus epigallocatechin-3-gallate in young adults with Down's syndrome (TESDAD): A double-blind, randomised, placebo-controlled, phase 2 trial. Lancet Neurol. 2016;
136. Manfredi-Lozano M, Leysen V, Adamo M, Paiva I, Rovera R, Pignat JM, et al. GnRH replacement rescues cognition in Down syndrome. Science. 2022 Sep 2;377(6610).
137. Altafaj X, Dierssen M, Baamonde C, Martí E, Visa J, Guimerà J, et al. Neurodevelopmental delay, motor abnormalities and cognitive deficits in

transgenic mice overexpressing Dyrk1A (minibrain), a murine model of Down's syndrome. Hum Mol Genet. 2001 Sep 1;10(18):1915–23.

138. Yu T, Li Z, Jia Z, Clapcote SJ, Liu C, Li S, et al. A mouse model of Down syndrome trisomic for all human chromosome 21 syntenic regions. Hum Mol Genet. 2010 Jul 15;19(14):2780–91.
139. Ferrés MA, Bianchi DW, Siegel AE, Bronson RT, Huggins GS, Guedj F. Perinatal Natural History of the Ts1Cje Mouse Model of Down Syndrome: Growth Restriction, Early Mortality, Heart Defects, and Delayed Development. PLoS One. 2016 Dec 1;11(12).
140. Jernigan TL, Bellugi U. Anomalous brain morphology on magnetic resonance images in Williams syndrome and Down syndrome. Arch Neurol. 1990;47(5):529–33.
141. Pinter JD, Brown WE, Eliez S, Schmitt JE, Capone GT, Reiss AL. Amygdala and hippocampal volumes in children with Down syndrome: a high-resolution MRI study. Neurology. 2001 Apr 10;56(7):972–4.
142. Weis S, Weber G, Neuhold A, Rett A. Down syndrome: MR quantification of brain structures and comparison with normal control subjects. AJNR Am J Neuroradiol. 1991;12(6):1207–11.
143. Lott IT, Dierssen M. Cognitive deficits and associated neurological complications in individuals with Down's syndrome. Vol. 9, The Lancet Neurology. 2010. p. 623–33.
144. Hartley T, Bird CM, Chan D, Cipolotti L, Husain M, Varga-Khadem F, et al. The hippocampus is required for short-term topographical memory in humans. Hippocampus. 2007;17(1):34–48.
145. Winocur G, Moscovitch M. Memory transformation and systems consolidation. J Int Neuropsychol Soc. 2011;17(5):766–80.
146. Debiec J, LeDoux JE, Nader K. Cellular and systems reconsolidation in the hippocampus. Neuron. 2002 Oct 24;36(3):527–38.
147. Zorrilla de San Martin J, Delabar JM, Bacci A, Potier MC. GABAergic over-inhibition, a promising hypothesis for cognitive deficits in Down syndrome. Free Radic Biol Med. 2018 Jan 1;114:33–9.
148. Fernandez F, Garner CC. Over-inhibition: a model for developmental

intellectual disability. Trends Neurosci. 2007 Oct;30(10):497–503.

149. Phillips RG, LeDoux JE. Differential contribution of amygdala and hippocampus to cued and contextual fear conditioning. Behav Neurosci. 1992;106(2):274–85.
150. Lever C, Wills T, Cacucci F, Burgess N, O'Keefe J. Long-term plasticity in hippocampal place-cell representation of environmental geometry. Nature. 2002 Mar 7;416(6876):90–4.
151. Nakashiba T, Cushman JD, Pelkey KA, Renaudineau S, Buhl DL, McHugh TJ, et al. Young dentate granule cells mediate pattern separation, whereas old granule cells facilitate pattern completion. Cell. 2012 Mar 30;149(1):188–201.
152. Bianchi P, Ciani E, Guidi S, Trazzi S, Felice D, Grossi G, et al. Early pharmacotherapy restores neurogenesis and cognitive performance in the Ts65Dn mouse model for down syndrome. J Neurosci. 2010 Jun 30;30(26):8769–79.
153. Leutgeb JK, Leutgeb S, Moser MB, Moser EI. Pattern separation in the dentate gyrus and CA3 of the hippocampus. Science. 2007 Feb 16;315(5814):961–6.
154. Bernier BE, Lacagnina AF, Ayoub A, Shue F, Zemelman B V., Krasne FB, et al. Dentate Gyrus Contributes to Retrieval as well as Encoding: Evidence from Context Fear Conditioning, Recall, and Extinction. J Neurosci. 2017;37(26):6359–71.
155. Poll S, Mittag M, Musacchio F, Justus LC, Giovannetti EA, Steffen J, et al. Memory trace interference impairs recall in a mouse model of Alzheimer's disease. Nat Neurosci. 2020 Aug 1;23(8):952–8.
156. Zhang Z, Ferretti V, Güntan I, Moro A, Steinberg EA, Ye Z, et al. Neuronal ensembles sufficient for recovery sleep and the sedative actions of α2 adrenergic agonists. Nat Neurosci. 2015 Apr 28;18(4):553–61.
157. Johnston ST, Parylak SL, Kim S, Mac N, Lim CK, Gallina IS, et al. AAV ablates neurogenesis in the adult murine hippocampus. Elife. 2021 Jul 1;10.
158. Tonegawa S, Liu X, Ramirez S, Redondo R. Memory Engram Cells Have

Come of Age. Neuron. 2015 Sep 2;87(5):918–31.
159. Cramer NP, Xu X, Haydar TF, Galdzicki Z. Altered intrinsic and network properties of neocortical neurons in the Ts65Dn mouse model of Down syndrome. Physiol Rep. 2015;3(12).
160. Stern S, Segal M, Moses E. Involvement of Potassium and Cation Channels in Hippocampal Abnormalities of Embryonic Ts65Dn and Tc1 Trisomic Mice. EBioMedicine. 2015 Sep 1;2(9):1048–62.
161. Nguyen TL, Duchon A, Manousopoulou A, Loaëc N, Villiers B, Pani G, et al. Correction of cognitive deficits in mouse models of Down syndrome by a pharmacological inhibitor of DYRK1A. Dis Model Mech. 2018 Sep 1;11(9).
162. Hyde LA, Frisone DF, Crnic LS. Ts65Dn mice, a model for Down syndrome, have deficits in context discrimination learning suggesting impaired hippocampal function. Behav Brain Res. 2001 Jan 8;118(1):53–60.
163. Kleschevnikov AM, Belichenko P V., Faizi M, Jacobs LF, Htun K, Shamloo M, et al. Deficits in cognition and synaptic plasticity in a mouse model of Down syndrome ameliorated by GABAB receptor antagonists. J Neurosci. 2012 Jul 4;32(27):9217–27.
164. Best TK, Cramer NP, Chakrabarti L, Haydar TF, Galdzicki Z. Dysfunctional hippocampal inhibition in the Ts65Dn mouse model of Down syndrome. Exp Neurol. 2012;
165. Mojabi FS, Fahimi A, Moghadam S, Moghadam S, Windy McNerneny M, Ponnusamy R, et al. GABAergic hyperinnervation of dentate granule cells in the Ts65Dn mouse model of down syndrome: Exploring the role of *App*. Hippocampus. 2016 Dec;26(12):1641–54.
166. Rao-Ruiz P, Yu J, Kushner SA, Josselyn SA. Neuronal competition: microcircuit mechanisms define the sparsity of the engram. Current Opinion in Neurobiology. 2019.
167. Miry O, Li J, Chen L. The Quest for the Hippocampal Memory Engram: From Theories to Experimental Evidence. Front Behav Neurosci. 2021 Jan 15;14.
168. Morrison DJ, Rashid AJ, Yiu AP, Yan C, Frankland PW, Josselyn SA.

Parvalbumin interneurons constrain the size of the lateral amygdala engram. Neurobiol Learn Mem. 2016 Nov 1;135:91–9.

169. Aimone JB, Deng W, Gage FH. Resolving new memories: a critical look at the dentate gyrus, adult neurogenesis, and pattern separation. Neuron. 2011 May 26;70(4):589–96.
170. Baker S, Vieweg P, Gao F, Gilboa A, Wolbers T, Black SE, et al. The Human Dentate Gyrus Plays a Necessary Role in Discriminating New Memories. Curr Biol. 2016 Oct 10;26(19):2629–34.
171. Smith GK, Kesner RP, Korenberg JR. Dentate Gyrus Mediates Cognitive Function in the Ts65Dn/DnJ Mouse Model of Down Syndrome. Hippocampus. 2014 Mar 1;24(3):354.
172. Josselyn SA, Tonegawa S. Memory engrams: Recalling the past and imagining the future. Science. 2020 Jan 3;367(6473).
173. Harashima C, Jacobowitz DM, Stoffel M, Chakrabarti L, Haydar TF, Siarey RJ, et al. Elevated expression of the G-protein-activated inwardly rectifying potassium channel 2 (GIRK2) in cerebellar unipolar brush cells of a down syndrome mouse model. Cell Mol Neurobiol. 2006;
174. Best TK, Siarey RJ, Galdzicki Z. Ts65Dn, a mouse model of Down syndrome, exhibits increased GABAB-induced potassium current. J Neurophysiol. 2007 Jan;97(1):892–900.
175. Chen X, Johnston D. Constitutively active G-protein-gated inwardly rectifying K+ channels in dendrites of hippocampal CA1 pyramidal neurons. J Neurosci. 2005 Apr 13;25(15):3787–92.
176. Johnston D, Magee JC, Colbert CM, Christie BR. Active properties of neuronal dendrites. Annu Rev Neurosci. 1996;19:165–86.
177. Takigawa T, Alzheimer C. Interplay between activation of GIRK current and deactivation of Ih modifies temporal integration of excitatory input in CA1 pyramidal cells. J Neurophysiol. 2003 Apr 1;89(4):2238–44.
178. Dong Y, Green T, Saal D, Marie H, Neve R, Nestler EJ, et al. CREB modulates excitability of nucleus accumbens neurons. Nat Neurosci. 2006;
179. Zhou Y, Won J, Karlsson MG, Zhou M, Rogerson T, Balaji J, et al. CREB regulates excitability and the allocation of memory to subsets of neurons in

the amygdala. Nat Neurosci. 2009 Nov;12(11):1438–43.
180. Guidi S, Stagni F, Bianchi P, Ciani E, Ragazzi E, Trazzi S, et al. Early pharmacotherapy with fluoxetine rescues dendritic pathology in the Ts65Dn mouse model of down syndrome. Brain Pathol. 2013 Mar;23(2):129–43.
181. Souchet B, Duchon A, Gu Y, Dairou J, Chevalier C, Daubigney F, et al. Prenatal treatment with EGCG enriched green tea extract rescues GAD67 related developmental and cognitive defects in Down syndrome mouse models. Sci Rep. 2019 Dec 1;9(1).
182. Stagni F, Giacomini A, Emili M, Trazzi S, Guidi S, Sassi M, et al. Short- and long-term effects of neonatal pharmacotherapy with epigallocatechin-3-gallate on hippocampal development in the Ts65Dn mouse model of Down syndrome. Neuroscience. 2016 Oct 1;333:277–301.
183. Araque A, Carmignoto G, Haydon PG. Dynamic signaling between astrocytes and neurons. Annu Rev Physiol. 2001;63:795–813.
184. Perea G, Navarrete M, Araque A. Tripartite synapses: astrocytes process and control synaptic information. Trends Neurosci. 2009 Aug;32(8):421–31.
185. Mederos S, Hernández-Vivanco A, Ramírez-Franco J, Martín-Fernández M, Navarrete M, Yang A, et al. Melanopsin for precise optogenetic activation of astrocyte-neuron networks. Glia. 2019 May 1;67(5):915–34.
186. Colgin LL. Rhythms of the hippocampal network. Nat Rev Neurosci. 2016 Apr 1;17(4):239–49.
187. Cho WH, Noh K, Lee BH, Barcelon E, Jun SB, Park HY, et al. Hippocampal astrocytes modulate anxiety-like behavior. Nat Commun. 2022 Dec 1;13(1).
188. Wang B, Zou L, Li M, Zhou L. Astrocyte: A Foe or a Friend in Intellectual Disability-Related Diseases. Front Synaptic Neurosci. 2022 Jun 23;14.
189. García O, Flores-Aguilar L. Astroglial and microglial pathology in Down syndrome: Focus on Alzheimer's disease. Front Cell Neurosci. 2022 Sep 20;16.
190. Antonarakis SE. Down syndrome and the complexity of genome dosage

imbalance. Nat Rev Genet. 2017 Mar 1;18(3):147–63.

191. Müller W, Heinemann U, Schuchmann S. Impaired Ca-signaling in astrocytes from the Ts16 mouse model of Down syndrome. Neurosci Lett. 1997 Feb 21;223(2):81–4.
192. Bambrick LL, Yarowsky PJ, Krueger BK. Altered astrocyte calcium homeostasis and proliferation in theTs65Dn mouse, a model of Down syndrome. J Neurosci Res. 2003 Jul 1;73(1):89–94.
193. Haustein MD, Kracun S, Lu XH, Shih T, Jackson-Weaver O, Tong X, et al. Conditions and constraints for astrocyte calcium signaling in the hippocampal mossy fiber pathway. Neuron. 2014 Apr 16;82(2):413–29.
194. Paxinos and Franklin's the Mouse Brain in Stereotaxic Coordinates - George Paxinos, Keith B.J. Franklin - Google Libros [Internet].
195. Boyce RW, Dorph-Petersen KA, Lyck L, Gundersen HJG. Design-based stereology: introduction to basic concepts and practical approaches for estimation of cell number. Toxicol Pathol. 2010 Dec;38(7):1011–25.
196. Dorph-Petersen KA, Lewis DA. Stereological approaches to identifying neuropathology in psychosis. Biol Psychiatry. 2011 Jan 15;69(2):113–26.
197. Mederos S, Sánchez-Puelles C, Esparza J, Valero M, Ponomarenko A, Perea G. GABAergic signaling to astrocytes in the prefrontal cortex sustains goal-directed behaviors. Nat Neurosci. 2021 Jan 1;24(1):82–92.
198. Martelotto LG. 'Frankenstein' protocol for nuclei isolation from fresh and frozen tissue for snRNAseq. 2020 Mar 6;
199. Hochgerner H, Zeisel A, Lönnerberg P, Linnarsson S. Conserved properties of dentate gyrus neurogenesis across postnatal development revealed by single-cell RNA sequencing. Nat Neurosci. 2018 Feb 1;21(2):290–9.
200. Wu T, Hu E, Xu S, Chen M, Guo P, Dai Z, et al. clusterProfiler 4.0: A universal enrichment tool for interpreting omics data. Innov (Cambridge. 2021 Aug 28;2(3).
201. Angerer P, Haghverdi L, Büttner M, Theis FJ, Marr C, Buettner F. *destiny* : diffusion maps for large-scale single-cell data in R. Bioinformatics. 2016 Apr 15;32(8):1241–3.

202. Ge SX, Jung D, Yao R. ShinyGO: a graphical gene-set enrichment tool for animals and plants. Bioinformatics. 2020 Apr 15;36(8):2628–9.
203. Cao Y, Lin Y, Ormerod JT, Yang P, Yang JYH, Lo KK. scDC: single cell differential composition analysis. BMC Bioinformatics. 2019 Dec 24;20(S19):721.
204. Hibaoui Y, Grad I, Letourneau A, Sailani MR, Dahoun S, Santoni FA, et al. Modelling and rescuing neurodevelopmental defect of Down syndrome using induced pluripotent stem cells from monozygotic twins discordant for trisomy 21. EMBO Mol Med. 2014;
205. Lein ES, Hawrylycz MJ, Ao N, Ayres M, Bensinger A, Bernard A, et al. Genome-wide atlas of gene expression in the adult mouse brain. Nat 2006 4457124. 2006 Dec 6;445(7124):168–76.
206. Miller FD, Gauthier AS. Timing Is Everything: Making Neurons versus Glia in the Developing Cortex. Neuron. 2007 May;54(3):357–69.
207. Halford J, Shen S, Itamura K, Levine J, Chong AC, Czerwieniec G, et al. New astroglial injury-defined biomarkers for neurotrauma assessment. J Cereb Blood Flow Metab. 2017 Oct 1;37(10):3278–99.
208. Hasel P, Rose IVL, Sadick JS, Kim RD, Liddelow SA. Neuroinflammatory astrocyte subtypes in the mouse brain. Nat Neurosci. 2021 Oct 1;24(10):1475–87.
209. Hoshi A, Yamamoto T, Shimizu K, Ugawa Y, Nishizawa M, Takahashi H, et al. Characteristics of aquaporin expression surrounding senile plaques and cerebral amyloid angiopathy in Alzheimer disease. J Neuropathol Exp Neurol. 2012 Aug;71(8):750–9.
210. Badaut J. Aquaglyceroporin 9 in brain pathologies. Neuroscience. 2010 Jul;168(4):1047–57.
211. Marx SO, Reiken S, Hisamatsu Y, Gaburjakova M, Gaburjakova J, Yang YM, et al. Phosphorylation-Dependent Regulation of Ryanodine Receptors. J Cell Biol. 2001 May 14;153(4):699–708.
212. Nestorowa S, Hamey FK, Pijuan Sala B, Diamanti E, Shepherd M, Laurenti E, et al. A single-cell resolution map of mouse hematopoietic stem and progenitor cell differentiation. Blood. 2016 Aug 25;128(8):e20–31.

213. Bazargani N, Attwell D. Astrocyte calcium signaling: the third wave. Nat Neurosci. 2016 Feb 27;19(2):182–9.
214. Corkrum M, Covelo A, Lines J, Bellocchio L, Pisansky M, Loke K, et al. Dopamine-Evoked Synaptic Regulation in the Nucleus Accumbens Requires Astrocyte Activity. Neuron. 2020 Mar;105(6):1036-1047.e5.
215. Van Den Herrewegen Y, Sanderson TM, Sahu S, De Bundel D, Bortolotto ZA, Smolders I. Side-by-side comparison of the effects of Gq- and Gi-DREADD-mediated astrocyte modulation on intracellular calcium dynamics and synaptic plasticity in the hippocampal CA1. Mol Brain. 2021 Dec 1;14(1).
216. Zdaniuk G, Wierzba-Bobrowicz T, Szpak GM, Stępień T. Astroglia disturbances during development of the central nervous system in fetuses with Down's syndrome. Folia Neuropathol. 2011;49(2):109–14.
217. Kanaumi T, Milenkovic I, Adle-Biassette H, Aronica E, Kovacs GG. Non-neuronal cell responses differ between normal and Down syndrome developing brains. Int J Dev Neurosci. 2013;
218. Lee HC, Tan KL, Cheah PS, Ling KH. Potential Role of JAK-STAT Signaling Pathway in the Neurogenic-to-Gliogenic Shift in Down Syndrome Brain. Neural Plast. 2016;2016.
219. Kawatani K, Nambara T, Nawa N, Yoshimatsu H, Kusakabe H, Hirata K, et al. A human isogenic iPSC-derived cell line panel identifies major regulators of aberrant astrocyte proliferation in Down syndrome. Commun Biol 2021 41. 2021 Jun 14;4(1):1–15.
220. Colombo E, Di Dario M, Capitolo E, Chaabane L, Newcombe J, Martino G, et al. Fingolimod may support neuroprotection via blockade of astrocyte nitric oxide. Ann Neurol. 2014 Sep 1;76(3):325–37.
221. Colombo E, Bassani C, De Angelis A, Ruffini F, Ottoboni L, Comi G, et al. Siponimod (BAF312) Activates Nrf2 While Hampering NFκB in Human Astrocytes, and Protects From Astrocyte-Induced Neurodegeneration. Front Immunol. 2020 Apr 8;11.
222. Colodner KJ, Montana RA, Anthony DC, Folkerth RD, De Girolami U, Feany MB. Proliferative potential of human astrocytes. J Neuropathol Exp

Neurol. 2005;64(2):163–9.

223. Horner PJ, Power AE, Kempermann G, Kuhn HG, Palmer TD, Winkler J, et al. Proliferation and differentiation of progenitor cells throughout the intact adult rat spinal cord. J Neurosci. 2000 Mar 15;20(6):2218–28.
224. Ma B, Buckalew R, Du Y, Kiyoshi CM, Alford CC, Wang W, et al. Gap junction coupling confers isopotentiality on astrocyte syncytium. Glia. 2016 Feb 1;64(2):214–26.
225. Scemes E, Spray DC. The astrocytic syncytium. In 2003. p. 165–79.
226. Rampon C, Jiang CH, Dong H, Tang YP, Lockhart DJ, Schultz PG, et al. Effects of environmental enrichment on gene expression in the brain. Proc Natl Acad Sci U S A. 2000 Nov 7;97(23):12880–4.
227. Dere E, De Souza-Silva MA, Frisch C, Teubner B, Söhl G, Willecke K, et al. Connexin30-deficient mice show increased emotionality and decreased rearing activity in the open-field along with neurochemical changes. Eur J Neurosci. 2003 Aug;18(3):629–38.
228. Pannasch U, Freche D, Dallérac G, Ghézali G, Escartin C, Ezan P, et al. Connexin 30 sets synaptic strength by controlling astroglial synapse invasion. Nat Neurosci. 2014;17(4):549–58.
229. Angulo MC, Kozlov AS, Charpak S, Audinat E. Glutamate released from glial cells synchronizes neuronal activity in the hippocampus. J Neurosci. 2004 Aug 4;24(31):6920–7.
230. Fellin T, Pascual O, Gobbo S, Pozzan T, Haydon PG, Carmignoto G. Neuronal synchrony mediated by astrocytic glutamate through activation of extrasynaptic NMDA receptors. Neuron. 2004 Sep 2;43(5):729–43.
231. Brose N, Rosenmund C, Rettig J. Regulation of transmitter release by Unc-13 and its homologues. Curr Opin Neurobiol. 2000 Jun 1;10(3):303–11.
232. Fox NC, Freeborough PA. Brain atrophy progression measured from registered serial MRI: validation and application to Alzheimer's disease. J Magn Reson Imaging. 1997 Nov;7(6):1069–75.
233. Green AJE, Harvey RJ, Thompson EJ, Rossor MN. Increased S100beta in the cerebrospinal fluid of patients with frontotemporal dementia. Neurosci Lett. 1997 Oct 10;235(1–2):5–8.

234. Rothermundt M, Peters M, Prehn JHM, Arolt V. S100B in brain damage and neurodegeneration. Microsc Res Tech. 2003;60(6):614–32.
235. King CM, Bohmbach K, Minge D, Delekate A, Zheng K, Reynolds J, et al. Local Resting Ca2+ Controls the Scale of Astroglial Ca2+ Signals. Cell Rep. 2020 Mar;30(10):3466-3477.e4.
236. Barger SW, Wolchok SR, Van Eldik LJ. Disulfide-linked S100 beta dimers and signal transduction. Biochim Biophys Acta. 1992 Nov 10;1160(1):105–12.
237. Rusakov DA, Zheng K, Henneberger C. Astrocytes as regulators of synaptic function: a quest for the Ca2+ master key. Neuroscientist. 2011 Oct;17(5):513–23.
238. Srinivasan R, Huang BS, Venugopal S, Johnston AD, Chai H, Zeng H, et al. Ca(2+) signaling in astrocytes from Ip3r2(-/-) mice in brain slices and during startle responses in vivo. Nat Neurosci. 2015 Apr 28;18(5):708–17.
239. Bindocci E, Savtchouk I, Liaudet N, Becker D, Carriero G, Volterra A. Three-dimensional Ca2+ imaging advances understanding of astrocyte biology. Science. 2017 May 19;356(6339).
240. Panatier A, Vallée J, Haber M, Murai KK, Lacaille JC, Robitaille R. Astrocytes are endogenous regulators of basal transmission at central synapses. Cell. 2011 Sep 2;146(5):785–98.
241. Burgess N, Maguire EA, O'Keefe J. The human hippocampus and spatial and episodic memory. Neuron. 2002 Aug 15;35(4):625–41.
242. Smith DM, Mizumori SJY. Hippocampal place cells, context, and episodic memory. Hippocampus. 2006;16(9):716–29.
243. Pearlson GD, Breiter SN, Aylward EH, Warren AC, Grygorcewicz M, Frangou S, et al. MRI brain changes in subjects with Down syndrome with and without dementia. Dev Med Child Neurol. 1998 May;40(5):326–34.
244. Strydom A, Hassiotis A, Walker Z. Magnetic resonance imaging in people with Down's syndrome and Alzheimer's disease. J Intellect Disabil Res. 2004 Nov;48(Pt 8):769–70.
245. Chakrabarti L, Best TK, Cramer NP, Carney RSE, Isaac JTR, Galdzicki Z, et al. Olig1 and Olig2 triplication causes developmental brain defects in

Down syndrome. Nat Neurosci. 2010 Aug;13(8):927–34.

246. Hernández S, Gilabert-Juan J, Blasco-Ibáñez JM, Crespo C, Nácher J, Varea E. Altered expression of neuropeptides in the primary somatosensory cortex of the Down syndrome model Ts65Dn. Neuropeptides. 2012 Feb;46(1):29–37.
247. Hernández-González S, Ballestín R, López-Hidalgo R, Gilabert-Juan J, Blasco-Ibáñez JM, Crespo C, et al. Altered distribution of hippocampal interneurons in the murine Down Syndrome model Ts65Dn. Neurochem Res. 2015 Jan 1;40(1):151–64.
248. Halassa MM, Fellin T, Takano H, Dong JH, Haydon PG. Synaptic islands defined by the territory of a single astrocyte. J Neurosci. 2007;27(24):6473–7.
249. Henneberger C, Papouin T, Oliet SHR, Rusakov DA. Long-term potentiation depends on release of D-serine from astrocytes. Nature. 2010 Jan 14;463(7278):232–6.
250. Jourdain P, Bergersen LH, Bhaukaurally K, Bezzi P, Santello M, Domercq M, et al. Glutamate exocytosis from astrocytes controls synaptic strength. Nat Neurosci. 2007 Mar;10(3):331–9.
251. Santello M, Bezzi P, Volterra A. TNFα controls glutamatergic gliotransmission in the hippocampal dentate gyrus. Neuron. 2011 Mar 10;69(5):988–1001.
252. Alldred MJ, Penikalapati SC, Lee SH, Heguy A, Roussos P, Ginsberg SD. Profiling Basal Forebrain Cholinergic Neurons Reveals a Molecular Basis for Vulnerability Within the Ts65Dn Model of Down Syndrome and Alzheimer's Disease. Mol Neurobiol. 2021 Oct 1;58(10):5141–62.
253. Alldred MJ, Lee SH, Petkova E, Ginsberg SD. Expression profile analysis of vulnerable CA1 pyramidal neurons in young-Middle-Aged Ts65Dn mice. J Comp Neurol. 2015 Jan 1;523(1):61–74.
254. Giaume C. Astroglial Wiring is Adding Complexity to Neuroglial Networking. Front Neuroenergetics. 2010;2.
255. Chever O, Dossi E, Pannasch U, Derangeon M, Rouach N. Astroglial networks promote neuronal coordination. Sci Signal. 2016 Jan 12;9(410).

256. Rouach N, Koulakoff A, Abudara V, Willecke K, Giaume C. Astroglial metabolic networks sustain hippocampal synaptic transmission. Science. 2008 Dec 5;322(5907):1551–5.

ABBREVIATIONS

ABBREVIATIONS

A_1R: Adenosine 1 Receptor
ACC: Anterior Cingulate Cortex
Aβ: Amyloid β peptide
AD: Alzheimer's Disease
Agt: Angiotensin
Akap6: A-Kinase Anchoring Protein 6
AMPA: α-amino-3-hydroxy-5-methyl-4-isoxazolepropionic acid receptor
AP: Action Potential
APP: Amyloid Precursor Protein
Aqp9: Aquaporin-9
Arc: Activity-Regulated Cytoskeleton-associated protein
BDNF: Brain-Derived Neurotrophic Factor
CA1: Cornu Ammonis Area 1
CA3: Cornu Ammonis Area 3
CBP: CREB-Binding Protein
CC: Current Clamp
CEEA-PRBB: Comité Ético de Experimentación Animal del PRBB
CF: Counting Frame
CFC: Contextual Fear Conditioning
CNO: Clozapine N-oxide
CP: Corner Point
CREB: Cyclic AMP-Responsive Element-Binding protein
Cx30: Connexin 30
Cx43: Connexin 43
DAG: Diacylglycerol
DEG: Differentially Expressed Gene
DG: Dentate Gyrus
DI: Discrimination Index
DNA: Deoxyribonucleic Acid
DS: Down syndrome

DSCR: Down syndrome critical region

DYRK1A: Dual-specificity tyrosine-regulated kinase 1A

EC: Entorhinal Cortex

EE: Environmental Enrichment

EGCG: Epigallocatechin-3-gallate

EPSC: Excitatory Postsynaptic Currents

ER: Endoplasmic Reticulum

FANS: Fluorescence-Activated Nuclear Sorting

Fabp7: Fatty acid binding protein 7

FC: Fear Conditioning

Fmr1: Fragile X Messenger Ribonucleoprotein 1

FXS: Fragile X syndrome

GABA: Gamma-Aminobutyric Acid

Gabbr2: Gamma-Aminobutyric Acid B Receptor 2

GC: Genome Copy

GECI: Genetically Encoded Calcium Indicator

GFAP: Glial Fibrillary Acidic Protein

Gjb6: Gap Junction Protein Beta 6

GLAST-1: Glutamate Aspartate Transporter 1

Gria5: Glutamate Ionotropic Receptor AMPA Type Subunit 5

Grin2c: Glutamate Ionotropic Receptor NMDA Type Subunit 2C

Grm5: Glutamate Metabotropic Receptor 5

GPCR: G Protein-Coupled Receptor

h: Hour

HSA21: Homo Sapiens Chromosome 21

ID: Intellectual Disability

IEG: Immediate Early Gene

Il17r: Interleukin-17 Receptor

$InsP_3R$: Inositol Triphosphate Receptor

IP_3: Inositol Triphosphate

iPSCs: Induced Pluripotent Stem Cells

KO: Knockout

LTD: Long-term Depression

LTP: Long-term Potentiation

min: Minute

mEPSC: Miniature Excitatory Postsynaptic Currents

mIPSC: Miniature Inhibitory Postsynaptic Currents

ml: Milliliter

mm: Millimeter

mM: Millimolar

Mmu: Mus Musculus Chromosome

mRNA: Messenger Ribonucleic Acid

MWM: Morris Water Maze

N: Number

NA: Numerical Aperture

NeuN: Neuronal Nuclear antigen

NORT: Novel Object Recognition Test

NMDA: *N*-methyl-d-aspartic acid

PAP: Perisynaptic Astroglial Process

PCA: Principal Component Analysis

PIP_2: Phosphatidyl (4,5)-bisphosphate

PLC: Phospholipase C

ROS: Reactive Oxygen Species

RT: Room Temperature

S100β: S100 calcium-binding protein β

SC: Schaffer Collaterals

SN = Single Nucleus

SOD1: SuperOxide Dismutase 1

STAT: Signal Transducer and Activator of Transcription

TBS: Tris-Buffered Saline

TeNT: Tetanus Toxin

TS: Trisomic mice

Ts65Dn Trisomic mice

TSP-1: Thrombospondin-1

UMAP: Uniform Manifold Approximation and Projection

WT: Wild-type

3D: Three-Dimensional

ETHICS, LIMITATIONS AND DATA AVAILABILITY

ETHICS, LIMITATIONS AND DATA AVAILABILITY

All studies of animal models and all procedures need to be approved by the institutional animal care and use Ethic Committee (PRBB) and will be implemented according to Local and National laws and the European directives in force on the protection of animals used for experimentation and other scientific purposes:

- Directive 2010/63/EU revising Directive 86/609/EEC on the protection of animals used for scientific purposes adopted on 22 September 2010.
- Commission Recommendation of 18 June 2007 on guidelines for the accommodation and care of animals used for experimental and other scientific purposes (2007/526/EC). This Recommendation compliments Annex III of Directive 2010/63/EU, which is based on provisions found therein, and sets down firm rules on requirements for accommodation and care of experimental animals.

- Spanish law: Real Decreto 53/2013, de 1 de febrero, del Ministerio de la Presidencia para la protección de los animales utilizados en experimentación y otros fines científicos, incluyendo la docencia BOE núm. 34, published on the Spanish official Journal of 8th of February.

- Local law: DECRET 214/1997, de 30 de juliol, pel qual es regula la utilització d'animals per a experimentació i per a altres finalitats científiques approved by the Catalan government.

- Statement of Compliance with Standards for Use of Laboratory Animals by Foreign Institutions no A5388-01, approved by the National Institutes of Health (NIH-USA).

All procedures to be performed have already been evaluated and approved by the Ethical Committee for Animal Experimentation (CEEA-PRBB), and approved by the Government of Catalunya. The Ethic Committee is an independent body formed by 8 people, 3 of them are not related with scientific experimentation including a lawyer.

All researchers involved in animal experimentations have the appropriate training as determined by the Local regulations of the Department of “Medi Ambient i Habitatge" for experiments with laboratory animal (decret 214/1997).
The CEEA ethical committee ensures that all procedures carried out at the CRG are done according to the three R´s: that is, Replacement, Reduction and Refinement.

- With respect to Replacement, given the nature of our proposed work it is not feasible to perform our experiments in cellular models.

- With respect to Reduction we are taking the approach to perform our functional
screens in a high-throughput manner, which should decrease the total number of animals used.

- With respect to Refinement, the animal unit of the PRBB has recently obtained the certificate from the Association for Assessment and Accreditation of Laboratory Animal Care (AAALAC-I, number of ref: 001339) which certifies that all animals are housed in conditions that enhance the welfare of the animals. Furthermore, all investigators in my lab involved in animal experimentations have the appropriate training as determined by the regulations of the National and Local Governments for experiments with laboratory animals (Spanish Law 10/2005; local law 214/1997). No worker in the CRG is allowed to handle any animals before taking this course and obtaining their personal license. Moreover, our experimental animals are under constant supervision from the Animal Unit Technicians and the Head Veterinarian, who ensure that the procedures performed do not cause any unnecessary distress to the mice.

Compliance of regulations and safety measures

The CRG has provided training for staff in the handling, storage, and disposal of radioactive and dangerous materials. All employees who handle these substances have received the necessary training. Additionally, it has created uniform working protocols in experimental laboratories, and each research group has a safety coordinator. To prevent inhalation and dispersion in the lab, the

laboratories feature a chemical gas hood. Additionally, they have personal protective equipment (gloves and safety glasses) to prevent direct contact when handling chemicals. The CRG conducts hygienic risk assessments with the objective of reducing the potential risk of inhalation and contact arising from the use of these materials. The CRG complies with Royal Decree 664/1997 on the protection of workers against chemical risk as well as the Occupational Risk Prevention Law (Law 31/1995). All CRG departments, laboratories, staff members, independent contractors, subcontractors, interns, volunteers, and site visits are subject to the CRG's requirements. The Occupational Risk Prevention Management System is subject to external audits.

Limitations

Animal studies on Chapter I and Chapter II have been performed on males. We understand how crucial it is for basic research to include both males and females to draw generalizable conclusions from basic research. For this reason, future studies will aim at replicating these results in female mice.
In like manner, all the experiments in this Thesis have been conducted using the Ts65Dn mice. Because we are aware that the Ts65Dn mouse model has several limitations, we are planning to replicate the most relevant results of every Chapter in Ts66Yah mice.

Data availability

The following link contains the raw data from each Chapter:

https://crgcnag-my.sharepoint.com/:f:/g/personal/afernandez_crg_es/EnaxQWd3wZRMr_n96AJvi0kB5Aqg1ZLu1ZdWOoee3IjBWg?e=BEQCCZ